LOCKHEED MARTIN ENERGY RESEARCH LIBRARIES
3 4456 0515724 6

CENTRAL RESEARCH LIBRARY
DOCUMENT COLLECTION

ORNL-4561
UC-25 – Metals, Ceramics, and Materials

cy 1

INFLUENCE OF TITANIUM ON THE HIGH-TEMPERATURE DEFORMATION AND FRACTURE BEHAVIOR OF SOME NICKEL BASED ALLOYS

(Thesis)

Charles Edward Sessions

OAK RIDGE NATIONAL LABORATORY
CENTRAL RESEARCH LIBRARY
DOCUMENT COLLECTION
LIBRARY LOAN COPY
DO NOT TRANSFER TO ANOTHER PERSON
If you wish someone else to see this document, send in name with document and the library will arrange a loan.
UCN-7969
(3 3-67)

OAK RIDGE NATIONAL LABORATORY
operated by
UNION CARBIDE CORPORATION
for the
U.S. ATOMIC ENERGY COMMISSION

Printed in the United States of America. Available from Clearinghouse for Federal Scientific and Technical Information, National Bureau of Standards, U.S. Department of Commerce, Springfield, Virginia 22151
Price: Printed Copy $3.00; Microfiche $0.65

LEGAL NOTICE

This report was prepared as an account of Government sponsored work. Neither the United States, nor the Commission, nor any person acting on behalf of the Commission:

A. Makes any warranty or representation, expressed or implied, with respect to the accuracy, completeness, or usefulness of the information contained in this report, or that the use of any information, apparatus, method, or process disclosed in this report may not infringe privately owned rights; or

B. Assumes any liabilities with respect to the use of, or for damages resulting from the use of any information, apparatus, method, or process disclosed in this report.

As used in the above, "person acting on behalf of the Commission" includes any employee or contractor of the Commission, or employee of such contractor, to the extent that such employee or contractor of the Commission, or employee of such contractor prepares, disseminates, or provides access to, any information pursuant to his employment or contract with the Commission, or his employment with such contractor.

ORNL-4561

Contract No. W-7405-eng-26

METALS AND CERAMICS DIVISION

INFLUENCE OF TITANIUM ON THE HIGH-TEMPERATURE DEFORMATION AND FRACTURE BEHAVIOR OF SOME NICKEL BASED ALLOYS

Charles Edward Sessions

A Dissertation
Presented to
the Graduate Council of
The University of Tennessee

In Partial Fulfillment
of the Requirements for the Degree
Doctor of Philosophy

JULY 1970

OAK RIDGE NATIONAL LABORATORY
Oak Ridge, Tennessee
operated by
UNION CARBIDE CORPORATION
for the
U.S. ATOMIC ENERGY COMMISSION

LOCKHEED MARTIN ENERGY RESEARCH LIBRARIES
3 4456 0515724 6

ACKNOWLEDGMENTS

The author would like to express his sincere appreciation to Dr. E. E. Stansbury, his major professor, for directing this research and offering encouragement during the course of this study. Dr. Stansbury's understanding of phase equilibria, microstructures and deformation processes has provided considerable insight into a complicated subject.

This work was performed in the Metal and Ceramics Division of the Oak Ridge National Laboratory, where the author is employed. The author expresses his appreciation to the Division director, Dr. J. H. Frye, the section heads involved in direction of the mechanical properties research, Dr. C. J. McHargue and Mr. J. R. Weir, and the author's immediate group leader, Dr. H. E. McCoy. A special debt of gratitude is extended to Drs. McHargue and McCoy for encouraging the author to select this thesis topic in mechanical metallurgy and in assisting the author in understanding certain phases of this work. The author is also grateful to Mr. Weir for allowing the author, a new engineer in his section, to propose and to research this dissertation problem.

Another very special debt of appreciation is expressed to Mr. Ralph E. Gehlbach for instructing the author in the techniques of electron microscopy and phase analysis. Without Mr. Gehlbach's valuable knowledge, experience, and assistance the effects of titanium on the phases and microstructures could not have been defined. Also the assistance of Mr. S. W. Cook is appreciated for the preparation of thin

film sample and performing electrolytic extractions of precipated phases.

The large amount of assistance provided by various technicians and service groups at the Oak Ridge National Laboratory* is appreciated. In particular the author would like to acknowledge the assistance in performing mechanical tests of Mr. E. M. Thomas, Mr. P. F. Huber and especially Mr. H. W. Kline and Mr. B. C. Williams. The author acknowledges the valuable assistance of J. Feltner who performed heat-treatments and processed the mechanical property data during the course of this study. Messrs. Feltner, Kline and Williams have worked for the last three years with unselfish assistance in performing the various tests required in this investigation. The metallographic sample preparation and photography of Mr. H. R. Tinch is also acknowledged. The assistance in performing the scanning electron microscopy given by Mr. R. K. Bennett of the Oak Ridge Y-12 plant and Mr. T. A. Nolan of the Oak Ridge Gaseous Diffusion Plant is appreciated. Mrs. Bette Thomas and the author's wife, Nancy, are acknowledged for typing drafts of this manuscript and the Graphic Arts department of ORNL is acknowledged for drawing the figures. Appreciation for critical review of the manuscript is expressed to Drs. F. W. Wiffen, C. J. McHargue, H. E. McCoy, Mr. D. G. Harman and Mr. H. Inouye.

---

*The Oak Ridge National Laboratory is operated by Union Carbide Corporation, Nuclear Division, for the U. S. Atomic Energy Commission.

Finally, the author would like to express his deepest felt appreciation to his immediate family. To his wife, Nancy, the author expresses his love and thankfulness particularly for the understanding and encouragement given over the last six years of part-time graduate work. Also, the author would like to express his heartfelt thanks to both his mother, Mrs. M. Earline Sessions, and his father, Mr. Harry E. Sessions, for encouragement and assistance in obtaining a college education.

ABSTRACT

Irradiation induced high temperature embrittlement of nickel alloys can be influenced by small additions of alloying elements such as titanium, zirconium, hafnium, and niobium. Thus, an investigation of the influence of titanium on the deformation and fracture behavior of nickel and a nickel base alloy, Hastelloy-N (Ni-12% Mo-7% Cr-0.07%C) was conducted. The purpose was to relate the influence of titanium on the precipitate types, morphology and distribution to the elevated temperature mechanical behavior in creep and tensile tests. This phase of the study involved (1) measuring creep-rupture properties at 650°C as a function of titanium and carbon content for laboratory heats of a Ni-12% Mo-7% Cr alloy, (2) defining the effect of titanium on the phase equilibria of four commercial heats of Hastelloy-N, and (3) correlating the carbide types, morphologies, and distributions established in these four heats with creep and tensile properties after aging at 650 or 760°C. In a second phase of this study the influence of titanium in the Ni-12% Mo-7% Cr alloy was compared with the beneficial influence of titanium in pure nickel by measuring the creep and tensile properties of a series of dilute nickel-titanium alloys at 600°C as a function of various test conditions.

It was shown that the influence of 0.5% Ti on the creep properties of the Ni-12% Mo-7% Cr alloy is small unless the alloy is aged prior to mechanical testing. An increase in the 650°C rupture life, a decrease

in creep rate, a small increase in ductility, and no change in the intergranular fracture mode were found when 0.5% Ti was added to the alloy. On the other hand, an increase in carbon content from 0.003% to 0.3% in an alloy containing Ni-12% Mo-7% Cr-0.5% Ti increased the rupture life by four orders of magnitude, decreased the creep rate by four orders of magnitude, and increased the creep ductility by a factor of three. A significant decrease in the grain size was found for the higher carbon contents.

It is proposed that a change in the strengthening mechanism occurs when titanium is added to the alloy. When titanium is present MC-type carbides precipitate on dislocations causing the growth of stacking faults. Under straining it is assumed that the formation of the stacking fault precipitate morphology is enhanced and the strength is increased due to dynamic strain aging. When titanium is not present coarse M_2C-type precipitates form primarily within the matrix.

Titanium contents up to 1.2% were found to affect the equilibrium carbide phases on aging at 650 and 760°C. Increasing concentrations of titanium favored the formation of an MC-type carbide rather than an M_2C-type. Titanium substitutes for chromium and for molybdenum in the MC carbide, increases the lattice parameter, and tends to stabilize the MC carbide to higher aging temperatures. The MC and M_2C-type carbides exists in several different morphologies. Alloys containing a favorable distribution of MC carbides had greater post-aging ductility in both creep and tensile tests than alloys containing M_2C carbides. A heavy, nearly continuous, grain boundary distribution of MC carbides resulted

in greater ductility than a rounded, widely spaced M_2C grain boundary precipitate distribution. The enhanced ductility was attributed to limiting the growth of grain boundary cracks by inhibitation of grain boundary shearing. Thus, one beneficial influence of titanium in the alloy was to promote the formation of a carbide type and distribution which allowed grain deformation to proceed to higher total strains at 650°C.

Titanium also promotes the formation of an MC-type carbide distribution detrimental to ductility but beneficial to tensile strength at 650°C. Precipitation of fine MC carbides on dislocations promotes the growth of a stacking fault precipitate morphology. The tendency to form stacking fault precipitates in the Ni-12% Mo-7% Cr-0.07%C alloys increases with an increase in either titanium content, solution annealing temperature, or aging temperature over the range of these variables investigated. For the Hastelloy-N containing 1.2% Ti and solution annealed at 1260°C, a maximum in the 650°C yield strength occurred after 200 hours and a minimum ductility after approximately 1500 hours of aging at 760°C. Stacking fault precipitates grew to a size resolvable in transmission electron microscopy on aging between 0.25 and 5 hours at 760°C. The strengthening influence of the stacking fault precipitate morphology was greater for short time tensile tests than for longer time creep tests. However, a loss of ductility was found in both creep and tensile tests for samples heat treated to form stacking fault precipitates. The tendency to nucleate and grow precipitates on stacking faults in this Ni-Mo-Cr-Ti system confirms the theoretical model

proposed by Silcock and Tunstall which was based on observations of NbC precipitation in austenetic stainless steels. However, grain boundary denuding of this type precipitate was not as extensive in the Ni-Mo-Cr-Ti alloys as reported for the stainless steels.

Although the mechanism by which titanium enhances the ductility of pure nickel was not defined in this study, it was shown that small concentrations of titanium drastically reduces the tendency for intergranular fracture in both creep and tensile tests at 600°C. Since the enhanced tensile ductility resulted from an increase in the "nonuniform" deformation, the strain rate sensitivity of the plastic flow is the parameter which best reflects the influence of the titanium. It is proposed that titanium acts as a scavenger and changes the distribution of impurities along the grain boundary so that enhanced ductility results because either (1) the grain boundaries have greater mobility for stress relieving migration or recrystallization or (2) the absence of impurities from the boundaries decreases the number of possible intergranular void nucleation sites so that fewer stress concentrations are present under mechanical test conditions.

Thus, it is proposed that titanium influences the mechanical behavior in the Ni-Mo-Cr-C alloy and in pure nickel in two significantly different ways. In one case (i.e., the Ni-Mo-Cr-C alloys) grain boundary shearing is reduced due to the influence of different carbide types and distributions and in the other case (i.e., the Ni-Ti alloys) enhanced grain boundary mobility is responsible for the enhanced hot ductility when titanium is added.

TABLE OF CONTENTS

CHAPTER		PAGE
I.	INTRODUCTION	1
II.	REVIEW OF LITERATURE	3
	High Temperature Fracture Processes	3
	Mechanisms	3
	Effect of composition and microstructure	7
	Effect of Selected Metallurgical Variables on Ductility	9
	Measures of ductility	10
	Effect of second phases on ductility	11
	Effect of temperature on ductility	12
	Effect of strain rate on ductility	13
	Microstructural effects on ductility	13
	Effect of stacking fault energy on ductility	14
	Ductility in creep	15
	Relating creep and rupture processes	16
	Strain rate sensitivity and work hardening	18
	Effect of Titanium on Strength and Ductility in Various Alloy Systems	20
	Titanium in iron-base alloys	21
	Titanium in nickel-base alloys	22
	Titanium in refractory metals	24

CHAPTER PAGE

III. EXPERIMENTAL PROCEDURE 27

Fabrication of Material 27

Mechanical Testing Procedure 31

Air environment 31

Argon environment 33

Microscopy and Phase Analysis 35

Optical metallography 35

Transmission microscopy 36

Scanning microscopy 36

Phase extraction and identification 37

Extractions for x-ray identification 37

Extraction replicas 37

IV. EXPERIMENTAL RESULTS 39

Influence of Titanium and Carbon Content on Creep Properties 40

Creep-rupture life 40

Effect of carbon content 40

Effect of titanium content 43

Secondary creep rate 46

Creep ductility 48

Elongation versus carbon content 48

Elongation versus creep rate 50

Elongation versus rupture life 53

CHAPTER PAGE

Influence of Titanium on Mechanical Properties of Commercial Alloys 53
Creep properties after aging 55
Tensile properties after aging 59
Properties at 650°C 59
Properties at room temperature 65
Influence of Titanium in Pure Nickel 65
Tensile properties 66
Effect of test temperature and composition 66
Effect of annealing time 68
Creep properties 70
Comparison of creep and tensile behavior 70
Effect of titanium content on elongation 70
Effect of deformation rate on elongation 73
Chemical analysis of tested alloys 73
Microscopy, Fractography, and Phase Analysis 75
Phases identified in aged alloys 75
Chemical analysis of phases 79
Optical metallography 81
Metallography of laboratory heats 81
Metallography of aged commercial heats 87
Transmission electron microscopy 91
Laboratory heats 91
Aged commercial heats 93

CHAPTER PAGE

Precipitate characterization from extraction replicas . 103

Fracture characterization 105

Optical examinations 105

Scanning microscopy 114

V. DISCUSSION OF RESULTS 121

Effect of Titanium and Carbon on Creep Properties 122

Discussions of Phase Stability on Aging 126

Influence of Titanium in Pure Nickel 130

Discussion of Microscopy 133

Relation of structures to properties 133

Stacking fault precipitation 135

Discussion of Models 140

Nucleation of precipitates on stacking faults 140

Model of creep cracking 147

VI. SUMMARY AND CONCLUSIONS 153

BIBLIOGRAPHY 159

APPENDIX 169

LIST OF TABLES

TABLE		PAGE
I.	Chemical Analyses of Laboratory Heats with Varying Carbon and Titanium Content	28
II.	Chemical Analyses of Nickel-Titanium Binary Alloys	29
III.	Chemical Analyses of Commercial Heats of Titanium Modified Hastelloy-N	30
IV.	Heat Treatments Given to Laboratory Heats	41
V.	Creep Properties of the 1.2% Ti Heat of Hastelloy-N for a One Hour at 1260°C Solution Anneal	58
VI.	Gas Analyses of Nickel and Nickel-Titanium Binary Alloys Tested in Argon at 600°C	76
VII.	Phases Identified in Various Aged Ni-12% Mo-7% Cr-Ti Alloys by Debye Scherrer X-Ray Analysis	77
VIII.	Heat Treatment Designations	169
IX.	Creep-Rupture Data at 650°C for Laboratory Heats of Hastelloy-N Varying Titanium and Carbon Concentration	170
X.	Creep Rupture Data for Nickel and Nickel-Titanium Alloys Tested in Argon at 600°C	175
XI.	Creep-Rupture Properties at 40000 psi and 650°C for Commercial Heats of Hastelloy-N Used to Evaluate the Thermal Stability	176
XII.	Tensile Data at 650°C for Commercial Heat 466535 for Various Heat Treatments	178

TABLE PAGE

XIII. Tensile Data at 650°C for Commercial Heat 466541 for Various Heat Treatments 179

XIV. Tensile Data at 650°C for Commercial Heat 466548 for Various Heat Treatments 180

XV. Tensile Data at 650°C for Commercial Heat 467548 for Various Heat Treatments 181

XVI. Tensile Data from Auxiliary Experiments on Heat 467548 to Define Conditions of Formation of the Stacking Fault Precipitate Morphology 182

XVII. Lattice Parameters of Carbide Phases from Aged Hastelloy-N Alloys Determined by X-ray Diffraction 183

XVIII. Tensile Data for Nickel and Nickel-Titanium Alloys Tested in Argon at 600°C and 0.002 Minute^{-1} Strain Rate 184

LIST OF FIGURES

FIGURE		PAGE
1.	Approximate Carbide Stability Range in Molybdenum-TZC Alloy (After Chang and Perlmutter[58])	26
2.	Mechanical Property Test Specimen	32
3.	Typical Strain-Time Curves for 40,000 psi Creep Tests in Air at 650°C	34
4.	Creep-Rupture Life at 650°C for Alloys Solution Annealed One Hour at 1177°C (Ni-12% Mo-7% Cr-0.5% Ti)	42
5.	Effect of Carbon on the Creep-Rupture Life of Ni-12% Mo-7% Cr-0.5% Ti Alloys at 650°C for Samples Solution Annealed One Hour at 1177°C	44
6.	Effect of 0.5% Ti on the Creep-Rupture Life of Ni-12% Mo-7% Cr-0.05% C Alloy at 650°C	45
7.	Change in the Secondary Creep Rate with Carbon and Titanium Content for the Ni-12% Mo-7% Cr-0.5% Ti Alloy at 40,000 psi and 650°C	47
8.	Variation in Creep Elongation with Carbon Content for 40,000 psi Creep Test at 650°C (Ni-12% Mo-7% Cr-0.5% Ti) .	49
9.	Fracture Strain Correlation with Secondary Creep Rate at 650°C for Specimens Annealed One Hour at 1177°C	51
10.	Fracture Strain Correlation with Secondary Creep Rate for Specimens Solution Annealed at 1177°C and Aged 100 Hours at 870°C (Ni-12% Mo-7% Cr-0.5% Ti)	52

FIGURE PAGE

11. Variation in Creep Elongation with Rupture Life at 650°C for Various Ni-12% Mo-7% Cr-0.5% Ti Alloys Annealed One Hour at 1177°C 54

12. Influence of Titanium Content and Aging Temperature on the 650°C Creep Properties at 40,000 psi for a Ni-12% Mo-7% Cr-0.07% C Alloy Annealed One Hour at 1177°C 56

13. Influence of Titanium Content and Aging Temperature on the 650°C Tensile Properties of Ni-12% Mo-7% Cr-0.07% C Alloys Annealed One Hour at 1177°C 60

14. Comparison of the Effects of Titanium Content and Aging Time on Three Measures of the Tensile Ductility (Hastelloy-N Solution Annealed One Hour at 1177°C) 61

15. Changes in the 650°C Tensile Properties with Aging Time for the 1.2% Ti Heat of Hastelloy-N Solution Annealed One Hour at 1260°C 63

16. Temperature Dependence of the Tensile Strength and Ductility of Nickel as a Function of Titanium Content . . 67

17. Effect of Annealing at 650°C on the Tensile Ductility for Nickel-270 and Ni-0.06% Ti Alloy at 600°C and 0.002 Minute^{-1} Strain Rate 69

18. Influence of Titanium Content on the Creep-Rupture Life of Nickel at 600°C 71

19. Effect of Titanium Concentration on the Elongation in Creep and Tensile at 600°C of Binary Nickel Alloys 72

FIGURE PAGE

20. Strain Rate Sensitivity of the Ductility of Nickel-Titanium Alloys at 600°C 74

21. Spectroscopic Analysis of Metallic Content of MC-type Carbides Extracted from Titanium Modified Ni-12% Mo-7% Cr-0.07% C Alloys 80

22. Effect of Carbon on the Microstructure of Ni-12% Mo-7% Cr-0.5% Ti Alloys Solution Annealed One Hour at 1260°C and Water Quenched 82

23. Effect of Carbon on the Microstructure of Ni-12% Mo-7% Cr-0.5% Ti Alloys Solution Annealed One Hour at 1177°C and Aged 100 Hours at 870°C 83

24. Effect of High Carbon Concentrations on the Microstructure of Ni-12% Mo-7% Cr-0.5% Ti Alloys Solution Annealed One Hour at 1260°C and Water Quenched. (a) Alloy 238-0.1% C, (b) Alloy 239-0.15% C, (c) Alloy 242-0.32% C 84

25. Changes in Microstructure Produced by Varying the Solution Annealing Temperature from 1040° to 1260°C for a Ni-12% Mo-7% Cr-0.5% Ti-0.05% C Alloy 86

26. Effect of Solution Annealing and Titanium Content on the Microstructure of Commercial Ni-12% Mo-7% Cr-0.07% C Alloys 88

27. Microstructure of Commercial Heats of Ni-12% Mo-7% Cr-0.07% C Alloy After Aging 3000 Hours at 760°C (100x) 89

FIGURE PAGE

28. Comparison of Structures of Aged Ni-12% Mo-7% Cr-0.07% C Alloys Using Interference Contrast Microscopy 90

29. Grain Boundary Carbides in Laboratory Heats of Ni-12% Mo-7% Cr-0.05% C Alloys After Aging 1500 Hours at 760°C. (a) Alloy 198, No Titanium, (b) Alloy 196, 0.5% Titanium 92

30. Carbide Distribution as a Function of Titanium Content in Ni-12% Mo-7% Cr-0.07% C Alloy After Aging 3000 Hours at 650°C (Solution Annealed One Hour at 1177°C) 94

31. Carbide Distribution as a Function of Titanium Content in Ni-12% Mo-7% Cr-0.07% C Alloy After Aging 3000 Hours at 760°C (Solution Annealed One Hour at 1177°C) 95

32. Precipitation of MC Carbides on Stacking Faults in a Ni-12% Mo-7% Cr-1.2% Ti-0.08% C Alloy (Annealed at 1260°C and Aged (a) 3000 Hours at 650°C and (b) 3000 Hours at 760°C) 98

33. Precipitates on Stacking Faults in the 1.2% Ti Heat of Hastelloy-N Solution Annealed One Hour at 1260°C and Aged 200 Hours at 760°C 99

34. Precipitates on Stacking Faults in the 1.2% Ti Heat of Hastelloy-N Solution Annealed One Hour at 1260°C and Aged 10,000 Hours at 760°C 100

35. Grain Boundary Structures After a 1260°C Solution Anneal and 3000 Hour Age at 760°C in a Sample of Hastelloy-N Exhibiting Stacking Fault Precipitates 102

FIGURE PAGE

36. Precipitates on Extraction Replicas Obtained from Samples of Hastelloy-N Solution Annealed at 1177°C and Aged 3000 Hours at 760°C 104

37. Effect of Titanium and Carbon on Creep Fractures at 40,000 psi and 650°C (Solution Annealed One Hour at 1177°C and Aged 100 Hours at 870°C with the Nominal Composition Ni-12% Mo-7% Cr-0.5% Ti-0.05% C, Except Where Noted) . . . 106

38. Tensile Fractures in 0.45% Ti Heat of Hastelloy-N Tested at 650°C and 0.002 Minute^{-1} Strain Rate After Aging 3000 Hours at Either 650°C or 760°C 108

39. Comparison of Tensile Fractures of Aged Hastelloy-N Alloys (35X). (a) 1.2% Ti Heat, Annealed at 1260°C and Aged 10,000 Hours at 760°C, 12% Elongation, 9.5% Reduction of Area (RA). (b) 0.15% Ti Heat, Annealed at 1177°C and Aged 10,000 Hours at 760°C, 17% Elongation, 13% RA. (c) 1.2% Ti Heat, Annealed at 1177°C and Aged 10,000 Hours at 760°C, 44% Elongation, 36% RA. (d) 0.45% Ti Heat, Annealed at 1177°C and Aged 10,000 Hours at 650°C, 43% Elongation, 31% RA 109

40. Mixed Transgranular and Intergranular Tensile Fracture of 1.2% Ti Heat of Hastelloy-N Heat-Treated to Produce Stacking Fault Precipitates Then Tensile Tested at 650°C. (a) 100X of Fracture. (b) 500X of Fracture 111

FIGURE PAGE

41. Creep Fractures of Commercially Pure Nickel and Ni-0.06% Ti Alloy for Tests in Argon at 600°C and 12,000 psi. (a) Nickel-270. (b) Ni-0.06% Ti. (c) Nickel-270, Near Fracture. (d) Ni-0.06% Ti, Near Fracture 113

42. Electron Scanning Fractographs of Intergranular Fracture in 1.2% Ti Heat of Hastelloy-N Showing Sheets of Precipitate on Grain Boundaries (Solution Annealed at 1260°C and Aged 1500 Hours at 760°C, Magnification Increases Progressive from (a) to (d)) 115

43. Room Temperature Fracture of Sample with Stacking Fault Precipitate Morphology. (a) Fracture at 20X. (b) Region of Intergranular Fracture 500X. (c) Isolated Region of Transgranular Failure on Grain Boundary 2000X. (d) Intergranular Dimples 5000X 117

44. Scanning Fractographs of 1.2% Ti Heat of Hastelloy-N Solution Annealed at 1260°C and Aged 1500 Hours at 760°C to Develop the Stacking Fault Precipitate Then Tested in Tension at Room Temperature. (Magnification Increases Progressively from (a) to (d)) 118

CHAPTER I

INTRODUCTION

Nickel-base alloys have two characteristics that are particularly detrimental in reactor applications at elevated temperatures. The first characteristic is a loss of both strength and ductility as the deformation temperature is increased. The temperature at which we observe the most significant decrease in ductility, the magnitude of the decrease, and the tendency to recover ductility at higher temperatures depend on several factors that have not been clearly separated. Important factors include (1) composition, (2) rate of deformation, (3) grain-boundary mobility, and (4) other metallurgical factors such as grain size and prior thermal history. The second important characteristic of nickel-base alloys is that under thermal neutron irradiation creep strength and ductility are further reduced. The postirradiation creep ductility of some alloys is often less than 1%. The irradiation damage has generally been attributed to gaseous helium produced by the transmutation of residual boron that results from thermal neutron capture. The neutron damage is manifest over the same temperature range as the ductility decrease in the unirradiated nickel alloys and thus compounds the problem.

As part of the Molten-Salt Reactor Program at the Oak Ridge National Laboratory a nickel-base alloy, Hastelloy-N, containing 16% Mo-7% Cr-4% Fe-0.06% C was developed which resists fluoride corrosion and has moderate resistance to air oxidation. The alloy is greatly

embrittled by thermal neutron irradiation. As a consequence further alloy development was initiated in which it was established that minor additions of certain alloying elements could beneficially influence the postirradiation mechanical properties of the alloy. The optimum concentrations of these small additions, the effects on the unirradiated properties, and the specific role of each alloying addition were not determined. A part of this alloy development program is represented by the present research which defines the role of titanium in the high-temperature deformation and fracture behavior of nickel and the nickel-base alloy, Hastelloy-N. More specifically, this dissertation compares the influence of titanium on the fracture process in pure nickel and in a modified Ni-12% Mo-7% Cr-0.06% C alloy. Emphasis is placed on the interaction of precipitate species and morphology on the high temperature mechanical behavior.

CHAPTER II

REVIEW OF LITERATURE

The influence of alloying on high temperature deformation involves too many aspects of physical metallurgy to permit extensive discussion in a literature review. As a consequence, this review will be restricted to a brief discussion of the following topics: (1) high temperature fracture processes, (2) effects of test and material variables on the ductility in creep and tensile deformation and (3) effects of titanium on phase stability and mechanical properties in selected alloys. Our limited understanding of the cause and control of intergranular fracture processes will be evident in each of these topics.

I. HIGH TEMPERATURE FRACTURE PROCESSES

A. Mechanisms

High-temperature fractures can be classified as a transgranular tearing, intergranular cracking, or a combination of the two. Transgranular fracture occurs below the so-called "equicohesive temperature" and generally is associated with appreciable ductility. Of considerably more interest are the two types of intergranular failure that can occur: (1) wedge type (w-type) fracture initiated at triple-point grain boundaries, and (2) intergranular cavitation (r-type cracks).

Zener[1] proposed that triple point fractures were initiated by concentration of the applied stress due to grain boundary sliding. The

stress, σ, in the vicinity of the triple junction is given by Stroh[2] as

$$\sigma = \left(\frac{L}{2\rho}\right)^{1/2} \tau \quad . \tag{1}$$

The distance between triple point junctions, L, is much larger than the radius of curvature of the grain boundary at the triple point, ρ, and τ is the shear stress acting across the grain boundary due to an applied stress. Other models also have been proposed, but all require grain-boundary sliding and a stress concentration at some grain-boundary inclusion or jog.

McLean[3] applied Stroh's ideas[2] of crack initiation at a dislocation pile-up to the case of wedge crack initiation at a grain boundary. The minimum stress, σ_m, needed to initiate a wedge crack on a grain boundary is given by McLean[3] as

$$\sigma_m = \left(\frac{12\gamma G}{\pi L}\right)^{1/2} \quad , \tag{2}$$

where γ is the effective surface energy of the crack surface, G is the shear modulus, and L is the length of the sliding interface. Equation (2) can be used to explain the effect of grain size, precipitate distribution, and other microstructural features on intergranular fracture. This stress, equation (2), also defines the demarcation between failures due to wedge cracking and those due to cavitation. Recent analyses of crack nucleation at dislocation pile-ups by Smith and Barnby[4] indicate that Stroh's analysis, equation (2), predicts too high a critical stress when applied to initiation of grain boundary wedge cracks. They assert that

equation (2) probably represents the stress needed to cause a crack to grow to observable size, but that actual crack nucleation based on their analysis would occur at a stress which is a factor of two lower than that given by equation (2).

Chen and Machlin[5] proposed another mechanism for void formation in high temperature creep due to grain boundary shear. They suggested that voids were nucleated at pre-existing jogs or grain corners and then grew by either vacancy condensation or plastic yielding. They indicated that the linking together of isolated voids led to formation of macroscopic intercrystalline cracks. Although a stress concentration due to grain boundary sliding appears to be necessary to initiate triple-point wedge type cracks, it is not clear which metallurgical factors determine the onset of sliding or the critical amount of sliding needed to start and propagate a crack. In the very high-purity metals neither wedge- nor cavity-type voids form. This is attributed to the dissipation of stress concentrations by plastic-flow and grain-boundary migration.[6]

The factors that determine the growth of wedge-type cracks are not clear, but continued grain-boundary sliding would undoubtedly increase the crack length. Weaver[7] has shown that the rate of growth of interparticle cracks depends on their instantaneous length. This in turn controls the stress concentration at the tip of each crack. The growth of w-type cracks by vacancy condensation or other thermally aided crack-propagation mechanisms has been proposed but not experimentally confirmed.[6] Generally, a change in fracture behavior occurs as the temperature is increased and the stress is decreased. The change is from w- to r-type cracks with both types observed at intermediate stresses and temperatures.

The formation of cavities (r-type voids) along grain boundaries is usually attributed to nucleation of voids at locations of high-stress concentration, such as grain-boundary jogs or particles. Grain-boundary sliding is again required for this mechanism. Balluffi and Seigle[8] have suggested that the rate of growth of these cavities is governed by the rate of vacancy migration through the lattice and along grain boundaries. Cavitation is found at stresses below that needed to initiate wedge-type cracks and can occur whenever the stress exceeds a critical value, σ_c, given by[8]

$$\sigma_c = \frac{2\gamma}{r \cos^2 \theta} , \qquad (3)$$

where γ is the surface energy, r is the radius of the void (crack), and θ is the angle between the applied stress axis and the given grain boundary.

Recently Stiegler et al.[9] pointed out that the mechanisms of cavity growth during creep (i.e., either due to mechanical processes or vacancy adsorption) remain controversial because of difficulties in observing the cavities in either transmission or optical microscopy. By using a replica fractographic technique these authors observed three-dimensional creep cavities in tungsten as a function of various creep test variables. In contrast to other accepted theories (Chang-Grant[10] and Zener[1]), Stiegler et al. concluded that the formation of r- and w-type creep cavities do not arise from different causes, but result from different limiting conditions of a common process. The cavities can grow by slip, grain boundary sliding, and stress-induced vacancy diffusion, but the relative contributions of each process depends on the temperature and stress of testing.[9] These authors point to a need to

study competing mechanisms that could be operative at intermediate temperatures where low ductilities are common.

Since grain-boundary sliding during creep is necessary for the initiation of intergranular fracture, one might conclude that below a certain temperature w-type cracks and r-type voids should not form. This conclusion follows from the observation that the extent of viscous grain-boundary sliding becomes very small, below some limiting temperature.[6]

B. Effect of Composition and Microstructure

Garofalo[6] lists four factors that can be classified as compositional or microstructural effects on intergranular fracture. First, fractures are often nucleated at inclusions such as precipitate particles within the grain boundary. Next, impurity segregation decreases the grain-boundary mobility which favors fracture and a decrease in ductility. A third factor is the formation of brittle films at grain boundaries which can lead to severe embrittlement. The fourth thing is a denudation of solute from a narrow zone near a grain boundary due to precipitation which can affect the grain-boundary sliding characteristics.

Alloying additions, heat treatments, neutron irradiation, and other metallurgical treatment affect microstructure and thus influence the fracture behavior of most materials. Since the microstructure is important in influencing the deformation behavior, a brief consideration will be given to some specific effects of grain-boundary precipitates in nickel- and iron-base alloys.

Precipitate particles within the grain boundary can inhibit the formation of grain boundary wedge cracks by decreasing the stress

generated at a triple point junction. Increasing the number of precipitate particles is equivalent to reducing L in equation (2): that is, the length of the sliding interface is reduced from the grain diameter to the average interparticle spacing and the stress needed to cause fracture is increased.

Garofalo[6] points out that the initiation of cracks or voids at grain boundaries containing second phase particles or inclusions does not necessarily lead to embrittlement in all cases. This is true especially when cracking is restricted to the interparticle spacing, in which case precipitates actually can be beneficial. Three conditions are given that cause them to have a favorable influence: (1) high cohesion between the particle and matrix, (2) interparticle spacing of 1 or 2 microns that allows grain-boundary migration, and (3) particles of high shear strength that are rounded in shape.

The effect of grain boundary carbides on the creep fracture behavior of nickel-based Nimonic alloys has been investigated by Weaver,[7,11] Betteridge and Franklin[12] and Heslop.[13] Betteridge and Franklin suggested that a solute depletion near the grain boundary due to precipitation prior to creep testing allowed for grain boundary relaxation and thus provided stress relieving under grain boundary shear. Weaver[11] observed a large number of grain boundary cracks (cavities) in the most ductile alloys and concluded that Gifkins' model[14] of crack nucleation around carbide particles rather than Zener's model[1] was operative, but that the good ductility resulted from limiting the crack growth to the interparticle spacing along the boundary. Thus, the cohesion of the carbide-matrix interface was the most important factor in promoting high fracture

ductility. Weaver suggested, however, that grain boundary sliding continued and that high ductilities and long rupture lives were obtained. Heslop[13] pointed out that a critical amount of strain was needed for cavity nucleation and also that the width of the solute depleted zone near a grain boundary was an important factor in the argument for a stress relieving influence of this zone. Weaver explained his results on the basis of Stroh's equation, equation (2), in which L is the precipitate particle spacing rather than the grain size, as generally used. At 750°C and 38,100 psi, he found that grain-boundary fracture occurred by wedge-crack formation when no precipitates were present and by intergranular cavitation in specimens heat treated to produce carbide precipitates. The transition in this case from wedge cracks to failure by cavitation was accompanied by an increase in stress-rupture life and ductility.

Harris[15] has shown that in magnesium intergranular cavities are nucleated at second-phase particles, but only at stresses below that necessary to form wedge-type cracks. Thus, the cavities are thought to result from the stress-concentration when the sliding grain boundary is held up by the isolated precipitate particle.

II. EFFECT OF SELECTED METALLURGICAL VARIABLES ON DUCTILITY

The problems of high-temperature embrittlement have focused attention on the cause and control of intergranular fracture. The American Society for Metals ductility seminar of 1967 is an excellent source of recent reviews of factors affecting fracture and ductility.

According to Dieter,[16] in the conference proceedings, the effects of grain size and solid solution additions on ductility are not well-documented. However, a large amount of work has been done on related aspects as listed below. Before discussing factors affecting ductility brief consideration is given to the selection of a measure of ductility, a problem that will become apparent in the following discussion.

A. Measures of Ductility

At low temperatures where fracture is normally preceded by necking, the uniform elongation is one of the best measures of ductility since the state of stress during uniform straining is uniaxial and well defined. Necking, however, is a local deformation that introduces a triaxial stress state within the material; thus, the total elongation at fracture represents straining that occurs under a varying state of stress, which is difficult to define.

Dieter[16] and Stiegler and Weir[17] have discussed the deformation at elevated temperatures in which the classical plastic instability (i.e., local necking) often is not observed in a tensile test because the rate of work hardening of the material is very low and the strain concentration is often not significant. In studies of high temperature deformation where the strain distribution along the gage length of a test specimen is fairly homogeneous the reduction of area and total elongation are more descriptive of the actual amount of deformation that precedes fracture.

Since the literature review and the subsequent experimental results are concerned with both intergranular creep-failures and ductile

transgranular tensile failures the most descriptive ductility parameter may differ depending on the strain distribution along the gage length of the sample. In the following discussions the total engineering elongation is consistently used as the measure of ductility. In some cases, additional measures of the ductility are compared with the total elongation in order to indicate the strain distribution.

B. Effect of Second Phases on Ductility

Edelson and Baldwin[18] found that the room temperature ductility of copper alloys containing various types and amounts of second phase particles (introduced by powder metallurgy techniques) decreased with increasing volume fraction of the second phase and did not depend on the mean free separation, shape, or type of the second phase particles. They suggest that the ductility was controlled by the concentration of strain locally in the matrix around the particles rather than homogeneous straining. It is interesting to note from this work that the yield strength of two alloys in the series studied did exhibit a correlation with interparticle spacing, precipitate size, and volume fraction while the ductility was a funtion of only the volume fraction of second phase precipitate in the alloy.

The importance of second phase particles on ductility at elevated temperatures was shown by Brindley.[19] In studies of the ductile fracture behavior of an Fe-21% Cr-0.05% C alloy Brindley found a drop in tensile ductility at intermediate temperatures (between 200 and 500°C) which he attributed to carbide precipitation. An inhomegeneous strain distribution due to the interruption of the slip process by void growth was given

as the reason for the ductility loss. The initiation of voids occurred at small 0.1 to 0.3 micron carbides precipitated during deformation.

Recent studies of throia-dispersed nickel indicate another aspect of the influence of second phases on mechanical behavior. Webster[20] has attributed differences in the recrystallization behavior of some TN-nickel samples to the influence of voids at the thoria-matrix interface. The voids were formed during fabrication or in other prior treatments and Webster argued that, under mechanical test conditions, the grain boundary mobility was decreased due to the presence of the voids associated with the dispersoid. Since the boundary mobility was reduced the stress concentrations were not relieved and grain boundary failure was enhanced.

C. Effect of Temperature on Ductility

The effect of temperature on ductility in nickel and other alloys has been studied by Rhines and Wray,[21] Reed-Hill, Smeal, and Rhines,[22] Shapiro and Dieter,[23] Smith,[24] Sessions,[25] Bloom,[26] Werner,[27] and Brindley,[19] to name a few. Most metals and alloys exhibit a decrease in ductility at intermediate temperatures, often in the hot-working region, and for nickel alloys the minimum is just below the recrystallization temperature. The cause has been attributed to various factors including strain aging, hot shortness, and grain-boundary shearing with associated intergranular failure. Although the cause of the drop in ductility is not clear, most investigators agree that the recovery at higher temperatures is a result of a reduction of stress concentrations by either recrystallization or grain-boundary migration. As pointed out by Stiegler *et al.*,[9] dynamic recrystallization requires prior deformation

and thus at intermediate temperatures, fractures may initiate prior to the introduction of enough strain into the matrix to cause recrystallization.

D. Effect of Strain Rate on Ductility

Deformation rates from slow creep test conditions (10^{-8} sec^{-1}) to high speed explosive forming (10^{6} sec^{-1}) have been divided into three ranges of strain rate:[16] a low region up to 10^{-2} sec^{-1}, an intermediate region to 10^{2} sec^{-1}, and the high strain rate region above 10^{2} sec^{-1}.

Orava[28] reported that the room temperature uniform elongation for face centered cubic and hexagonal-close-packed structures increases with increasing strain rate in the low strain rate region but that body-centered cubic metals show a corresponding decrease in ductility. In the intermediate strain rate region (10^{-2} to 10^{2} sec^{-1}) many metals show an increase in elongation and reduction of area at fracture but there is no clear-cut trend and no reliable theoretical basis for the prediction of this behavior.[16] In the high strain rate region, represented by impact loading, the fracture strain drops off significantly with increasing strain rates for impact velocities above some critical velocity.

E. Microstructural Effects on Ductility

Rogers[29] states that the presence of particles and holes in metals before straining does not necessarily mean that fracture will result from void linkup since the failure mode can be changed from ductile rupture to void-initiated, shear fractures by simply lowering the temperature. Thus, the influence of particles is affected by test temperature.

Rogers considers the evidence for void formation either by dislocation interactions, by second phase particles, and by pre-existing holes: he concludes that in the absence of definitive evidence to the contrary, void formation (i.e., grain boundary crack formation) likely occurs by the growth of an internal pre-existing hole or at second phase particles. Since void formation at second phase particles as small as 50Å have been reported in Cu-Si,[30] Rogers feels there is no shortage of void initiation sites even in very high purity metals.

F. Effect of Stacking Fault Energy on Ductility

Rogers[29] has proposed that the most important influence on ductility is associated with the tendency of a microstructure to either concentrate or distribute strain. Strain (and stress) is concentrated if dislocations pile up at obstacles: the concentration is avoided and the strain distributed if dislocations can climb or cross-slip to by-pass obstacles such as precipitates. Important variables governing the dislocation behavior include stacking fault energy, temperature, strain rate, and strain hardening; however, other than the deformation temperature the stacking fault energy is the most important since it determines the magnitude of the separation of a dislocation into partial dislocations.[29] Thus, if the stacking fault energy is low, the partials will be widely separated and cross-slip will be limited by the difficulty of contraction of the partials. In alloy systems where the deformation relates to the ease of cross-slip, then a higher stacking fault energy should tend to produce greater strain at fracture.

Nickel has a stacking fault energy which is intermediate with respect to other pure metals. The value for nickel is lower than that for iron and aluminum, but is higher than that for gold, silver, and zinc. The influence of alloying on the stacking fault energy has been reviewed by Christian and Swann.[31]

G. Ductility in Creep

Creep ductility is controlled by competition between creep deformation and crack initiation and growth. Creep deformation represents a balance between work hardening and recovery processes. Garofalo[30] acknowledges that although ductility can be defined in terms of creep strain preceding fracture, it is not a true material property because it depends on stress, temperature, and the wide assortment of metallurgical factors previously discussed. The difficulty in evaluating ductility in creep lies in the fact that uniform creep strain is difficult to determine in conventional tests and that the total strain to fracture (i.e., total elongation) actually represents three contributions to the apparent strain: (1) true matrix deformation, (2) elongation from grain boundary separation (voiding), and (3) strain due to grain boundary sliding or grain rotation. Garofalo has attacked this problem by proposing that the relation between elongation in the absence of voids ε_r', and the fracture elongation ε_r is given by[32]

$$\varepsilon_r' = \frac{\rho_o}{\rho}(1 + \varepsilon_r) - 1 \quad , \tag{4}$$

where ρ_o is the density of the material and ρ is the apparent density

after deformation, reduced below ρ_o by void formation. Corrections for the contribution of grain boundary sliding to the total creep elongation are difficult to assess and are quite temperature dependent.

Grant and Bucklin[33] point out that the total creep elongation is a difficult parameter to correlate because the third stage elongation during creep is primarily a reflection of intergranular cracking (i.e., grain boundary separation) which is a highly variable event and, thus, difficult to reproduce. They proposed that a better measure of creep ductility was the "true creep elongation," defined by the sum of the strain accumulated during stage I and stage II of the creep test.

H. Relating Creep and Rupture Processes

With most materials the rupture life at elevated temperatures is a function of the creep rate and the inherent ductility of the material. Previous attempts to understand the relation between creep deformation and ductility have been unsuccessful.[32] However, empirical correlation seems to indicate a relationship between these two parameters.

Under certain limiting conditions of stress and temperature, a variety of metals obey the relation

$$t_r \dot{\varepsilon}_s = \text{constant} = K \qquad (5)$$

where t_r is the time to rupture at constant temperature and $\dot{\varepsilon}_s$ is the steady-state creep rate. Garofalo et al.[34] have shown that type-316 stainless steel follows this relation and that the constant, K, is proportional to both the strain during steady-state creep, ε_s, and

the strain, ε, that one calculates assuming that the steady-state creep rate, $\dot{\varepsilon}_s$, operates for the full rupture life (i.e., $\varepsilon = \dot{\varepsilon}_s t_r$). However, a relation between the steady-state creep rate and the strain at fracture has not been found.

A relationship between the rupture life, t_r, and the creep rate, $\dot{\varepsilon}_s$, which is independent of stress and temperature was found by Monkman and Grant[35] for a wide variety of materials.

$$t_r \, \dot{\varepsilon}_s^X = \text{constant} = C \quad . \tag{6}$$

In their studies, the constant C varied appreciably with composition and the exponent X varied only slightly for a large range of alloy compositions.[35] A large effort, primarily in Europe, has been attempted to define the value of the exponent in equation (6) for creep-rupture of high-purity material. It has recently been shown[36] that a Ni-0.1 atomic percent Pd alloy tested at 500°C under a constant stress obeys equation (6) with X = 1.

A theoretical treatment giving an equation of the form of equation (5), or equation (6) with X = 1, was made by Hoff[37] in 1952. Hoff derived equation (5) on the basis of a one-dimensional stress analysis of a constant load creep test. He assumed constant volume, ignored primary creep, and considered that steady-state creep was maintained until failure occurred by local necking. Agreement of the creep behavior of a nickel-palladium alloy with Hoff's theoretical equation[37] is probably coincidental since the density of the alloy continuously decreased due

to growth of internal cavities with increasing creep strain. This could negate the constancy of volume assumed by Hoff in the theoretical derivation. The theoretical and experimental stress conditions also differed.

Garofalo[32] makes the important point that although there are many empirical relations, it is not at all obvious that creep ductility (strain to fracture) should depend on the creep rate except that equation (5) implies that part of the deformation prior to rupture should depend on the steady-state creep rates.

Attempts to study factors affecting ductility in creep such as the growth of creep cavities as a function of strain (for example, reference 36) and other creep test variables may eventually lead to a better understanding of the fundamental relationship between creep deformation and fracture initiation. However, the question of the basic influence of creep parameters on ductility is, in general, not well-established.

I. Strain Rate Sensitivity and Work Hardening

The observation that the ductility of nickel alloys at intermediate temperatures is further reduced by irradiation, particularly in the same temperature range, has led to the current investigation of the influence of alloying additions on the ductility. It was presumed that if improvement could be obtained in the intermediate temperature ductility through alloying, then the ductility after irradiation would also be increased. Since the deformation behavior has been studied in relationship to the work hardening and strain rate sensitivity of those metal showing the behavior, pertinent information relative to these variables is reviewed in this section.

Two important relationships pertaining to stress, strain, and strain rate have been established empirically for a large number of materials.[38] The power law relating stress, σ, and true strain, ε, is

$$\sigma = A\varepsilon^n \tag{7}$$

where n is the strain hardening coefficient and A is a constant. With increasing test temperature n decreases and approaches zero at temperatures above approximately one-half the absolute melting temperature, T_m. A second equation relates stress, σ, to strain rate, $\dot{\varepsilon}$, in the form

$$\sigma = K\dot{\varepsilon}^m \quad , \tag{8}$$

where m is the strain rate sensitivity coefficient and K is a constant.

The Consideré construction for a material whose tensile stress-strain behavior follows equation (7) shows that at the onset of plastic instability (local necking) the true strain is equal to the strain hardening coefficient and thus n relates to uniform tensile elongation. After necking, however, the amount of further deformation relates more to the strain rate sensitivity of the plastic deformation as discussed by Hart.[39] The effect of these two material parameters, n and m, on the argument for a ductility minimum is as follows. For test temperatures below approximately 0.5 T_m, n and m both decrease and thus the plastic deformation (ductility) decreases with increasing temperature. However, above approximately 0.5 T_m the work hardening coefficient is virtually zero and m, and thus ductility, increases with increasing temperature.

Therefore, a minimum range of ductility in the vicinity of 0.5 T_m could be expected for systems where σ, ε, and $\dot{\varepsilon}$ are related to the two power laws of equations (7) and (8).

Plastic deformation in some ranges of temperatures responds to decreases in strain rate in a manner similar to the behavior expected for a temperature increase. Increasing temperature and decreasing strain rate both generally decrease ductility below the temperature of the ductility minimum. Therefore, correlations of ductility versus strain rate can also show a ductility minimum just as ductility versus temperature does. Glen[40] has discussed his observations on this correlation and argues that the minimum creep ductility as a function of strain rate for alloys undergoing precipitation reaction could reflect the critical time at temperature necessary for the formation of a precipitation distribution responsible for the reduced ductility.

III. EFFECT OF TITANIUM ON STRENGTH AND DUCTILITY IN VARIOUS ALLOY SYSTEMS

Small additions of titanium, zirconium, and aluminum to various metals can significantly affect both the strength and ductility of the alloy, particularly at elevated temperatures. Addition of these elements for purposes of deoxidation improve the mechanical properties: in recent years the additional benefit of having these elements in solid solution has been realized. Our limited understanding of the role of titanium additions for various systems is discussed below.

A. Titanium in Iron-Base Alloys

The early use of titanium additions in steels is discussed by Comstock and Urban.[41] A large effect of 1% Ti in solid solution on the 625°C rupture life of an 8% Cr-3% Mo steel was reported by Bardgett in 1956.[42] The formation of both TiC and Fe_2Ti strengthened this alloy, but a maximum rupture life was found when approximately 1% Ti remained in solid solution. The effect of titanium in type-321 stainless steel was investigated by White and Freeman.[43] They found that the 650°C creep rupture strength increased with a decrease in Ti:C ratio at a constant carbon level. The effects of titanium and niobium on the formation of the sigma phase and Ni_3Ti in Cr-Ni stainless steels were studied by Nakagawa, Kawabe, and Otoguro.[44] They found that the 650°C rupture life reached a minimum value between 0 and 2%, for additions of both titanium and niobium, yet the tensile strength increased progressively with increased additions of either element for tests up to 800°C. The effects of solid solution hardening and of ferrite formation were indicated as the reason for the minimum rupture life as a function of alloying addition.

The potent effect of titanium for gettering oxygen, nitrogen, and carbon is illustrated by the research of Leslie and Sober,[45] who used 0.15% Ti in iron to effectively eliminate the contribution of these interstitials to low temperature yielding and flow characteristics of iron. They reported that this alloy exhibited ductility at all test temperatures which was higher by a factor of two to three than that found for zone refined iron. They concluded that the few hard, second-phase precipitates formed by reaction of the titanium with the

interstitials might be beneficial to the ductility and thus could have been a factor in producing ductilities greater than in zone refined iron.

Bloom and Weir[46] have studied the influence of small titanium additions on the pre- and post-irradiation tensile and creep rupture properties of type 304 and 304L stainless steels. They found the optimum post-irradiation creep and tensile ductilities to occur for a titanium level of 0.2%. The most striking influence of the small titanium addition in these steels was a pronounced change in the creep fracture mode in the unirradiated alloy from intergranular to transgranular when titanium was added. Apparently the basic influence of titanium in these steels is on the precipitate morphology or on the chemistry of the grain boundary regions, both of which could affect the fracture mode of the unirradiated alloy.

B. Titanium in Nickel-Base Alloys

Guard[47] and Garofalo[6] have discussed work on the potent effect of titanium on the creep behavior of nickel and the Ni-20% Cr alloy. Hazlett and Parker[48] in 1954 showed a rapid decrease in the initial creep rate of nickel-titanium binary alloys at 700°C with increasing titanium up to 4 atomic %. A correlation by Guard[47] between lattice parameters for various alloying additions and room temperature yield strength of Ni-20% Cr illustrates that the greatest strength increase for a given change in lattice parameter is produced by titanium and that aluminum, vanadium, molybdenum, and chromium give smaller amounts of strengthening.

Correlations of increases in the 900°C yield strength of Ni-20% Cr indicate that molybdenum and titanium are both potent strengtheners and that, on an atom fraction basis, aluminum, vanadium, and chromium produce less high temperature strengthening, in that order.

A fundamental study of solute hardening and the substructure development in nickel-titanium alloys was reported by Ancker and Parker.[49] They found that both the density of the substructure and the room temperature strength of nickel were increased with increasing titanium content. However, they concluded that even though impurity atmospheres undoubtedly form around dislocations in nickel-titanium alloys due to large misfit strains in the nickel lattice, these atmospheres are no more effective in hindering dislocation migration than are impurity atoms in "pure nickel." Nevertheless, strengthening was vaguely attributed to possible Cottrell hardening rather than effects of titanium on the development of substructures in the alloys.

The role of titanium in most nickel-base superalloys is that of precipitate hardening through the formation of the gamma prime type intermetallic compounds, Ni_3Ti and $Ni_3(Ti, Al)$.[50,51] Generally, titanium and aluminum are both added in concentrations of 2-4% to achieve this strengthening. Strengthening of superalloys is also possible through carbide precipitation and the influence of titanium[50] and molybdenum[52] on the phase relationships in these complex alloys has previously been discussed. Beattie and Ver Snyder[52] found that with increasing molybdenum content between zero and 11% in a Ni-20% Cr-10% Co-2% Ti-0.1% C

alloy there was a decrease in the amount of TiC and an increase in M_6C-type carbides after various heat treatments. They also observed that Ti(C,N) was generally stable at low aging temperatures but was unstable and often redissolved at higher aging temperatures.

Decker and Freeman[53] showed that the beneficial influence on creep behavior of trace additions of boron and zirconium to a titanium and aluminum hardened superalloy was related to the suppression of structural changes that affect crack formation in creep. Trace additions of either boron or zirconium retarded the agglomeration of $M_{23}C_6$-type carbides and Ni_3Ti at grain boundaries and longer times (thus higher strains) were obtained in creep before the precipitation and solute depletion near grain boundaries led to initiation of microcracking and failure.

As in the iron-base alloys, the addition of small amounts of titanium to some nickel-base alloys[54] can significantly improve the post-irradiation mechanical properties. The benefit of titanium increases progressively with increasing titanium contents in the range zero to 1.2% for a Ni-12% Mo-7% Cr-0.06% C alloy. The lack of information on the mechanism of the effect of titanium in this alloy system led to the present research and has become the subject of this dissertation.

C. Titanium in Refractory Metals

A large amount of research[55-59] has been done during the last ten years on development of a titanium-containing molybdenum alloy. The role of titanium in the Mo-0.5% Ti alloy involves Mo_2C and TiC precipitate phases. Chang has shown[58] that the property changes relate to the

titanium to carbon ratio and to the relative stability of the carbides. The approximate stability of the phases in this system as a function of temperature is given in Figure 1. Titanium carbide, TiC, is stable at low temperatures, whereas Mo_2C and ZrC coexist (if zirconium is present) at higher solutioning or aging temperatures. In most cases, aging involved the precipitation of TiC below approximately 1650°C accompanied by simultaneous dissolution of preexisting Mo_2C from prior alloy fabrication. Chang further pointed out that small zirconium additions stabilized the TiC precipitates to higher aging temperatures, presumably by changing the composition of the second phase to a (Ti,Zr)C compound.

Studies of the interaction of titanium with interstitial impurities in vanadium were recently completed. Keith[60] concluded from internal friction studies that some free oxygen and nitrogen remained in solution for titanium additions up to 1% and that strain aging due to interstitial precipitation was not eliminated until the titanium content of the vanadium exceeded approximately 1.5%. Thus, the evidence indicated titanium was being partitioned between compound formation and solid solution and that a titanium content approximately five times the stoichiometric amount (based on amount of interstitials) was required in this system for complete reaction. Thus, even in relatively simple systems the location and strengthening effects of alloying additions is complicated.

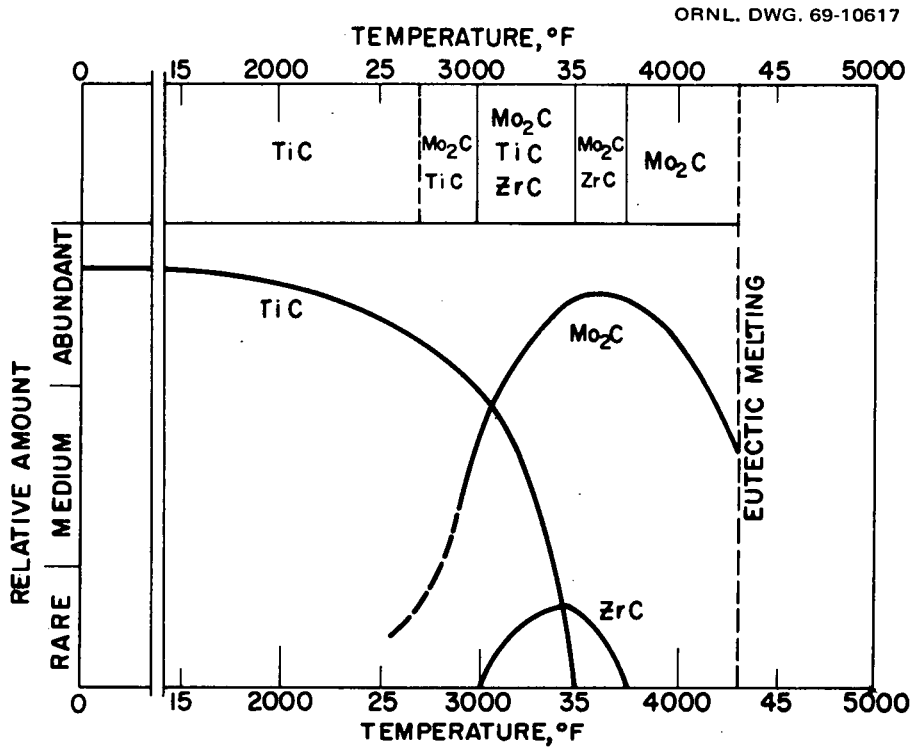

Figure 1. Approximate carbide stability range in molybdenum-TZC alloy (after Chang and Perlmutter[58]).

Chang, W. H., and I. Perlmutter, "Solutioning and Aging Reactions in Molybdenum-Base Alloys," High Temperature Materials Part II, Metallurgical Society of the AIME Conference, Vol. 18. New York: Interscience Publishers, 1963. Pp. 347-370.

CHAPTER III

EXPERIMENTAL PROCEDURE

I. FABRICATION OF MATERIAL

The material used in this study included both high-purity laboratory heats and 100-pound commercial heats. High-purity commercial nickel, International Nickel Company Nickel-270, electrolytic chromium, and high-purity molybdenum were used to make laboratory nickel-molybdenum-chromium-carbon alloy and binary nickel-titanium alloys. The chemical analyses of a series of alloys in which the carbon content was varied are given in Table I. The analyses of the binary alloys which were investigated are given in Table II. Samples from four commercial melts of Hastelloy-N were used to evaluate the thermal stability of the titanium-modified alloy and the compositions of these heats are given in Table III.

The laboratory melts were melted ten times on a water-cooled copper hearth of a "beehive" furnace containing an argon atmosphere. Each alloy was fabricated in the following sequence: (1) hot swaged at 1260°C from 1 to 0.75 inch diameter, (2) swaged at 870°C from 0.75 to 0.44 inch, (3) annealed 15 minutes at 870°C, and (4) cold swaged in increments from 0.44 to 0.28 inch with intermediate anneals, when needed, of 15 minutes at 870°C. The binary alloys were melted and cast in the same manner, but after initial breakdown at 1260°C the alloys were fabricated to 0.25 inch diameter rods by cold swaging from 0.75 inch with intermediate anneals at 870°C in air. Samples of the commercial heats

TABLE I

CHEMICAL ANALYSES OF LABORATORY HEATS WITH VARYING CARBON AND TITANIUM CONTENT

Element	Chemical Analyses (wt, %)								
	193[a]	194	195	196	197	198	238	239	242
Mo	13.5	13.3	13.7	11.5	11.3	12.4	12.5	12.0	12.0
Cr	7.0	7.3	7.6	6.7	6.6	7.3	7.2	7.2	7.2
Ti	0.48	0.47	0.54	0.51	0.47	<0.01	0.50	0.52	0.53
C	0.003	0.007	0.037	0.053	0.27	0.045	0.096	0.146	0.32
Fe	0.03	0.03	0.03	0.07	0.07	0.13	0.22	0.30	0.31
Si	0.01	0.02	0.01	0.01	0.01	0.01	0.02	0.02	0.02
Mn	<0.02	<0.02	<0.02	<0.02	<0.02	<0.02	0.08	0.13	0.12
W	--	--	--	--	--	--	0.09	0.09	0.03
Zr	--	--	--	--	--	--	0.001	0.0003	0.003
Hf	--	--	--	--	--	--	0.001	<0.001	<0.001
V	<0.02	<0.02	<0.02	<0.02	<0.02	<0.02	0.003	0.003	0.001
Co	<0.03	<0.03	<0.03	<0.03	<0.03	<0.03	0.1	0.05	0.1
Cb	<0.05	<0.05	<0.05	<0.05	<0.05	<0.05	0.002	0.005	0.0005
Al	<0.05	<0.05	<0.05	<0.05	<0.05	<0.05	<0.03	<0.03	<0.03
S	<0.002	0.003	<0.002	<0.002	<0.002	<0.002	0.004	0.005	0.004
B							0.0005	0.0005	0.002
O	0.0057	0.0035	0.0105	0.0058	0.003	0.0032	0.0031	0.0038	0.003
N	0.0052	0.0054	0.0014	0.0028	0.0016	0.0068	0.0009	0.0063	0.005
H	0.0007	0.0007	0.0004	0.0009	0.0008	0.0006	<0.0001	<0.0001	0.000
Ni	Balance	Balance	Balance	Balance	Balance	Balance	Balance	Balance	Balance

[a]Alloy heat number.

TABLE II

CHEMICAL ANALYSES OF NICKEL-TITANIUM BINARY ALLOYS

Element	Chemical Analyses (wt %)			
	253[a]	222	223	226
Mo	<0.02	<0.02	<0.02	<0.02
Cr	0.03	<0.05	<0.05	<0.05
Ti	<0.02	0.062	0.26	1.53
C	0.004	0.006	--	0.007
Fe	0.07	0.02	--	0.05
Si	<0.01	<0.01	0.01	<0.01
Mn	0.08	<0.01	<0.01	<0.001
W	0.01	0.03	0.03	0.01
Zr	<0.01	<0.01	<0.01	<0.01
V	<0.01	0.03	0.01	<0.01
Co	0.10	0.003	0.001	0.001
Cu	0.04	0.0005	0.0005	0.001
Nb	0.005	0.0002	0.0002	<0.0001
Al	0.001	<0.03	--	<0.03
S	0.003	<0.002	--	<0.002
P	0.001	0.001	--	<0.002
B	0.0006	0.00007	0.00007	<0.00002
O	0.0021	0.015	0.0049	0.021
N	0.0011	0.0004	0.0003	0.0006
H	0.0018	0.0006	0.0003	0.0008
Ni	Balance	Balance	Balance	Balance

[a]Alloy heat number.

TABLE III

CHEMICAL ANALYSES OF COMMERCIAL HEATS OF TITANIUM MODIFIED HASTELLOY-N

Element	Chemical Analyses (wt %)			
	466535[a]	466541	466548	467548
Mo	12.8	13.2	12.4	12.0
Cr	7.2	6.8	7.7	7.1
Ti	0.15	0.27	0.45	1.2
C	0.073	0.07	0.04	0.08
Fe	0.03	0.03	0.03	0.04
Si	0.07	0.05	0.05	0.03
Mn	0.12	0.10	0.14	0.12
Mg	0.034	0.01	0.023	--
W	0.007	0.07	0.007	0.004
Zr	0.0002	0.0007	<0.0001	0.002
V	<0.01	<0.01	<0.01	0.001
Co	0.02	0.04	0.03	0.15
Cu	0.002	0.005	0.0005	0.01
Nb	<0.0001	0.0001	0.0003	0.0005
Al	<0.03	<0.03	<0.03	0.05
S	0.003	<0.002	0.003	<0.002
P	--	--	--	0.0004
B	0.0002	0.0002	0.00007	0.0007
O	0.0012	0.0008	0.001	0.0003
N	0.007	0.0005	0.0009	0.0002
H	0.0002	0.0002	0.0002	0.0003
Ni	Balance	Balance	Balance	Balance

[a]Alloy Heat number.

were obtained from vendor-supplied 0.5 inch-thick plate, which was cut into strips and then hot swaged at 870°C to 0.25 inch-diameter rod.

II. MECHANICAL TESTING PROCEDURE

Creep and tensile tests of the various alloys were performed on samples machined from swaged 0.25-inch-diameter rods to the dimensions shown in Figure 2 and then heat treated at temperatures up to 1260°C in an argon atmosphere. Samples generally were cooled from the heat-treating temperature in a water-cooled extension outside the heated zone of the furnace. The cooling rate was quite rapid for this procedure: form 1260°C the specimens temperature decreased to approximately 760°C in one minute, to 540°C in two minutes, to 370°C in four minutes, and to below 150°C in 10 minutes. Tests of the nickel-molybdenum-chromium-titanium alloys were performed in air at 650°C. Because of poor oxidation resistance of the binary nickel-titanium alloys, they were tested in an argon environment at temperatures from 400 to 800°C. Heat-up times varied for different tests but were never longer than four hours.

A. Air Environment

The tensile tests were run in an Instron Universal Testing Machine at a nominal cross-head speed of 0.002 inch minute^{-1}, which is equivalent to approximately 12% strain per hour or 0.002 minute^{-1} strain rate for a one inch gage length specimen. Temperature was controlled at 650 ± 4°C with two chromel-alumel thermocouples and an L & N temperature controller, and the specimen was heated by a small two-zone resistance furnace. The

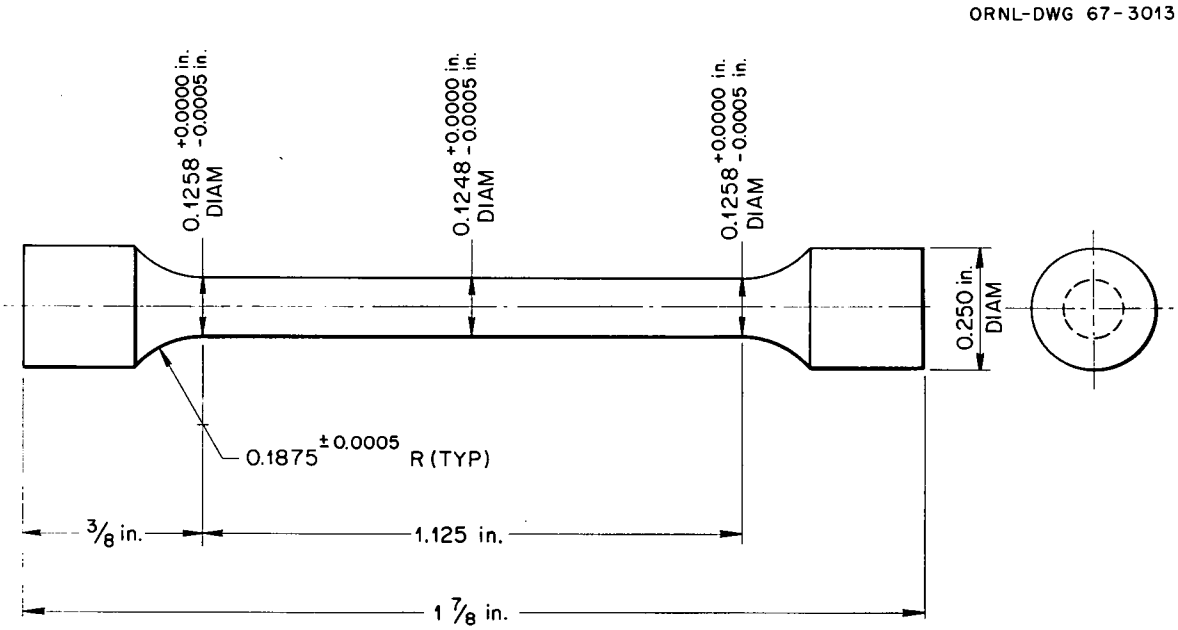

Figure 2. Mechanical property test specimen.

tensile properties were obtained from a curve of load versus cross-head movement plotted by the Instron from the load cell signal and gear-drive movement. Heat-up times in tensile testing required approximately one hour and the temperature was maintained constant at the desired level 15-30 minutes before starting the tests.

Lever arm creep rupture machines with multiple zone resistance furnaces were used in creep testing and the temperature was controlled at 650 ± 3°C during the test. Strain was measured by a dial indicator that measured the total movement of the specimen and part of the load train. Initial strain measurements were normally taken after the load was applied, thus the instantaneous extension was not reflected in the strain-time curves. Total elongation and reduction-in-area measurements were made after testing.

Strain-time curves were obtained by plotting the strain measurements from dial gage reading as a function of time under the load. The actual plotting of the creep curve was done using a computer program[61] which converted the dial gage readings to strain and then plotted strain as a function of the time at which the strain was measured. Typical creep curves obtained at 40,000 pounds per square inch (psi) and 650°C for several alloys are shown in Figure 3.

B. Argon Environment

In order to exclude the influence of test environment on the fracture ductility of the dilute nickel-titanium alloys, tensile and creep test were run in an argon atmosphere. The tensile test furnace

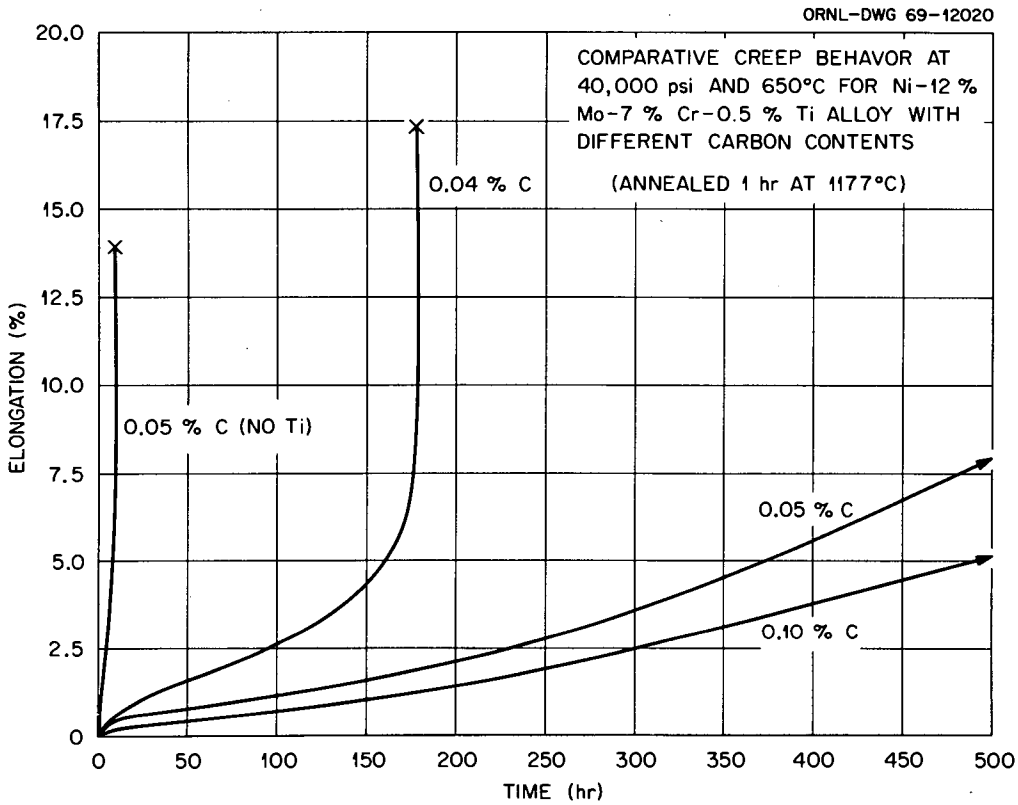

Figure 3. Typical strain-time curves for 40,000 psi creep tests in air at 650°C.

was a small stainless steel system with rubber, O-ring fittings. The system was evacuated by mechanical and oil diffusion pumps. Tests were conducted with a slow argon purge at temperatures up to 800°C. At 700° and 800°C, small but visible contamination was apparent for samples containing 0.5 to 1.5% Ti.

The environmental creep machines were evacuated and outgassed overnight to approximately 5×10^{-6} torr and then backfilled with argon prior to starting the creep test. Sacrificial zirconium foil was placed around the test specimen to reduce contamination and no appreciable changes in visual appearance were evident after tests. Creep tests were conducted at 600°C for times varying between 10 and 2000 hours. Strain measurements and temperature control for the argon tests were similar to those for the tests in air.

III. MICROSCOPY AND PHASE ANALYSIS

A. Optical Metallography

Standard metallographic examination was performed on aged and tested samples. Vibratory polishing was used for sample preparation. The Hastelloy specimens were etched by swabbing with an etchant containing 33% glycerine-50% HCl-17% HNO_3 and the nickel and nickel-titanium binary alloys were etched by immersion in a mixture containing equal parts of a 10% NaCN solution and 10% NH_4HSO_4 solution. A research metallograph and an interference contrast microscope were used for metallographic examination.

B. Transmission Microscopy

In addition to standard metallographic evaluation of microstructures developed during aging and mechanical testing, many samples were examined using transmission electron microscopy.

Normally, electron microscopy samples were obtained from the unstressed ends of tested tensile or creep specimen, but in several auxiliary experiments heat treatments were performed on small 0.25 inch diameter tabs. In either case, the 0.25 inch section was machined to 0.125-inch-diameter and circular discs 0.02 inch thick were cut for thinning. These discs were electrolytically dimpled and thinned in a solution of 33% HNO_3 + 67% methanol at temperatures between 0 and 10°C using the technique developed by DuBose and Stiegler.[62] The thin area adjacent to the hole which developed during electrolytic thinning was examined in a 200 kilovolt electron microscope. Selected area electron diffraction patterns were often used to identify precipitate types, and a general examination was conducted to characterize the precipitate distributions as a function of alloy composition and heat treatment.

C. Scanning Microscopy

Fractured samples were examined in both a JEOLCO and Cambridge scanning electron microscope to compare the fracture appearance as a function of heat treatment and test temperature. No replication of the sample was required and both high temperature and room temperature fractures were examined to 5000X. The operating principles and potential use of the scanning microscopy in fractography have been discussed

elsewhere.[63,64] However, the interpretation of elevated temperature fractures is somewhat uncertain based on our current understanding of these fracture processes.

D. Phase Extraction and Identification

1. Extractions for x-ray identification. Samples from the creep and tensile tests were chosen for extensive phase analysis. Electrolytic extractions were conducted on the unstressed portion of test specimens using a 10% HCl-methanol solution and a current density of approximately 4 milliamperes/square centimeter. The extraction was continued for 20-40 minutes with frequent interruption to remove the extracted precipitate by ultrasonic vibration. After three washing steps which involved ultrasonic agitation, centrifugation, and decantation of excess alcohol, the remaining alcohol solution was pipetted onto a heated glass slide. The precipitates on glass slides were then either analyzed using the goniometer x-ray technique or removed and placed in a capillary tube for determining a Debye-Scherrer powder pattern.

2. Extraction replicas. Extraction replicas were prepared from the unstressed portion of test samples using two techniques. One method involved heavily etching the specimen in 10% HCl-methanol at 3 to 4 volts for 10 to 30 seconds followed by careful washing and air drying. Replicating tape, softened with aceton, was firmly held against the etched surface and, after drying, was stripped from the sample. Precipitates were embedded in the plastic replica. The replica was cut into 1/8 inch

pieces and coated with a thin layer of carbon. The plastic was then dissolved in acetone leaving the precipitates clinging to the carbon film. After being washed in acetone and ethanol, the carbon extraction replicas were placed in water and picked up on electron microscope grids for examination by both optical and electron microscopy.

The second extraction replica technique used in this study was the direct carbon method. A thin layer of carbon was evaporated onto a lightly etched metallographic specimen. The carbon film was then scribed into 1/8 inch squares and removed from the specimen by electrolytic etching in 10% HCl-alcohol to dissolve the matrix. Etching was continued until the replica floated free with those precipitates originally at the specimen surface clinging to the carbon. After several washings in ethanol the replicas were straightened by placing them in water and then picked up on electron microscope grids for observation.

Precipitates extracted by either of these methods could then be observed optically or in the electron microscope. In addition, the extracted phases could be analyzed by electron diffraction to determine the crystal structure of the phases or with an electron microprobe attachment for the electron microscope to determine the chemical analysis of the precipitate.

CHAPTER IV

EXPERIMENTAL RESULTS

The influence of small titanium additions on the mechanical behavior of nickel and a nickel alloy (Hastelloy-N, Ni-12% Mo-7% Cr-0.06% C) was determined in both creep and tensile tests. The influence of titanium and carbon on the strengthening of the Hastelloy was investigated by (1) analysis of the phases developed on aging, (2) determination of the morphology and distribution of these phases, and (3) measurement of the resulting mechanical behavior in creep and tensile loading.

In order to isolate the effect of titanium, an evaluation of the influence of titanium in nickel was made by studying the deformation behavior of a series of dilute binary alloys as a function of temperature and strain rate. However, primary emphasis was placed on the influence of titanium in the nickel-molybdenum-chromium alloy since technologically the alloy is more important than the pure material.

In section I, results are presented which show the influence of titanium and carbon concentration on the creep properties of the nickel-molybdenum-chromium alloy at 650°C after various heat treatments. Section II covers the influence of titanium content on the creep properties at 650°C and tensile properties at 25 and 650°C for four aged commercial alloys. The third section, III, presents results on the influence of titanium in binary nickel-titanium alloys on their creep and tensile behavior in an argon environment. In the final section, IV, results

are presented of phases identified in aged alloys and of microstructures examined for all alloys in this study. The evaluation of microstructures is based on optical metallography, thin film and scanning electron microscopy.

I. INFLUENCE OF TITANIUM AND CARBON CONTENT ON CREEP PROPERTIES

Alloys with various carbon and titanium contents listed in Table I, page 28, were given one of the heat treatments listed in Table IV and creep tested at 650°C in air at stresses which gave rupture lives in the range 0.01 to 2000 hours. The results presented here are representative of the data obtained, and the complete results are tabulated in the Appendix. The behavior is discussed in the order (A) creep-rupture life, (B) creep rate, and (C) creep ductility.

A. Creep-Rupture Life

1. Effect of carbon content. The stress-rupture properties as a function of alloy composition are given in Figure 4 for specimens solution annealed one hour at 1177°C (hereafter denoted simply as 1177°C). Seven of the alloys (with the nominal base composition Ni-12% Mo-7% Cr-0.5% Ti) included vary only in carbon content from 0.003 to 0.32 weight %. The eighth alloy contained 0.045% C, but with no titanium present. The numbers in parentheses in Figure 4 denote the total creep elongation which will be discussed in a subsequent section.

TABLE IV

HEAT TREATMENTS GIVEN TO LABORATORY HEATS

Anneal Designation[a]	Time at Temperature (hr)	Temperature (°C)	Purpose of Heat Treatment
121	1	1177	Mill-anneal treatment that produces optimum creep properties for this Ni-12% Mo-7% Cr alloys.
123	1	1260	Solution anneal that produces virtually a single-phase alloys with properties inferior to the 121 treatment.
22	1 100	1177 870	Solution anneal and age treatment that precipitates large amounts of carbides both within the grain and at grain boundaries.

[a]See data in the Appendix for use of anneal designation.

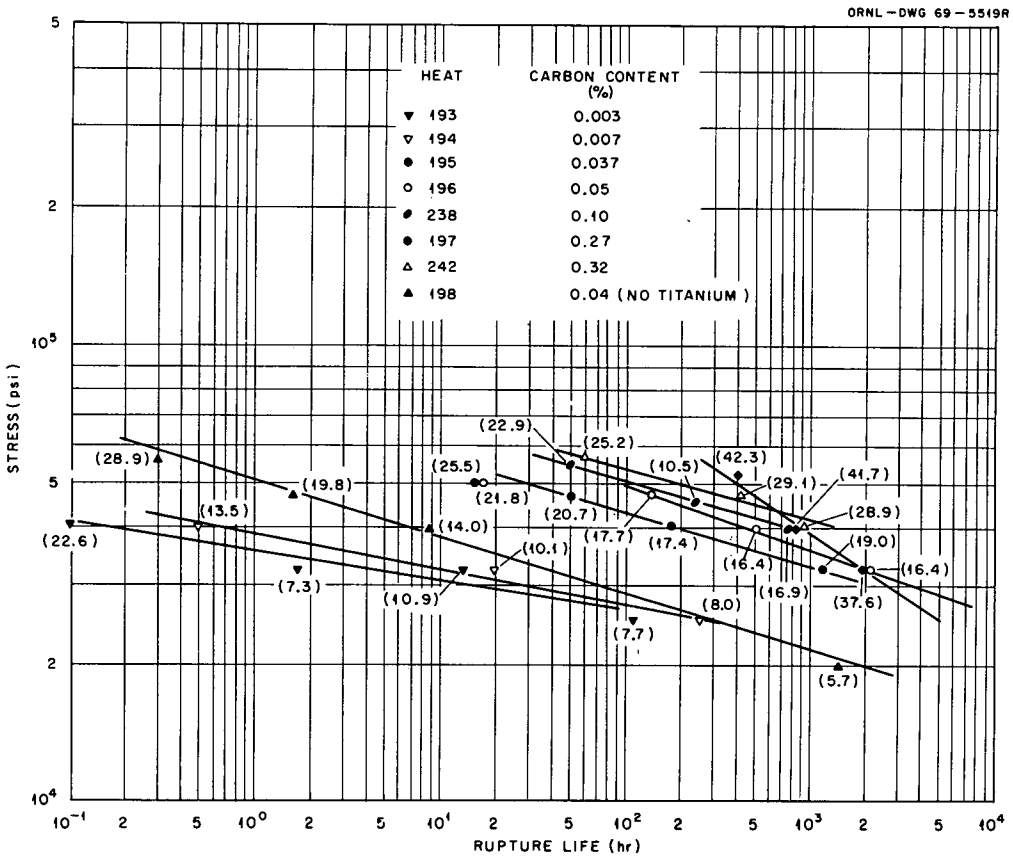

Figure 4. Creep-rupture life at 650°C for alloys solution annealed one hour at 1177°C (Ni-12% Mo-7% Cr-0.5% Ti).

The creep life in air at 650°C increases by four orders of magnitude with increasing carbon content. Although not plotted, the other heat treatments investigated exhibited a similar range in creep rupture life. The alloy without the 0.5% Ti (Heat 198) failed at approximately one-tenth the time of its carbon equivalent which contained titanium (i.e., Heat 196). The 1177°C heat treatment produced higher rupture lives than did the heat-treatment at 1260°C, indicating that the higher annealing temperature which results in essentially complete solution of the alloying constituents reduces the creep resistance. The influence of aging 100 hours at 870°C (after an 1177°C solution anneal) on the creep rupture life was dependent on the carbon level. No effect was found for the lower carbon contents, but a factor of five reduction in the rupture life was found for higher contents (data in the Appendix).

The progressive increase in rupture life (and thus creep strength) with increasing carbon content is better illustrated in Figure 5 in which data are plotted for each of three stress levels following the same heat-treatment. The rate of change in rupture life decreases above approximately 0.04% C at each stress level.

2. Effect of titanium content. The influence of 0.5% Ti and heat-treatment on the creep-rupture life of alloys containing 0.05% C is illustrated in Figure 6. The alloy without titanium (Heat 198, open symbols) contained 12.4% Mo and the alloy with titanium (Heat 196, filled symbols) contained 11.5% Mo. These molybdenum contents are sufficiently close that the increased rupture life of the alloy containing 0.5% Ti

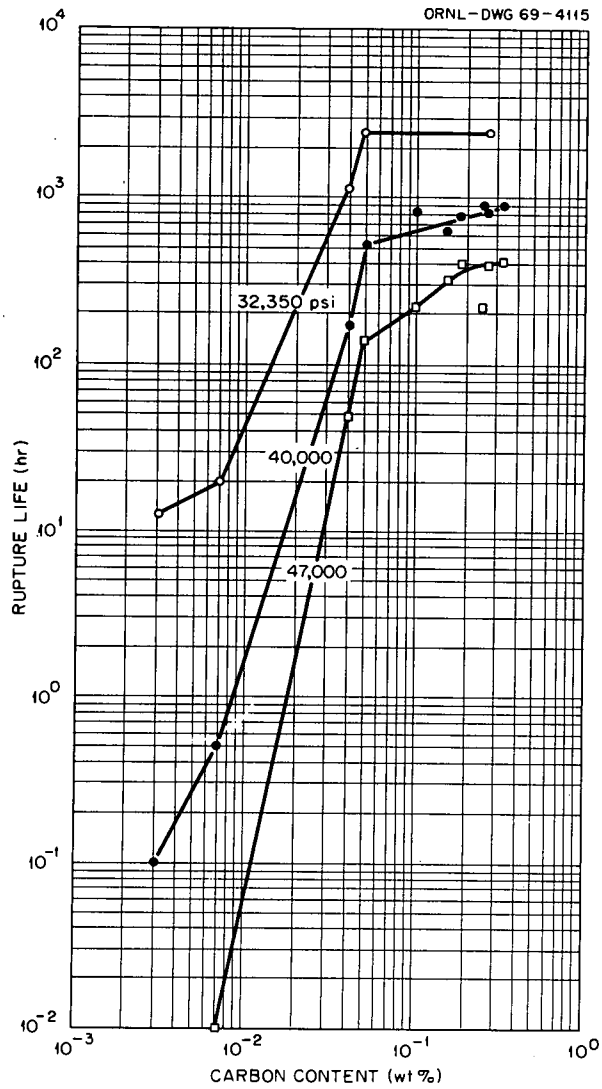

Figure 5. Effect of carbon on the creep-rupture life of Ni-12% Mo-7% Cr-0.5% Ti alloys at 650°C for samples solution annealed one hour at 1177°C.

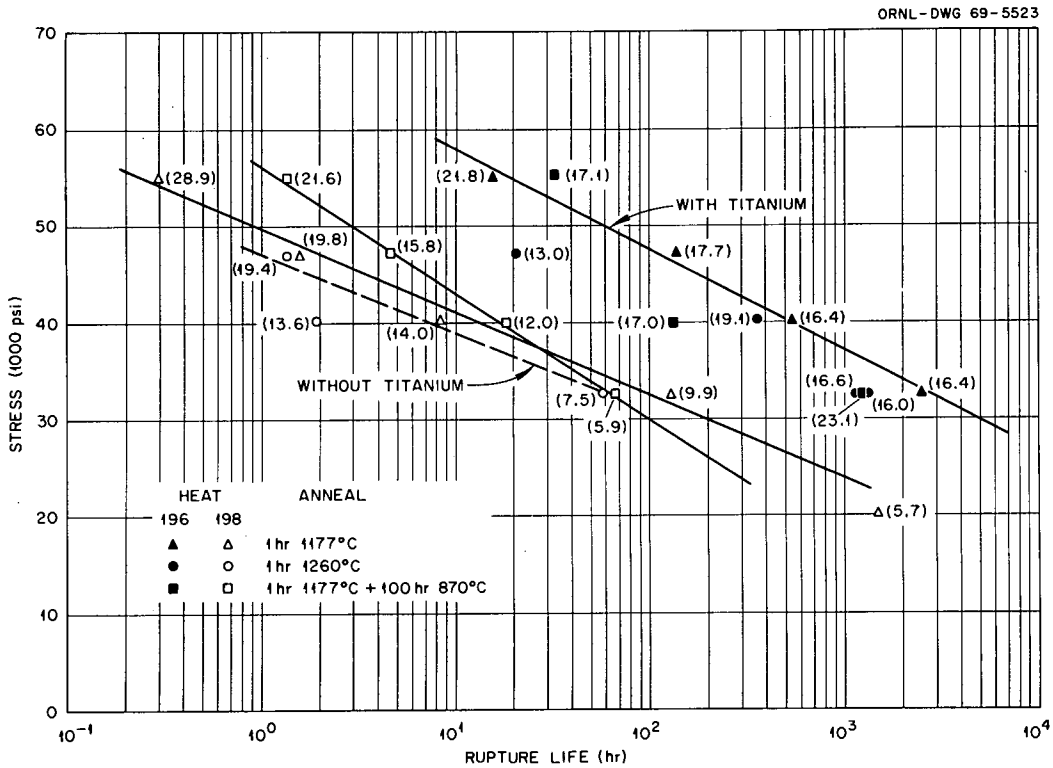

Figure 6. Effect of 0.5% Ti on the creep-rupture life of Ni-12% Mo-7% Cr-0.05% C alloy at 650°C.

can be attributed to the titanium. The rupture life of the alloy containing 0.5% Ti is from five to twenty times that of the titanium-free alloy, depending on the stress level and heat treatment considered.

The fracture strains (elongations), which are given in parentheses in Figure 6, indicate higher ductility for a given heat-treatment in the alloy containing 0.5% Ti than for the alloy without titanium. This is particularly true at lower stress levels and is a factor in producing the higher rupture lives at low stresses. The largest difference in the ductility between the two heats is for the samples aged 100 hours at 870°C prior to creep testing.

B. Secondary Creep Rate

The change in secondary creep rate with carbon content for a test at 40,000 psi and 650°C is given in Figure 7. In agreement with the rupture life data, the secondary creep rate decreases with increasing carbon content. As the carbon content increases from 0.003 to 0.04% C (with 0.5% Ti), the creep rate decreases by three orders of magnitude. Between 0.04 and 0.3% C there is an additional factor of five to ten decrease for the solution annealed condition. The differences in creep rate for the various heat-treatments are greater at higher carbon concentrations. The secondary creep rate of the higher carbon alloys aged 100 hours at 870°C is a factor of eight to ten greater than that found for samples tested in either of the solution annealed conditions. Thus, the aging process which causes precipitation actually decrease the resistance to creep deformation, as measured by the secondary creep rate.

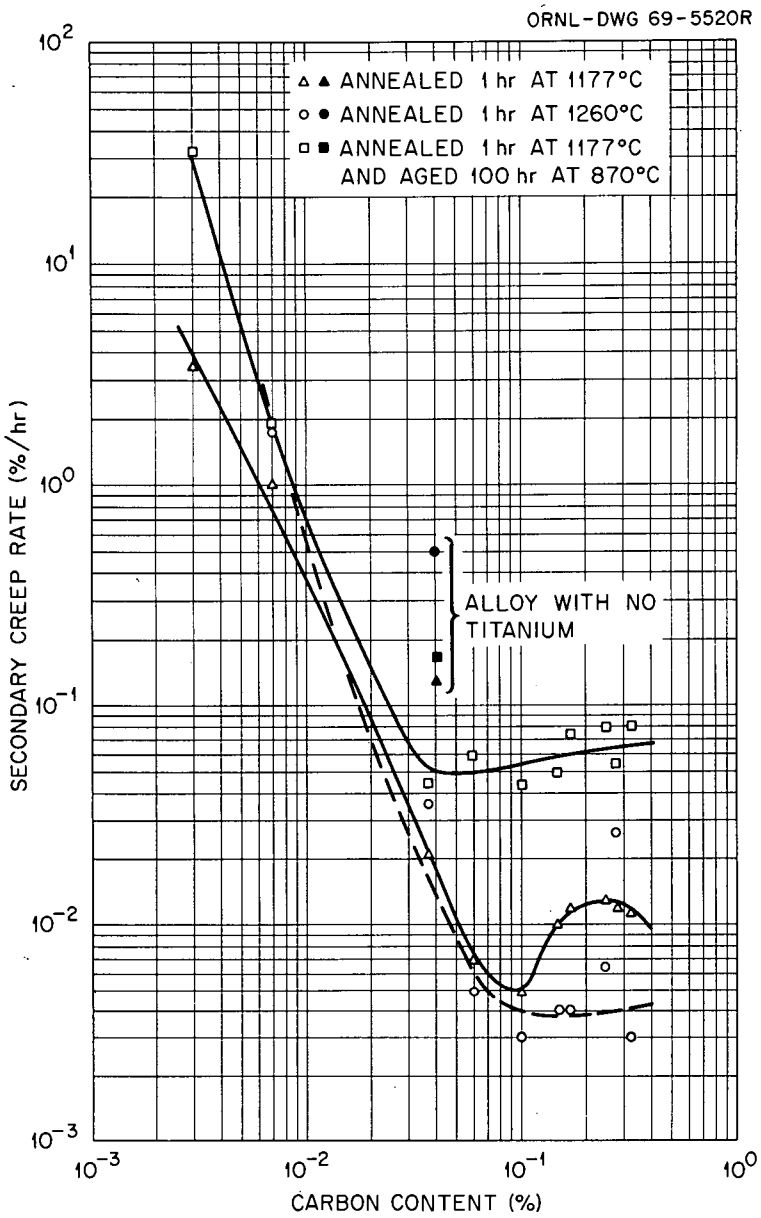

Figure 7. Change in the secondary creep rate with carbon and titanium content for the Ni-12% Mo-7% Cr-0.5% Ti alloy at 40,000 psi and 650°C.

The effect of 0.5% Ti (at the 0.05% C concentration) is to reduce the creep rate by a factor of approximately ten, which is concluded by reference to the filled data points in Figure 7 for the titanium free alloy (Heat 198). This effect of titanium on the creep rate agrees with the effect on the rupture life behavior (Figure 6, page 45).

C. Creep Ductility

Since the creep strain is the result of complicated internal deformation processes that vary with the composition, microstructure, strain rate, and other test variables, a test temperature of 650°C and an air environment were selected to assess the effects of as many of these parameters as possible. The resulting influence of alloying on the ductility in creep is presented in three ways in order to separate the important parameters.

1. Elongation versus carbon content. Figure 8 gives the total creep strain at 650°C and 40,000 psi as a function of carbon content. At this stress the fracture strain varies between 10 and 20% for concentrations up to approximately 0.1% C. A sharp increase is observed at higher carbon contents; however, this trend was not as marked at the higher stresses (see Appendix). In general, however, creep elongation increases with increasing carbon content for samples showing increased rupture life above 0.1% C. This qualification is made since at higher stress levels, the data for the 1260°C heat treatment did not show the increase in ductility with carbon content.

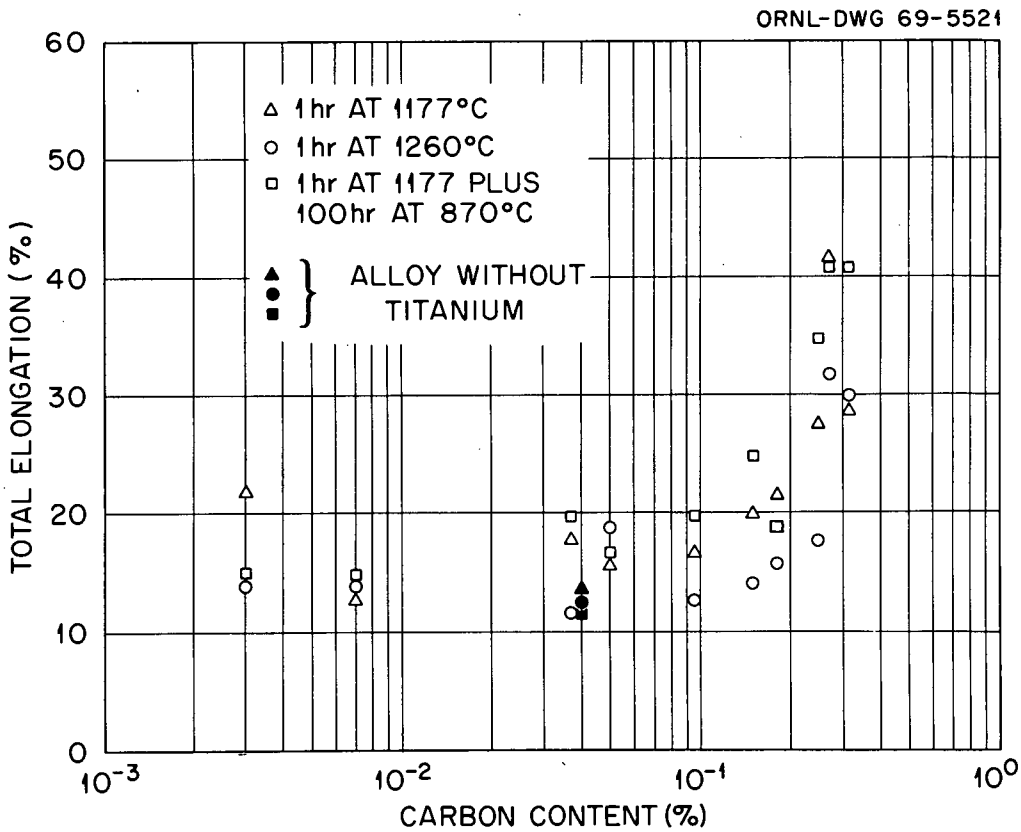

Figure 8. Variation in creep elongation with carbon content for 40,000 psi creep test at 650°C (Ni-12% Mo-7% Cr-0.5% Ti).

2. Elongation versus creep rate. The strong influence of strain rate on fracture processes in the temperature range 500° to 700°C makes it instructive to plot the creep ductility as a function of the rate of deformation. This relationship is shown in Figures 9 and 10 for two different heat-treatments. As discussed by Glen,[40] one might expect that a material undergoing precipitation during testing could show a minimum ductility value at some intermediate strain rate. The data from these creep test show no consistent correlation on this basis, with one exception.

In both solution treated and aged alloys those containing titanium had higher ductility than those with the same carbon content but no titanium (i.e., Heats 195 and 196 versus Heat 198). It is clear from Figure 9 that one heat of material (Heat 197 with 0.27% C) exhibited significantly higher fracture strains than the other solution-annealed alloys for the same rate of secondary creep. Figure 10 shows that if aged 100 hours at 870°C before creep testing the heat with an equivalent carbon content to alloy 197 (i.e., Heat 242 with 0.32%) also exhibited a large amount of creep deformation before fracture at similar strain rates. The reason for the difference in the ductility behavior of the 0.32 and 0.27% C heats in Figure 9 is probably related to differences in grain size as discussed later. Comparison of Figures 9 and 10 shows that aging at 870°C prior to creep testing shifts the curves upward and to the right, giving higher fracture strains for a given creep rate. This is particularly evident for the higher carbon contents, where the prior aging treatment has precipitated large amounts of carbides.

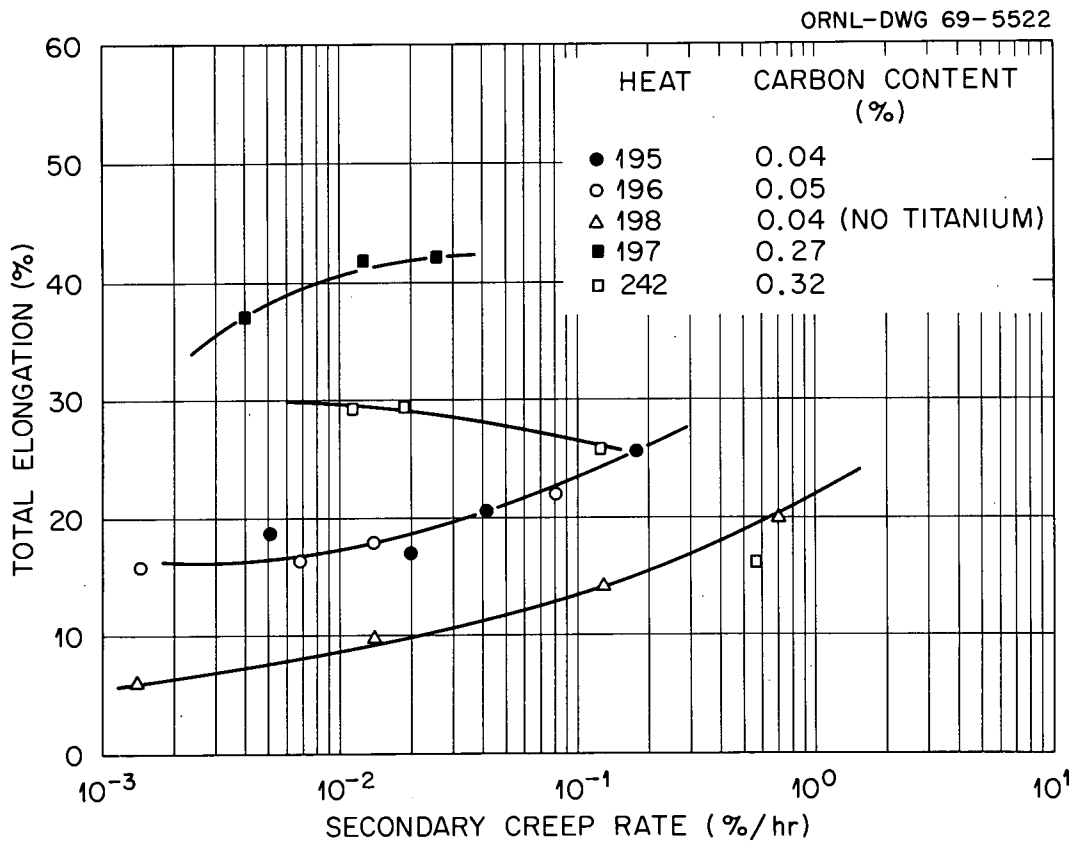

Figure 9. Fracture strain correlation with secondary creep rate at 650°C for specimens annealed one hour at 1177°C.

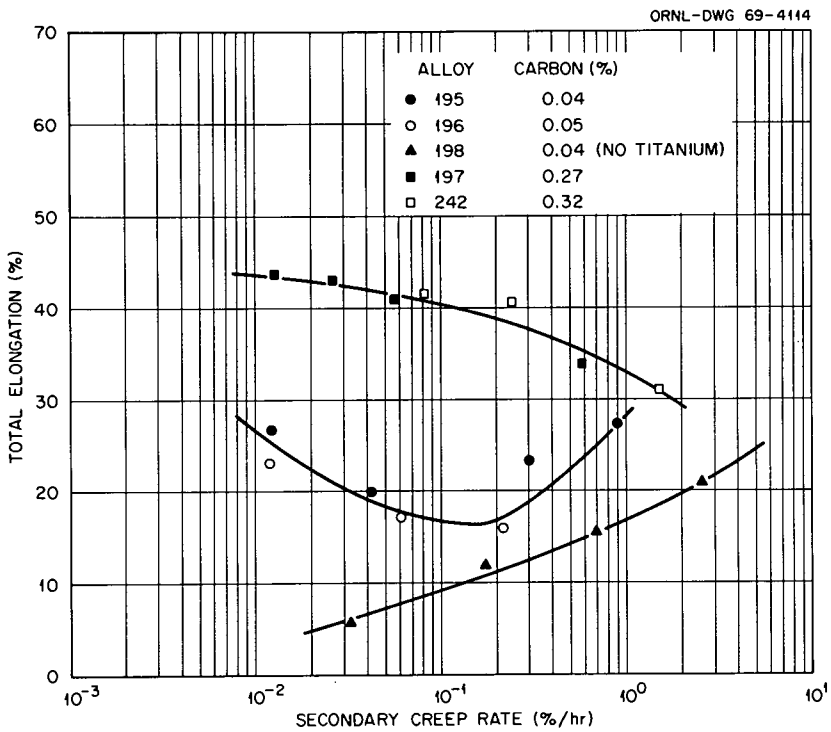

Figure 10. Fracture strain correlation with secondary creep rate for specimens solution annealed at 1177°C and aged 100 hours at 870°C (Ni-12% Mo-7% Cr-0.5% Ti).

3. Elongation versus rupture life. In alloys subject to strain rate and aging effects, there is often a decrease in creep ductility with increasing rupture time. Figure 11 shows the elongation (fracture strain) as a function of rupture life for the various carbon levels after an 1177°C heat-treatment. The results for some heats show the expected decrease in this measure of ductility, but for the 0.32% C heat an increase in ductility with rupture life was found. When reduction-of-area of the creep-rupture samples is correlated in this way, the trends are similar and the magnitude of the ductility is in good agreement with the measured elongation.

II. INFLUENCE OF TITANIUM ON MECHANICAL PROPERTIES OF COMMERCIAL ALLOYS

To assess the influence of titanium concentration on aging reactions a series of commercial alloys (Table III, page 30) with different titanium contents was studied. Initially, the thermal stability of these alloys was evaluated by aging at 650° and 760°C and testing in creep or tensile at 650°C. Subsequent experiments were performed to define the effect of certain deleterious heat-treatments on the structures and on the room temperature and 650°C tensile properties. The results which follow contrast the differences in the properties after 650° and 760°C aging for a given alloy rather than emphasize the trends with titanium content. The reason for this approach is to avoid, or at least minimize, arriving at conclusion influenced by possible heat-to-heat variations in properties.

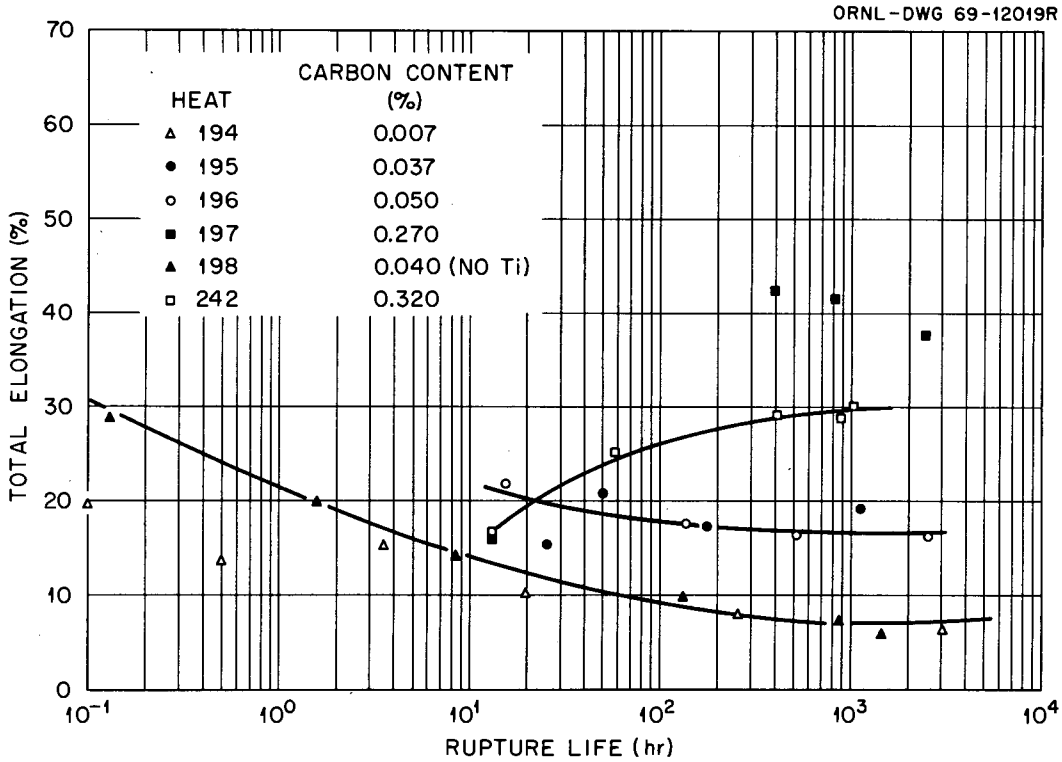

Figure 11. Variation in creep elongation with rupture life at 650°C for various Ni-12% Mo-7% Cr-0.5% Ti alloys annealed one hour at 1177°C.

A. Creep Properties After Aging

A comparison of the creep behavior of four commercial heats of Hastelloy N as a function of titanium content is given in Figure 12. These data correspond to three different histories: (1) solution annealed at 1177°C, (2) annealed at 1177°C and aged 3000 hours at either 650°C or (3) 760°C. Samples with these three thermal histories were then creep tested in air at 40,000 psi and 650°C.

In the as-annealed condition the secondary creep rate for the four different alloys is identical, but both the rupture-life and the creep elongation was appreciably higher for the 1.2% Ti heat than for the three heats with lower titanium contents. For the aged conditions, the creep rate of the three heats with low titanium contents has increased by a factor of from three to six, but no change in creep rate due to aging was found for the 1.2% Ti heat.

In the aged condition the creep rate of these materials decreases by a factor of four with increasing titanium content from 0.15 to 1.2%. The total creep elongation increases from 13 to 53% as a function of titanium after the 650°C aging treatment and increases from 9 to 37% for samples aged at 760°C. This significantly higher ductility for the 1.2% Ti heat accounts for the greater rupture life observed for that heat as compared to the heats containing lower titanium concentrations. The differences in creep behavior as a function of titanium content represent the influence of different carbide phases and distributions established by the aging treatments and will be discussed in a subsequent section.

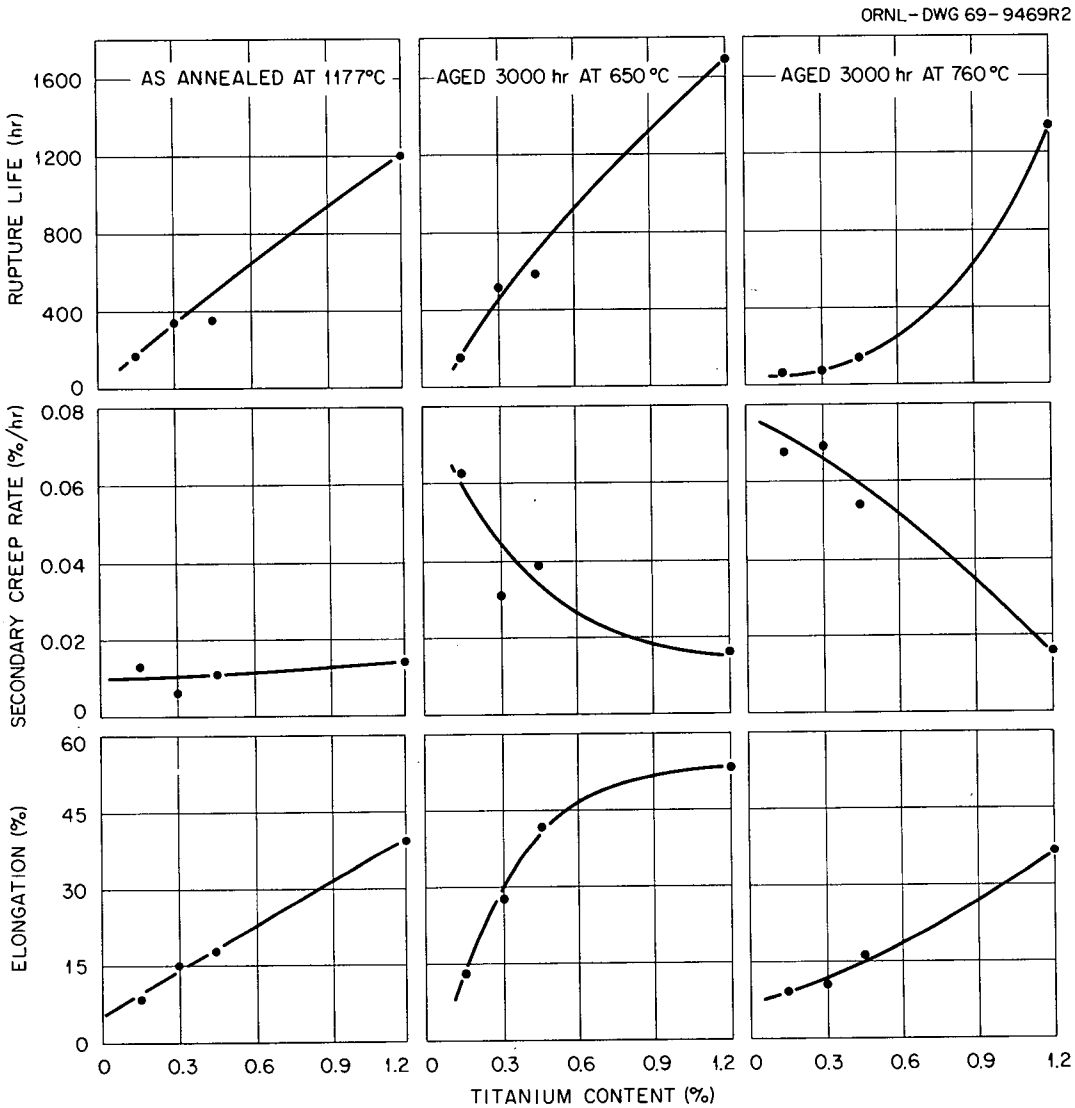

Figure 12. Influence of titanium content and aging temperature on the 650°C creep properties at 40,000 psi for a Ni-12% Mo-7% Cr-0.07% C alloy annealed one hour at 1177°C.

A comparison of the creep curves, corresponding to these data plotted in Figure 12, shows the time required for 5 percent strain to be approximately a factor of two shorter after the 760°C age than for the 650°C age, with the exception of the highest titanium heat which exhibited no difference. The fraction of the time to rupture spent in the first two stages of creep (primary plus secondary creep) varied from 0.7 to 0.95, with samples of the more ductile, high titanium heat (1.2% Ti) spending the smallest portion (lower fraction) of its creep life in the first two creep stages.

The influence of solution annealing at 1260°C and aging 3000 hours at 760°C for the heat with 1.2% Ti is shown in Table V. This particular heat and heat-treatment produced a radically different carbide distribution, which will be discussed in the Microscopy and Phase Analysis section, and thus the influence of that structure on the creep behavior is of interest. The effect of annealing at 1260°C and aging for this 1.2% Ti heat of Hastelloy N (Table V) was to increase the secondary creep rate by a factor of two to three and decrease the rupture life a small amount, but the treatments did not significantly change the creep ductility.

Comparing the results of aging this high titanium heat after an 1177°C and a 1260°C solution anneal indicates that there is little difference in the creep-rupture life, but the creep rates and the ductilities are appreciably lower if solution annealed at the higher temperature before aging. For example, the post-age creep elongations for the 1260°C anneal (i.e., 24 and 20%, Table V) are appreciably lower than for that found for a prior 1177°C anneal (53 and 37%, Figure 12).

TABLE V

CREEP PROPERTIES OF THE 1.2% Ti HEAT OF HASTELLOY-N FOR A ONE HOUR AT 1260°C SOLUTION ANNEAL

History[a]	Rupture Life[b] (hr)	Secondary Creep Rate (%/hr)	Fracture Strain (%)
As annealed one hour at 1260°C	2472	0.003	21.6
Annealed at 1260°C and aged 3000 hours at 650°C	2095	0.007	24.5
Annealed at 1260°C and aged 3000 hours at 760°C	1454	0.010	20.4

[a]Heat 467548.

[b]Tested in air at 40,000 psi stress and 650°C.

B. Tensile Properties After Aging

1. Properties at 650°C. The 650°C tensile properties measured at a low strain rate of 12% per hour (or 0.002 minute^{-1} strain rate) are plotted in Figure 13. The heat treatments are identical to the creep test results previously discussed and include an 1177°C solution anneal and two aging treatments of 3000 hours at 650 or 760°C. The yield strength (0.2% offset stress) and ultimate tensile strength show a minimum near 0.5% Ti and are higher at 1.2% Ti for all three heat-treatments. The large strength difference represents differences in both carbon and titanium contents as shown in Table III, page 30. The trends, plotted in Figure 13, of the total elongation with titanium differ for the three thermal treatments. For the as-annealed material the elongation increases slowly from 28 to 39% with increasing titanium content up to 1.2%, but after the 650°C age the elongation increases more rapidly (from 19 to 44%) and levels out above 0.5% Ti.

After the 760°C age the elongation for the three lower titanium levels is appreciably reduced as compared to an unaged sample, but for the 1.2% Ti heat no loss of high-temperature ductility occurred. Thus, as evident in the creep behavior, the stability and favorable precipitate distribution for the higher titanium concentration can be inferred from the differences in these tensile test results.

Effect of aging time. A comparison of three common measures of tensile ductility is given in Figure 14 as a function of aging time at 650°C following an 1177°C solution anneal. As measured by total

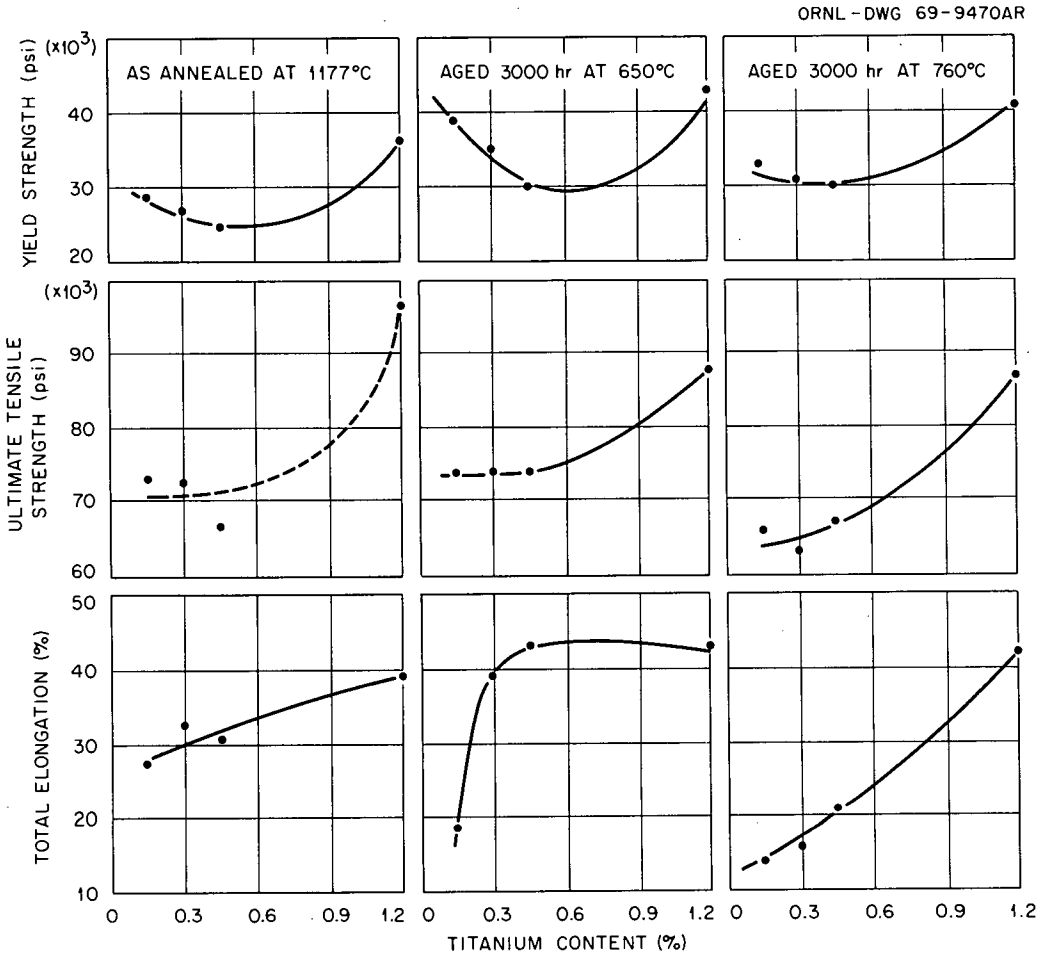

Figure 13. Influence of titanium content and aging temperature on the 650°C tensile properties of Ni-12% Mo-7% Cr-0.07% C alloys annealed one hour at 1177°C.

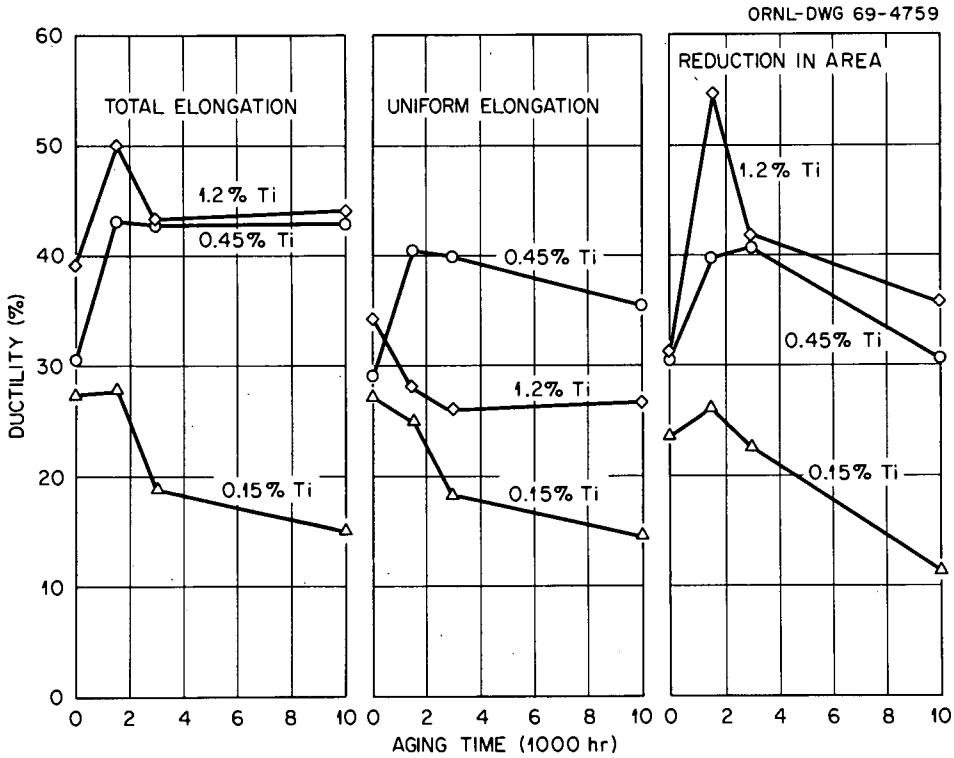

Figure 14. Comparison of the effects of titanium content and aging time on three measures of the tensile ductility (Hastelloy-N solution annealed one hour at 1177°C).

elongation at 650°C, the tensile ductility of the intermediate and high titanium material increases during the first 1500 hours of aging, but changes very little with further time. Comparing the total and uniform elongation values shows that nearly all of the strain is "uniform strain" (i.e., occurs prior to reaching the ultimate stress) for the 0.15 and 0.45% titanium alloys. For the 1.2% Ti heat there is a decrease in the uniform elongation over the first 3000 hours. Over the same period of time the total elongation is enhanced relative to the starting condition for the 1.2% Ti heat. Therefore, the beneficial influence of titanium is manifested as an increase in the amount of nonuniform strain. That is to say, the enhancement of tensile ductility caused by the higher titanium concentration (1.2% Ti) is attributable to the alloys ability to plastically deform or neck-down after local necking has begun in the tensile test.

Effect of a 1260°C solution anneal. The aging response of one particular commercial heat of Hastelloy-N (i.e., the 1.2% Ti heat) was significantly different after an 1177° and a 1260°C solution anneal. The reason for the difference is discussed in a subsequent metallography section. In Figure 15, the tensile properties at 650°C are given for aging after a one hour at 1260°C solution anneal. Both the 0.2% yield strength and total elongation are plotted as a function of aging time at 650 and at 760°C. These particular tests were run to correlate the property changes which result from the development of precipitates on stacking faults, a precipitate phenomenon that will be discussed in the Microscopy and Phase Analysis section. These data (Figure 15) show a

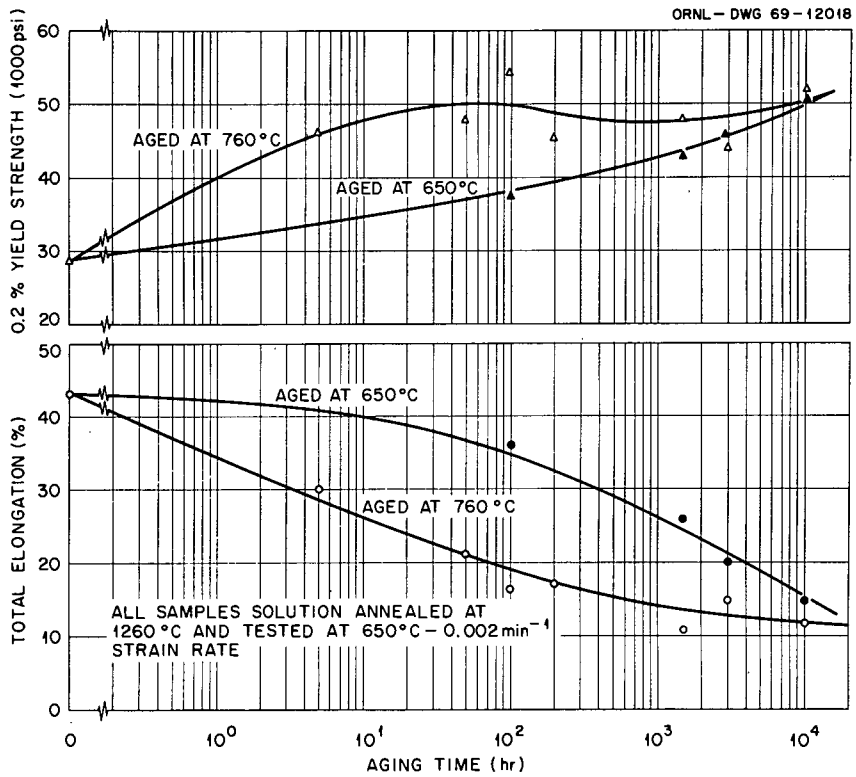

Figure 15. Changes in the 650°C tensile properties with aging time for the 1.2% Ti heat of Hastelloy-N solution annealed one hour at 1260°C.

rapid increase in the yield strength from 30,000 to 45,000 psi after only five hours of aging at 760°C, and the strength approaches a value of approximately 50,000 psi at 10,000 hours. For aging at 760°C the yield strength reaches a maximum value after approximately 100 hours. The yield strength for aging at 650°C, however, increases at a slower rate, but approaches the same strength level after approximately 10,000 hours. The tensile ductility (elongation) exhibits a rapid decrease with aging time at 760°C and approaches an equilibrium value of 12% between 1500 and 3000 hours. For the 650°C age, the ductility decrease is more sluggish but at longer times it approaches the same level of ductility as that found for the 760°C aging treatment.

Although the results are not presented in detail, the influence of a 1260°C anneal on the aging response of commercial heats of Hastelloy was determined for heats containing 0.15, 0.27, and 0.45% Ti, in addition to the 1.2% Ti heat discussed in Figure 15. The results, however, indicated that even though the aging behavior after a 1260°C solution was similar to that found for an 1177°C anneal (Figures 12 and 13, pages 56 and 60) the magnitude of the 650°C tensile ductility was consistently lower, and the rate of ductility loss with aging time was more rapid if samples were preannealed at 1260°C. One heat of material, 0.45% Ti, was an exception to this rule and exhibited no greater ductility loss for aging after a 1260°C solution anneal than was found for an 1177°C anneal. Nevertheless, the data presented in Figure 15 for the 1.2% Ti heat represents the most significant property changes attributable directly to the

use of the higher solution anneal temperature for these commercial alloys with titanium contents between 0.15 and 1.2%.

2. Properties at room temperature. The changes in the room temperature tensile properties were measured for a few samples after solution annealing at 1177°C and aging 1500 hours at 650 and 760°C and the results are given in the Appendix. Generally, the room temperature ductilities in the as-solution annealed condition were between 50 and 65%. The lowest post-age ductility was 41% for the 0.15% Ti heat and the maximum ductility was 59% for the 0.45% Ti heat. As measured at room temperature the yield strength increased approximately 20%, the ultimate strength increased about 10%, and the total elongation decreased approximately 10 to 25% as compared to unaged samples at room temperature.

In the case of the 1.2% Ti alloy that showed the large loss of hot ductility after a 1260°C solution anneal,(Figure 15, page 63), the corresponding room temperature ductility was 40% after 1500 hours at 760°C. This value should be compared to 68% elongation for the as-annealed condition. Thus, the precipitation on stacking faults, which occurs on aging if pre-annealed at 1260°C, had a considerably smaller effect on the room-temperature tensile ductility than on the ductility at 650°C.

III. INFLUENCE OF TITANIUM IN PURE NICKEL

The beneficial effects of titanium additions on the high-temperature properties of complicated engineering alloys prompted an

evaluation of the effects of small titanium additions in pure nickel. Five alloys melted from commercially pure nickel (INCO-270) stock with titanium concentrations of 0, 0.06, 0.26, 0.58 and 1.5% Ti (Table II, page 29) were tested in tensile and creep in order to seek information on causes of enhanced ductility.

The tensile properties were first determined as a function of temperature and composition. Then measurements were made of the properties for certain compositions at a particular temperature (600°C) in order to assess the effects of other test variables on the creep and tensile fracture behavior. The tensile results are presented first, followed by the creep property measurements.

A. Tensile Properties

1. Effect of test temperature and composition. The effect of composition and test temperature on the tensile ductility is shown in Figure 16 for a 0.002 minute^{-1} strain rate test. The curve marked "Nickel-270" corresponds to samples of the commercial nickel which were melted and fabricated just like other laboratory heats, but with no alloying additions added. The other two sets of data correspond to nickel-titanium binary alloys with 0.06% Ti and 1.5% Ti concentration. The Nickel-270 exhibits a drop in both uniform and total elongation from approximately 35% at temperatures of 400° and 600°C to approximately 12% at 700°C. For both alloys containing titanium, the total tensile elongation increases as the test temperature increases, but the uniform strain decreases with increasing temperature. At a given test

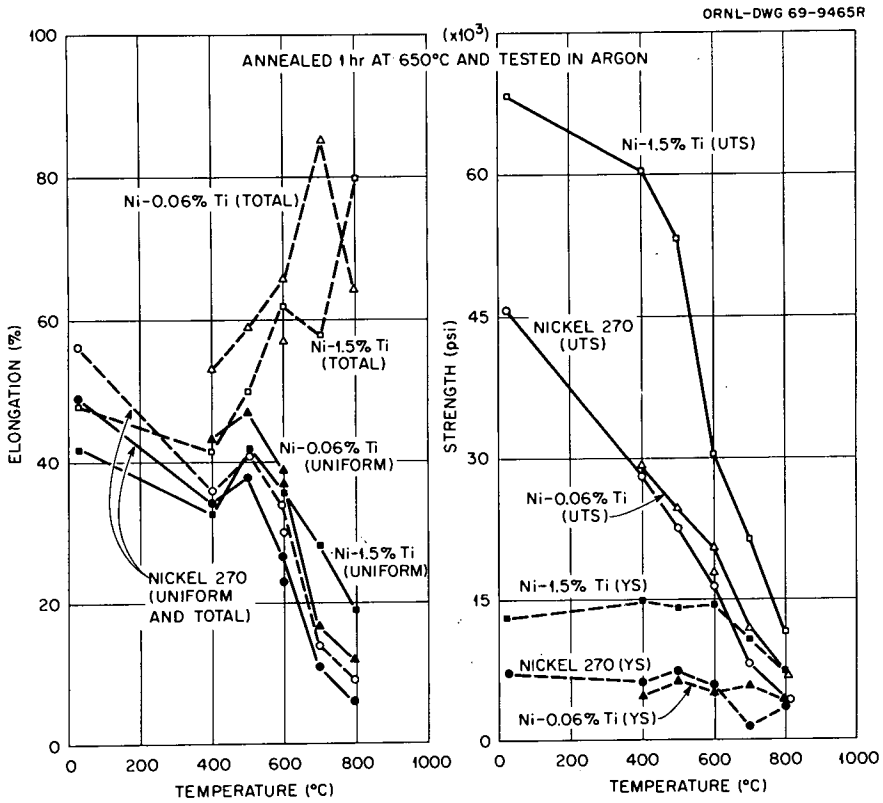

Figure 16. Temperature dependence of the tensile strength and ductility of nickel as a function of titanium content.

temperature titanium has slightly increased the amount of uniform elongation, but the primary influence of titanium is to greatly increase the nonuniform elongation as compared to the alloy without titanium. Since the necking strain and not the uniform strain is affected most by the additions of titanium to nickel, it is suggested that the rate sensitivity of the plastic deformation is significantly affected.

The change in strength for these alloys is also shown in Figure 16. One finds an increase in both the 0.2% yield and ultimate strengths on alloying with titanium, and each alloy shows a decrease in strength with temperature, as expected. The maximum strength at each temperature occurs for the highest titanium level and very little strengthening is found for the 0.06% Ti heat. The lack of significant strengthening and the large increase in ductility for this dilute 0.06% Ti alloy indicate that the titanium is operating as a gettering addition that removes or changes the distribution of some impurities.

2. Effect of annealing time. The effect of annealing time at 650°C prior to tensile testing at 600°C is shown in Figure 17. Both the uniform and total elongation are independent of annealing time between 0.25 and 165 hours at 650°C. The 600°C yield strength of these two alloys, which are not plotted, also showed no consistent change with aging time at 650°C up to 165 hours. These observations indicate that structures produced on annealing are achieved quite rapidly and that no detrimental grain growth, precipitation, or contamination resulted during the heat-treatment of the samples in quartz capsules.

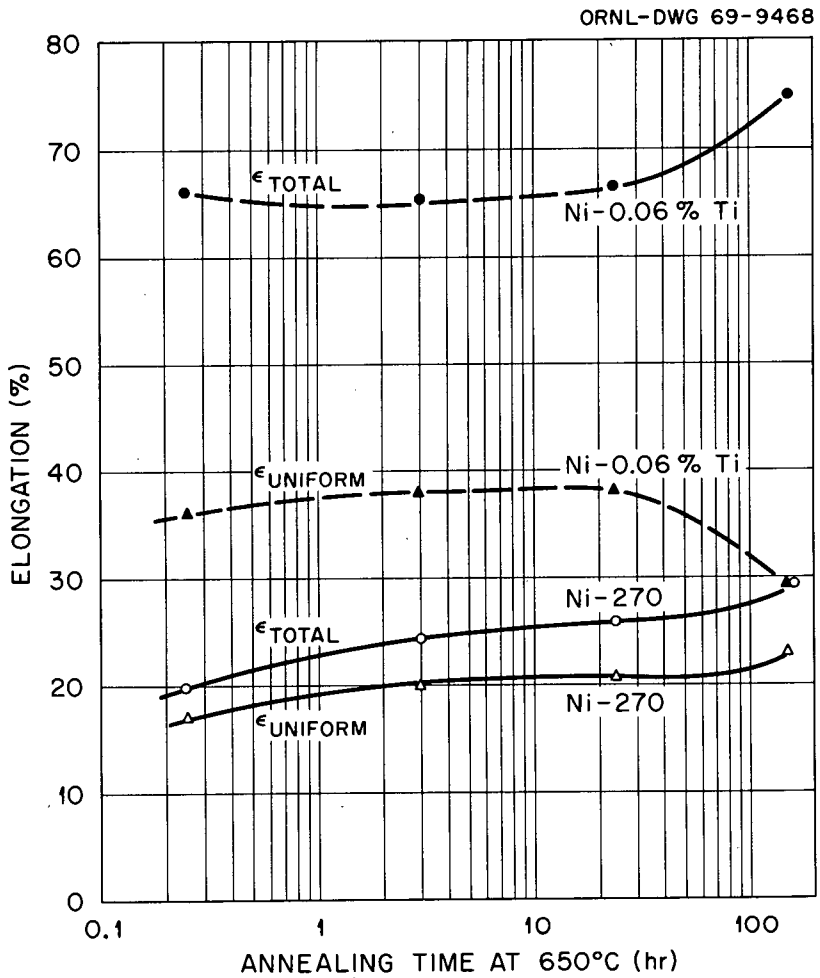

Figure 17. Effect of annealing at 650°C on the tensile ductility for Nickel-270 and Ni-0.06% Ti alloy at 600°C and 0.002 minute^{-1} strain rate.

B. Creep Properties

Creep properties of pure nickel (Nickel-270) and several dilute nickel-titanium binary alloys were measured in argon to substantiate the assumption that titanium enhanced the grain-boundary mobility of nickel and to investigate the effects of this enhanced mobility on creep deformation and fracture.

The creep-rupture lives of the various alloys with and without titanium are shown in Figure 18. The rupture life increases with increasing titanium, as expected. This increase in rupture life with increasing titanium content is due to two factors. The factors are (1) a decrease in the secondary creep rate and (2) a large increase in creep elongation as shown by the numbers in parentheses in Figure 18. The creep rate for example at 12,000 psi and 600°C decreases by a factor of 50 for progressive increases in titanium content up to 1.5%.

C. Comparison of Creep and Tensile Behavior

1. Effect of titanium content on elongation. Data from Figures 16, page 67, and 18 are replotted in Figure 19 to compare the influence of increasing titanium concentration on the strain at fracture (total elongation) of nickel for creep and tensile test conditions. The data plotted in Figure 19 correspond to samples annealed one hour at 650°C and then tested at 600°C in either tension at 0.002 minute^{-1} strain rate or in creep at 12,000 psi stress. In addition, a sample of Nickel-270 was tensile tested after a two-pass zone refining operation which was

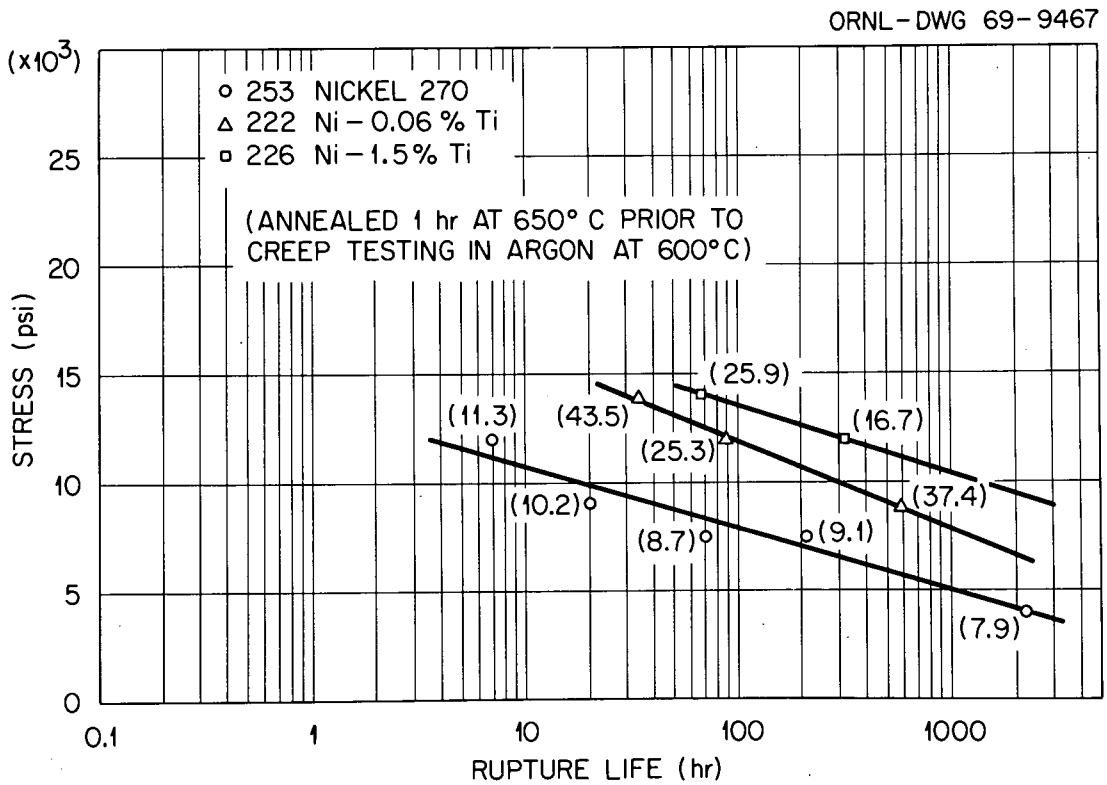

Figure 18. Influence of titanium content on the creep-rupture life of nickel at 600°C.

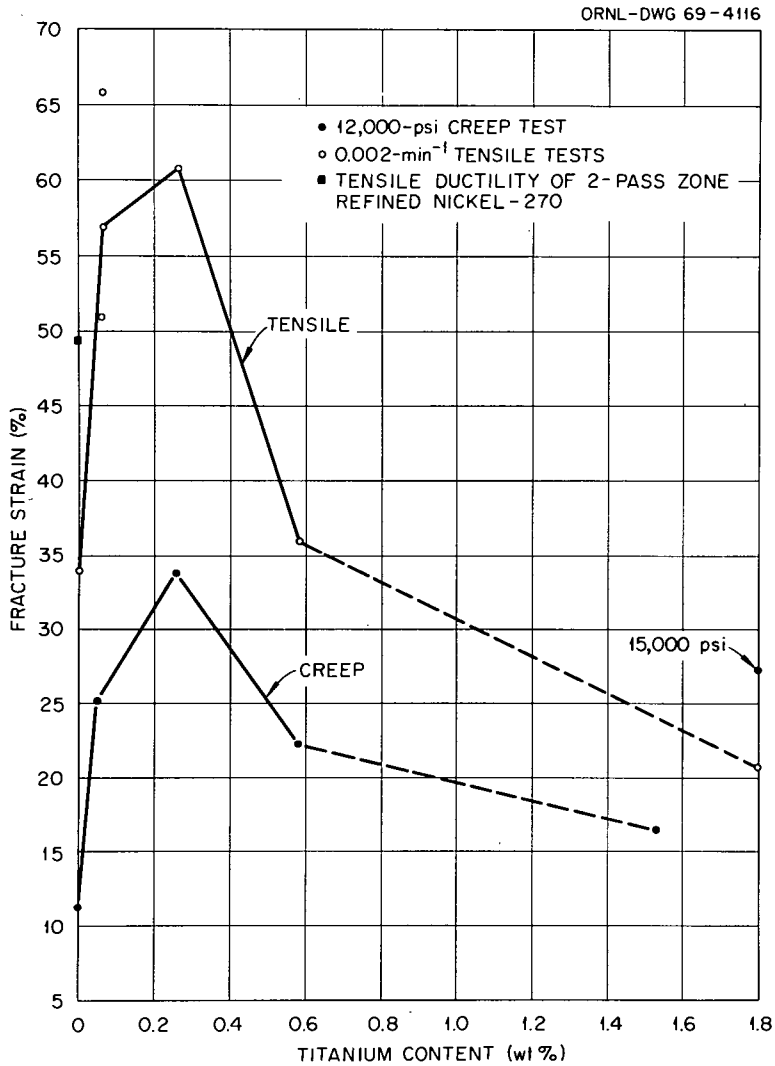

Figure 19. Effect of titanium concentration on the elongation in creep and tensile at 600°C of binary nickel alloys.

given to change the impurity distribution. The changes in composition for this treatment were insignificant.

The results in Figure 19 indicate a maximum ductilizing effect of titanium in both creep and tensile testing at 600°C. The maximum ductility in both types of test corresponds to 0.26% Ti; however, in tensile the 0.06% Ti alloy exhibited ductility values equivalent to those at the 0.26% Ti concentration. Above 0.26% Ti both the creep and tensile ductility decreased with titanium concentration, for two higher titanium contents evaluated. The two-pass zone refining operation resulted in a structure that was more ductile in tensile than the starting material, commercial purity nickel-270 that had been remelted and fabricated.

2. Effect of deformation rate on elongation. The strain rate sensitivity of the fracture strain for both tensile and creep testing conditions at 600°C is shown in Figure 20. Alloys with and without titanium show a general decrease in fracture strain with decreasing rates of deformation. The alloys containing titanium exhibit significantly higher ductilities than the alloy without titanium at all rates of deformation. Thus, the stronger titanium-containing alloys, which require a higher stress level to produce the same secondary creep rate, exhibit greater resistance to fracture than the unalloyed nickel.

D. Chemical Analysis of Tested Alloys

Since the effect of test environment can confuse an evaluation of alloying effects per se several samples were chemically analyzed after testing in argon creep and tensile tests. The results, given in

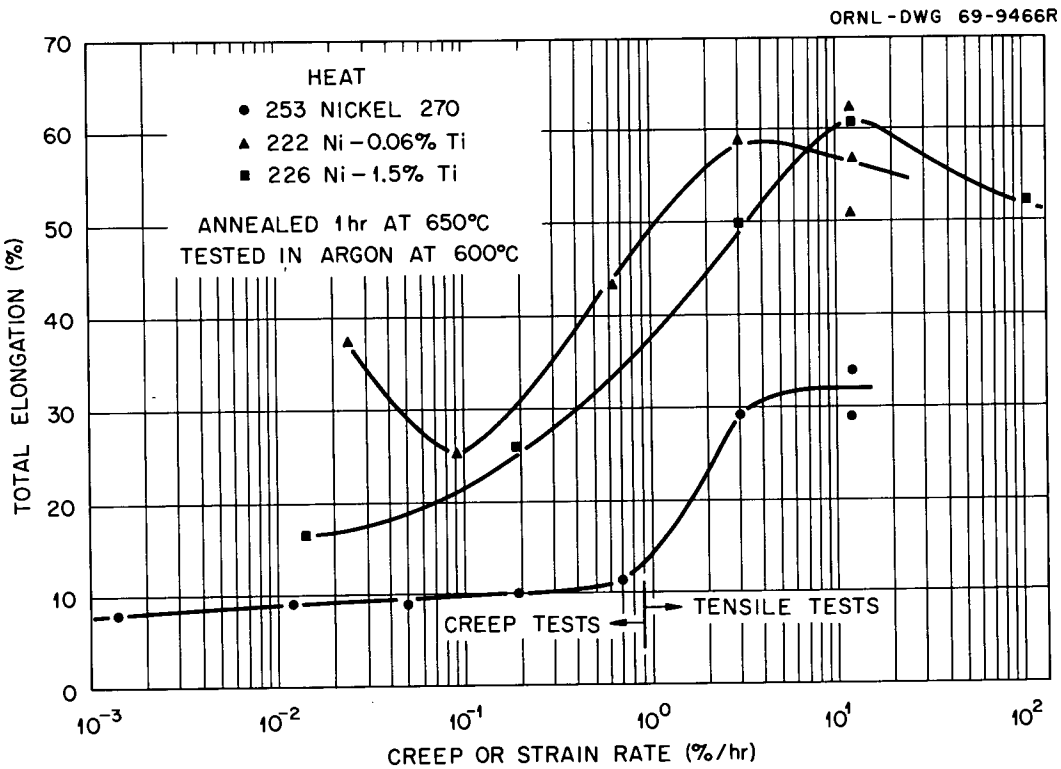

Figure 20. Strain rate sensitivity of the ductility of nickel-titanium alloys at 600°C.

Table VI, indicate that no gaseous contamination of any consequence was observed. In fact, in three of the six samples the concentration of oxygen after testing was somewhat lower than the before test analysis. Thus, the effect of the argon test environment on the ductility of these binary nickel alloys should be insignificant.

IV. MICROSCOPY, FRACTOGRAPHY, AND PHASE ANALYSIS

In order to correlate the microstructure with alloy content, heat-treatment, and testing conditions, selected samples were analyzed to determine the phases present, the phase morphology, and the phase distribution within the alloy. The first section presents the results of x-ray phase analysis of precipitate particles extracted from aged alloys. Following sections include optical metallography, electron transmission microscopy, extraction replica microscopy, and scanning electron examination of fractured samples. All of the different materials examined in microscopy will be discussed under the specific experimental technique.

A. Phases Identified in Aged Alloys

The heats used, heat-treatments, and phases identified by x-ray and confirmed generally by electron diffraction are listed in Table VII. The lattice parameters measured by the Debye Scherrer x-ray diffraction technique are given in Table XVII of the Appendix. These results indicate that in the Ni-12% Mo-7% Cr-0.04% C alloy with no titanium (i.e., alloy 198) the only second phase precipitate after 1500 hours at either 650 or 760°C is the M_2C-type carbide. The "M" in M_2C denotes metal content and the "C" denotes carbon in the compound. For the most dilute titanium

TABLE VI

GAS ANALYSES OF NICKEL AND NICKEL-TITANIUM BINARY ALLOYS TESTED IN ARGON AT 600°C

Alloy	Gas and Carbon Content Before Test (ppm)[a]				Gas Content After Tests in Argon (ppm)[a]		
	Oxygen	Nitrogen	Hydrogen	Carbon	Oxygen	Nitrogen	Hydrogen
Nickel-270	21	11	18	40	75	7	4
Nickel-270	21	11	18	40	83	6	4
Ni-0.06% Ti	150	4	6	60	51	5	3
Ni-0.06% Ti	150	4	6	60	61	4	3
Ni-0.27% Ti	--	--	--	--	49	3	3
Ni-1.5% Ti	210	6	8	70	44	4	3
Ni-1.8% Ti	140	8	6	40	200	7	4

[a]Parts per million by weight.

TABLE VII

PHASES IDENTIFIED IN VARIOUS AGED NI-12% Mo-7% Cr-Ti ALLOYS BY DEBYE SCHERRER X-RAY ANALYSIS

Heat	Heat-Treatments			Titanium Content (%)	Phases Present
	Solution Anneal (°C)	Age Time (hr)	Age Temperature (°C)		
198	1177	1500	650	None	M_2C
	1177	1500	760	None	M_2C
466535	1177	3000	650	0.15	(MC)[a] + M_2C
	1177	3000	760	0.15	M_2C
466548	1177	0		0.45	b
	1260	0		0.45	b
	1177	3000	650	0.45	MC
	1177	3000	760	0.45	(MC)[a] + M_2C
196	1177	1500	650	0.5	MC + M_2C
	1177	1500	760	0.5	MC + M_2C
467548	1177	0		1.2	MC
	1260	0		1.2	MC
	1177	3000	650	1.2	MC
	1177	3000	760	1.2	MC
	1260	3000	650	1.2	MC
	1260	3000	760	1.2	MC

[a]Minor amounts present.

[b]Too little second phase present to extract electrolytically.

addition (0.15% Ti) the MC-type carbide forms at 650° C in addition to M_2C type; however, at 760°C the MC is not stable and only M_2C exists. For the 0.45% Ti heat only MC was found at the lower aging temperature: at the higher age temperature, 760°C, minor amounts of MC are present, but primarily M_2C was found. The laboratory heat, alloy 196, with 0.5% Ti contained four precipitate phases after 1500 hours at 650°C, which were identified as two discrete MC-type carbides and two different M_2C-type carbides. At 760°C, however, only one MC-type phase and one M_2C-type phase were found. For the highest titanium content evaluated (1.2% Ti) only the MC-type carbide was found after aging for 3000 hours at 650 or 760°C.

These results show that adding titanium to this basic alloy has promoted the formation of an MC-type carbide and, furthermore, that higher concentrations of titanium stabilize the MC phase to higher aging temperatures. In alloys containing 0.5% Ti or less there is a transition in the type of carbide that is precipitated during aging at 650 and 760°C. The transition is from an MC-type at lower temperatures to an M_2C-type carbide at higher aging temperatures. In the 1.2% Ti alloy this transition is not found since only the MC-type carbide was identified.

Titanium carbide (TiC) was not found in any of the alloys listed in Table VII. Rather, the MC-type carbide corresponded to a range of lattice parameters from 4.21 to 4.28 angstroms (Å), based on the molybdenum-chromium-carbon system,[65] which is smaller than the 4.33 Å parameter for TiC. However, small amounts of titanium in the alloy

affected the composition of the MC phase as discussed in the following section.

The M_2C carbide actually has an orthorhombic crystal structure, but the x-ray diffraction pattern of the M_2C phase can be indexed based on the hexagonal crystal structure. Two particular unit cells were found for the M_2C phase in these alloys (Table XVII, Appendix). One structure had the cell parameter a = 2.92, c = 4.58, c/a = 1.57, and the other structure had a = 2.98, c = 4.69, c/a = 1.57. The compositional differences of these two M_2C carbides was not determined.

1. Chemical analysis of phases. In order to study the increased stability of the MC phase with titanium content, milligram quantities of second phase MC-type carbides were extracted from the samples aged at 650°C, where primarily MC was precipitated. Using both a microprobe attachment to the electron microscope and quantitative spark emission spectroscopy techniques, the concentration of molybdenum, chromium, and titanium in the carbides was determined.

The metallic composition (normalized to 100%) of molybdenum, chromium, and titanium from the spectroscopic technique is given in Figure 21 as a function of the titanium content of the alloy from which the precipitates were extracted. The results show an increase in the titanium content and a decrease in chromium content of the MC phase with increasing titanium in the alloy. The change in the molybdenum concentration of the MC phase is not clear from the results in Figure 21, but one would expect it to change only slightly if titanium were

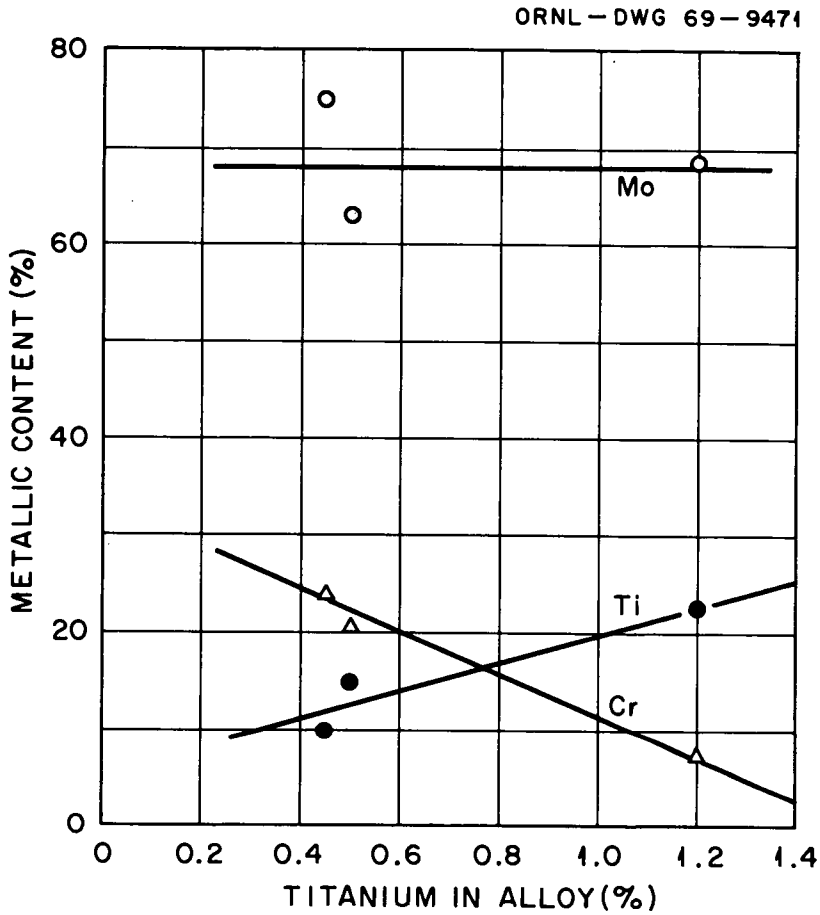

Figure 21. Spectroscopic analysis of metallic content of MC-type carbides extracted from titanium modified Ni-12% Mo-7% Cr-0.07% C alloys.

substituting for chromium in the precipitate. The replacement of either chromium or molybdenum with increasing titanium in the alloy would be possible, however, since the observed increase in lattice parameter of MC from 4.21 to 4.28 Å (Table XVII, in the Appendix) is consistent with the fact that the atomic diameter of titanium (2.93 Å) is larger than either that of chromium (2.57 Å), or molybdenum (2.80 Å).[66] As mentioned previously, the observed parameters of these MC carbides were significantly lower than that reported for TiC which is 4.33 Å.

Similar chemical analyses were made on samples that contained primarily M_2C carbides. In this case M_2C was rarely present as a single phase and the trends with titanium content in the alloy were not clear. The results indicated that the M_2C phase of the 0.15% Ti heat contained molybdenum and chromium, but no titanium. It is possible that titanium does not affect the M_2C, but only the composition and stability of the MC carbide.

B. Optical Metallography

1. Metallography of laboratory heats. The effect of carbon content on the structure of the Ni-12% Mo-7% Cr-0.5% Ti alloy is shown in Figures 22-24. The influence of 0.5% Ti on microstructures can be found from comparing the alloy without titanium (heat 198) with the alloy containing titanium and 0.05% C (heat 196) in Figures 22 and 23.

The microstructures in Figure 22 show that solution annealing at 1260°C followed by water quenching produces a single-phase alloy for carbon contents below 0.05%. Solution annealing at 1177°C followed by

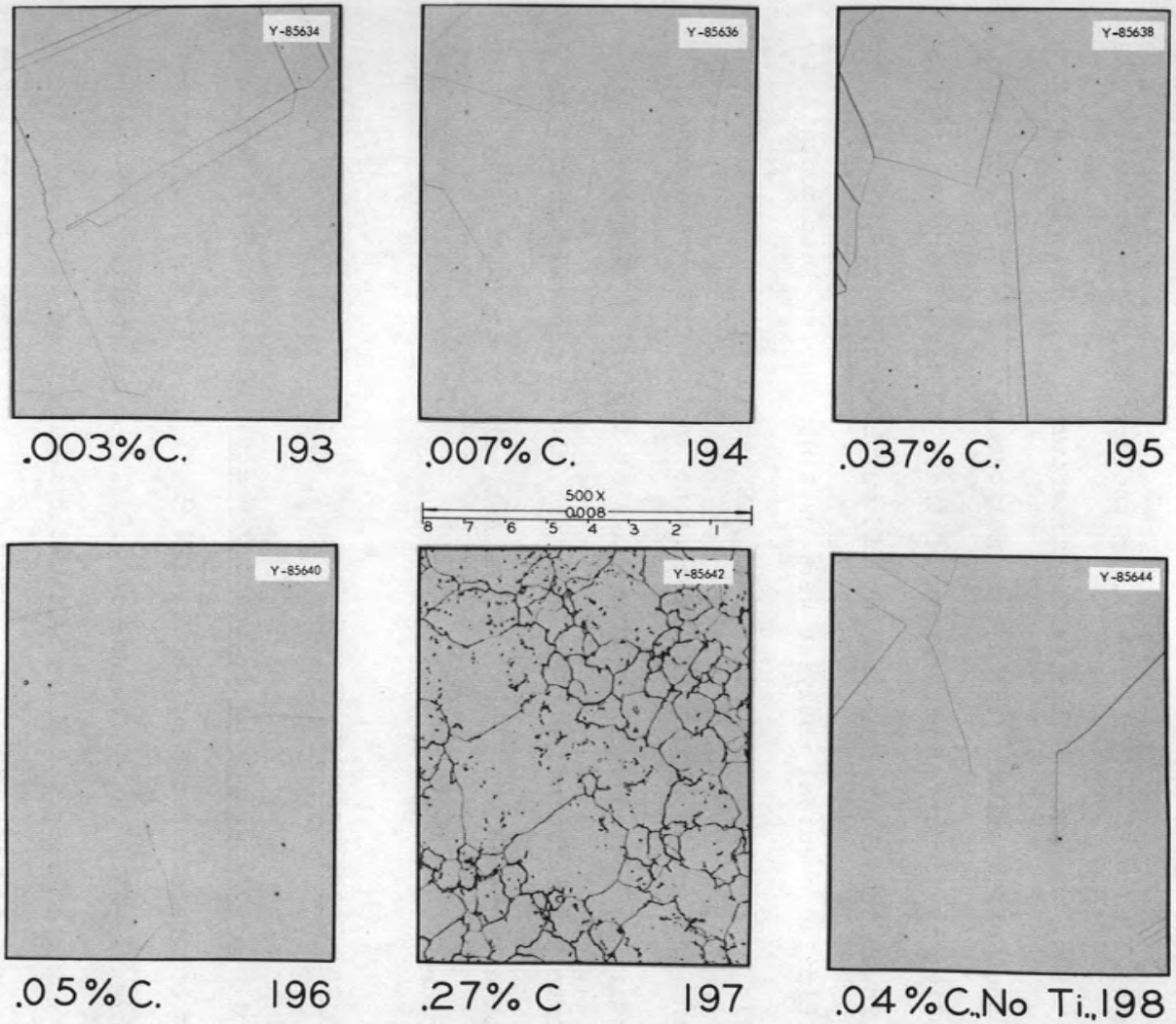

Figure 22. Effect of carbon on the microstructure of Ni-12% Mo-7% Cr-0.5% Ti alloys solution annealed one hour at 1260°C and water quenched.

PHOTO 91879

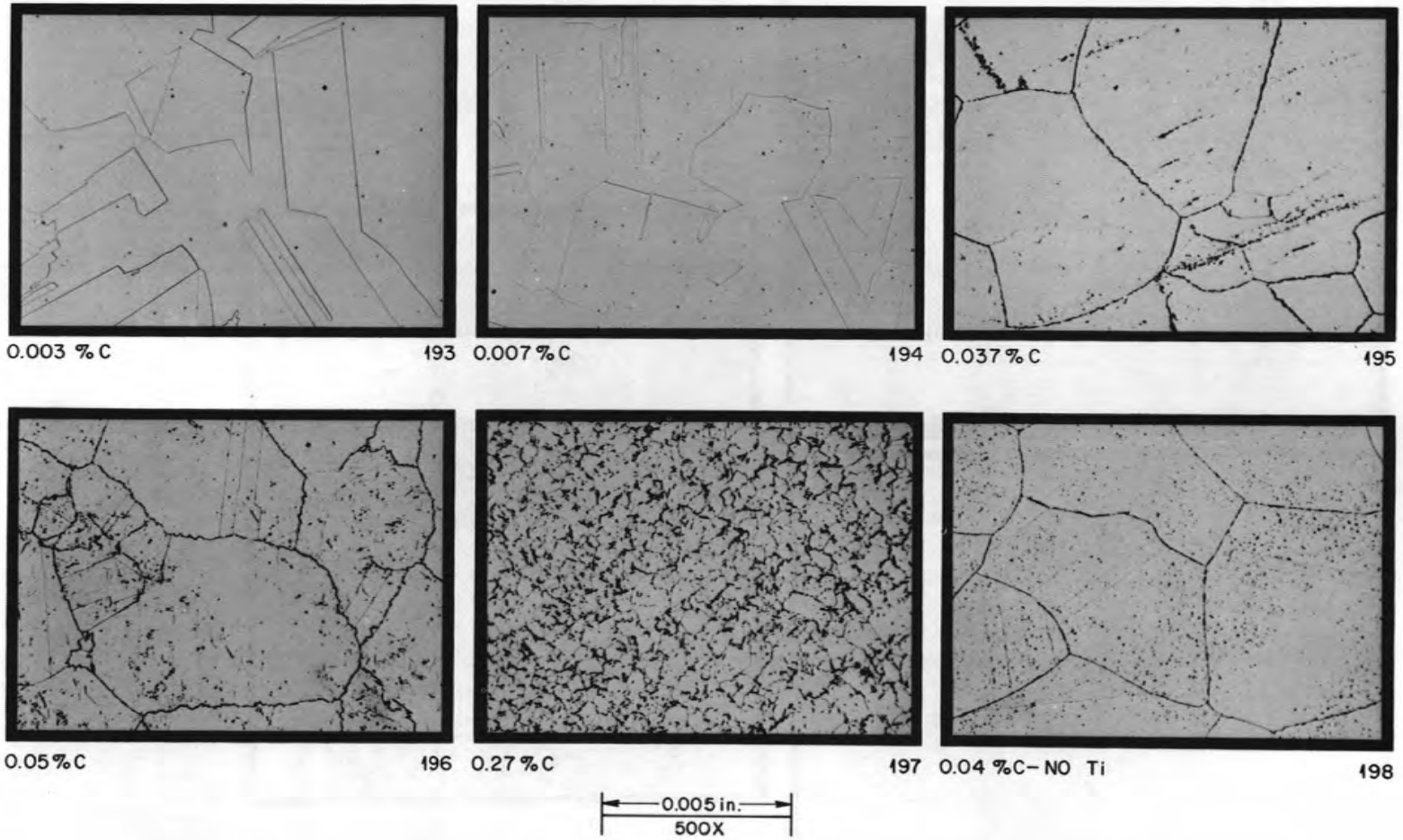

Figure 23. Effect of carbon on the microstructure of Ni-12% Mo-7% Cr-0.5% Ti alloys solution annealed one hour at 1177°C and aged 100 hours at 870°C.

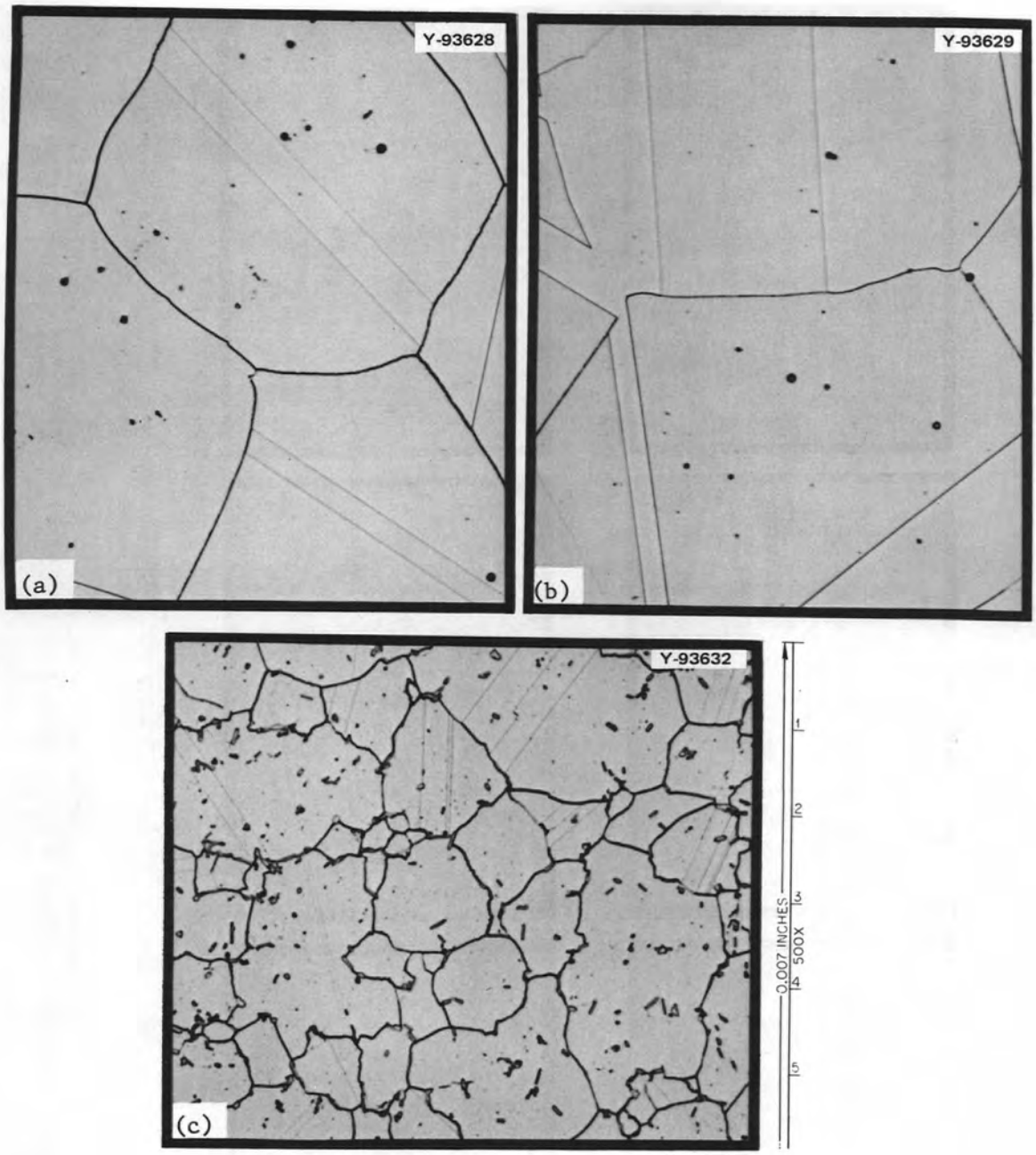

Figure 24. Effect of high carbon concentrations on the microstructure of Ni-12% Mo-7% Cr-0.5% Ti alloys solution annealed one hour at 1260°C and water quenched. (a) Alloy 238-0.1% C, (b) Alloy 239-0.15% C, (c) Alloy 242-0.32% C.

water quenching also produces a single-phase alloy. In contrast to this, slow cooling within the cold zone of the furnace (80°C per minute) from either of the two annealing temperatures produces a small amount of second phase. The structure produced by solution annealing at 1177°C, and aging 100 hours at 870°C is shown in Figure 23. Rather coarse precipitates are evident optically for carbon contents of 0.007% and higher. That there is some precipitation in the sample containing 0.003% C was confirmed by transmission electron microscope.

Precipitate distributions in a second set of alloys containing carbon contents between 0.1 to 0.32% are shown in Figure 24 for the 1260°C solution annealed and water-quenched condition. The grain size for alloys with less than 0.15% C is comparable to that of the lower carbon alloys (Figure 22). For the 0.32% C alloy second-phase particles have limited the grain growth significantly and the sample has a finer grain size. Transmission microscopy of the 0.32% C sample showed continuous grain boundary precipitates in addition to the large carbides that are visible optically.

Figure 25 shows the microstructure produced by a one hour heat treatment at either 1040°, 1095°, 1177°, or 1260°C. This alloy composition (Ni-12% Mo-7% Cr-0.5% Ti-0.05% C) corresponds to carbon contents in the midrange between the high and low contents evaluated in creep. The structures produced at 1040° and 1095°C are similar. Increasing the temperature from 1095° to 1177°C causes a significant increase in grain size and a decrease in the amount of second phase. Small differences in grain size for the 1177° and 1260°C treatments were evident in optical metallography at this carbon content.

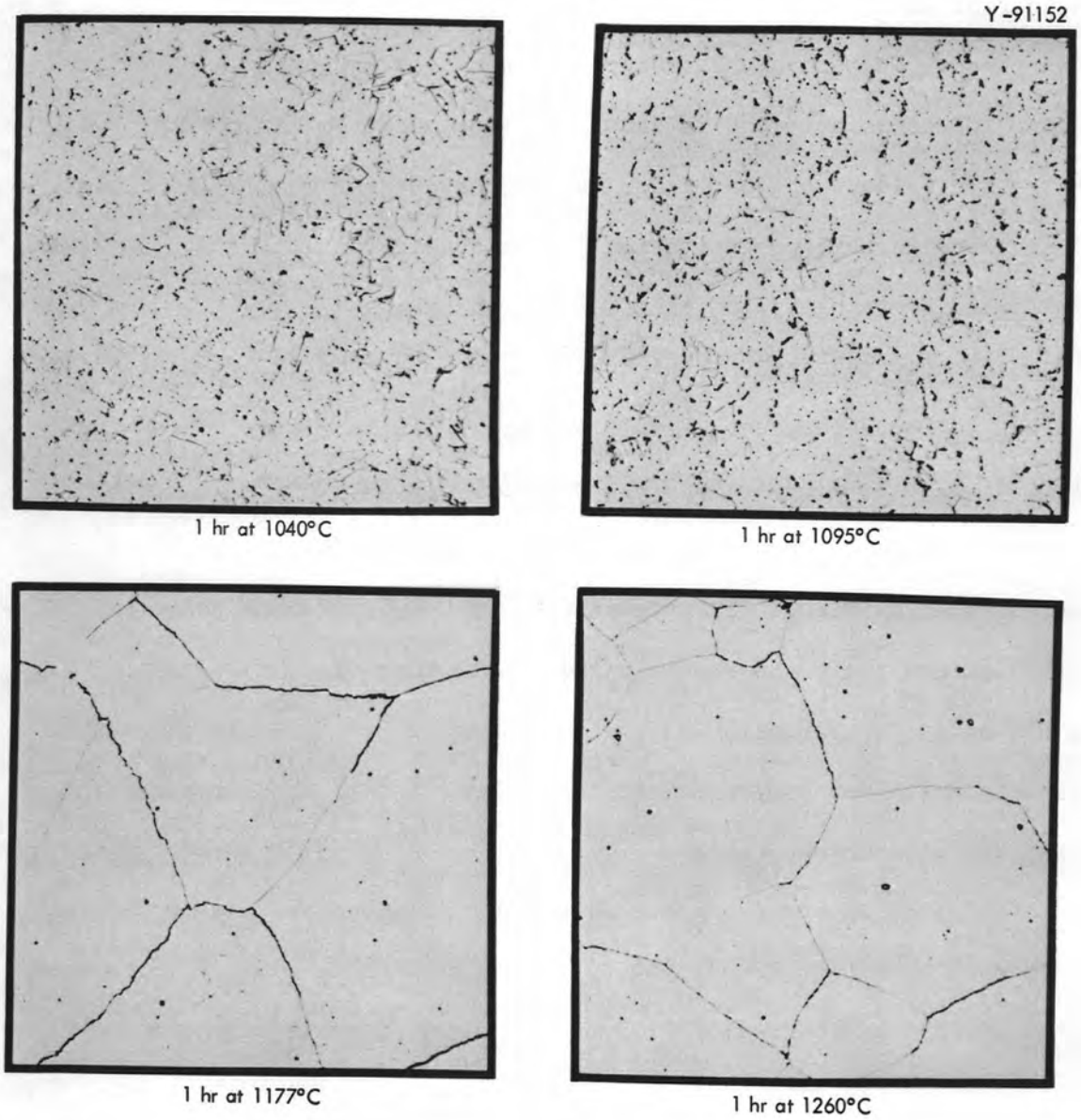

Figure 25. Changes in microstructure produced by varying the solution annealing temperature from 1040° to 1260°C for a Ni-12% Mo-7% Cr-0.5% Ti-0.05% C alloy.

2. Metallography of aged commercial heats. The effect of solution annealing temperature on the structure of alloys with three titanium contents and nominally 0.07% C are shown in Figure 26. An 1177°C anneal does not produce a single phase alloy and the grain size varies with titanium content, but not in a consistent manner. The highest titanium alloy, 1.2% Ti, has large amounts of stringers which are made up of clusters of second phase particles. The grain size for each heat after one hour at 1260°C is larger by a factor of two to four than that for an 1177°C anneal. The amount of second phase differs significantly for these two treatments only at the 1.2% Ti level.

The microstructures for the aged conditions were taken from tensile samples tested one to four hours at 650°C after the specific aging treatment. Aging 3000 hours at 650°C produces heavy concentrations of grain boundary precipitates at each titanium concentration. Matrix precipitation is more extensive in the two lower titanium heats, but in the 1.2% Ti heat large patches of precipitates are present that were not taken into solution during heat treatment at 1177°C. Figure 27 compares the microstructure of the alloys with the four titanium concentrations at areas near the tensile fracture after aging 3000 hours at 760°C. No important differences are evident at this magnification for the three lower titanium levels. The 1.2% Ti alloy shows a banded structure due to precipitate stringers remaining from the preanneal structure. Figure 28 shows the structure of specimens from two heats aged 3000 hours at 650° and 760°C. The areas photographed were near the tensile fracture. Interference contrast microscopy was used to reveal the second phases

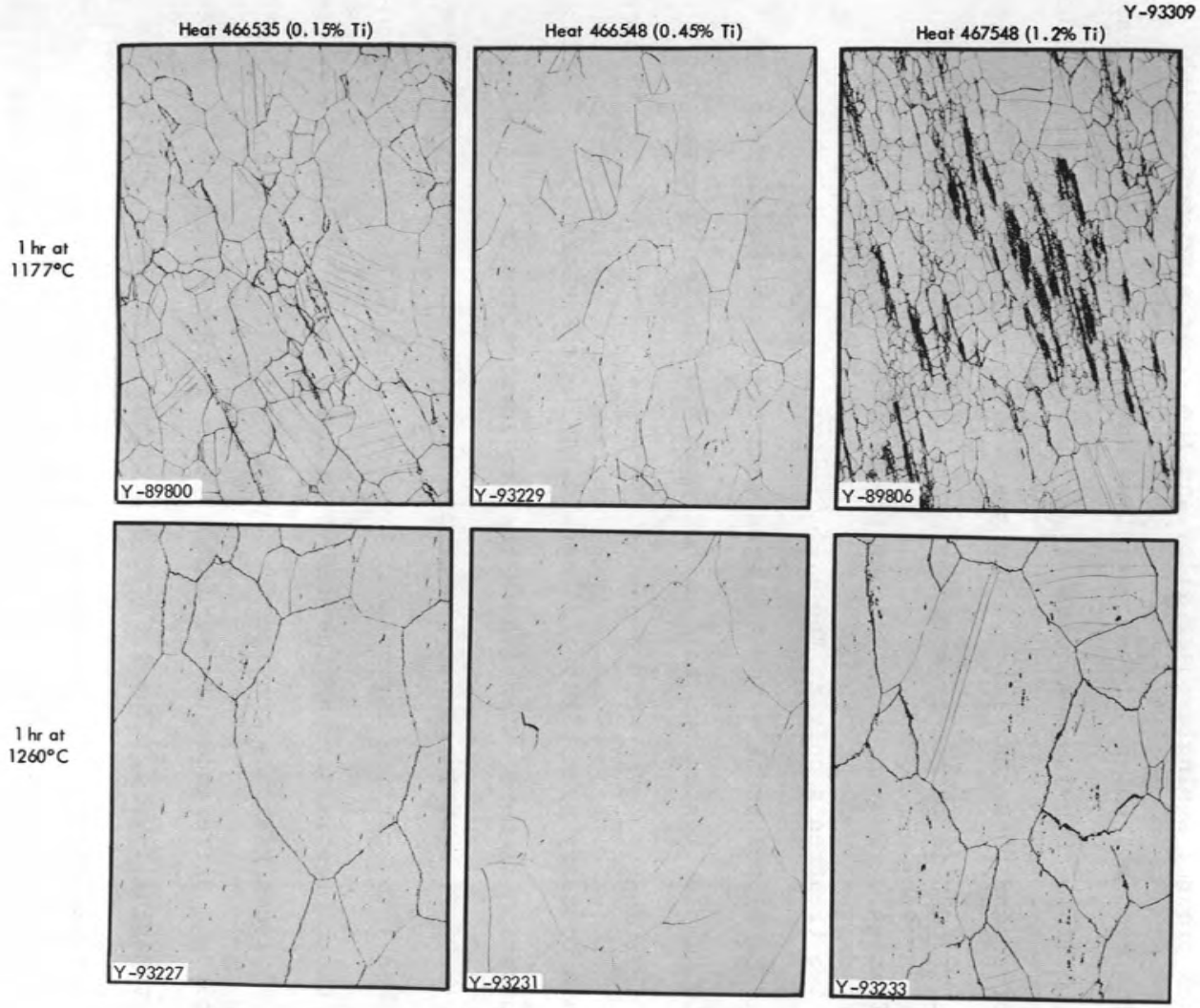

Figure 26. Effect of solution annealing and titanium content on the microstructure of commercial Ni-12% Mo-7% Cr-0.07% C alloys.

Y-88809

1 HOUR AT 1177°C PLUS 3000 HOURS AT 760°C

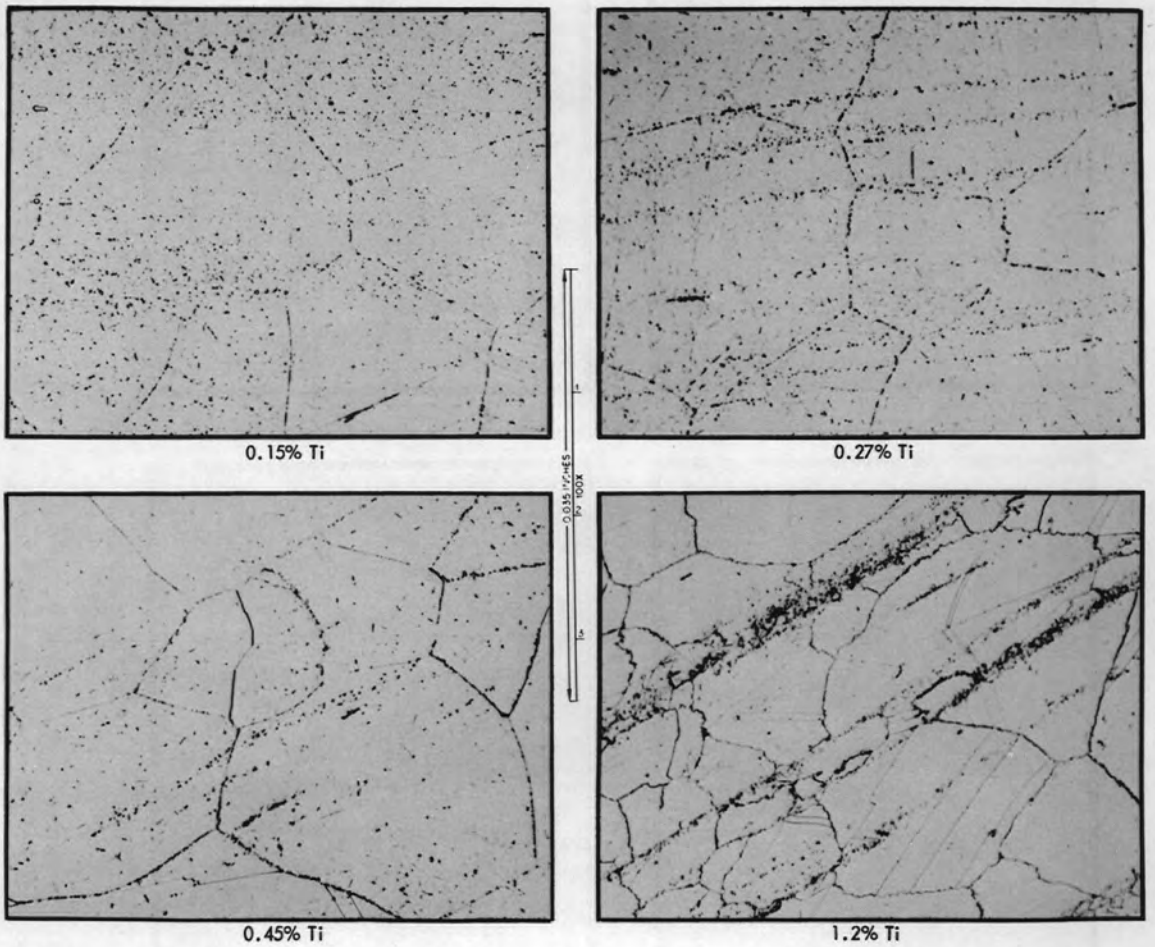

Figure 27. Microstructure of commercial heats of Ni-12% Mo-7% Cr-0.07% C alloy after aging 3000 hours at 760°C (100x).

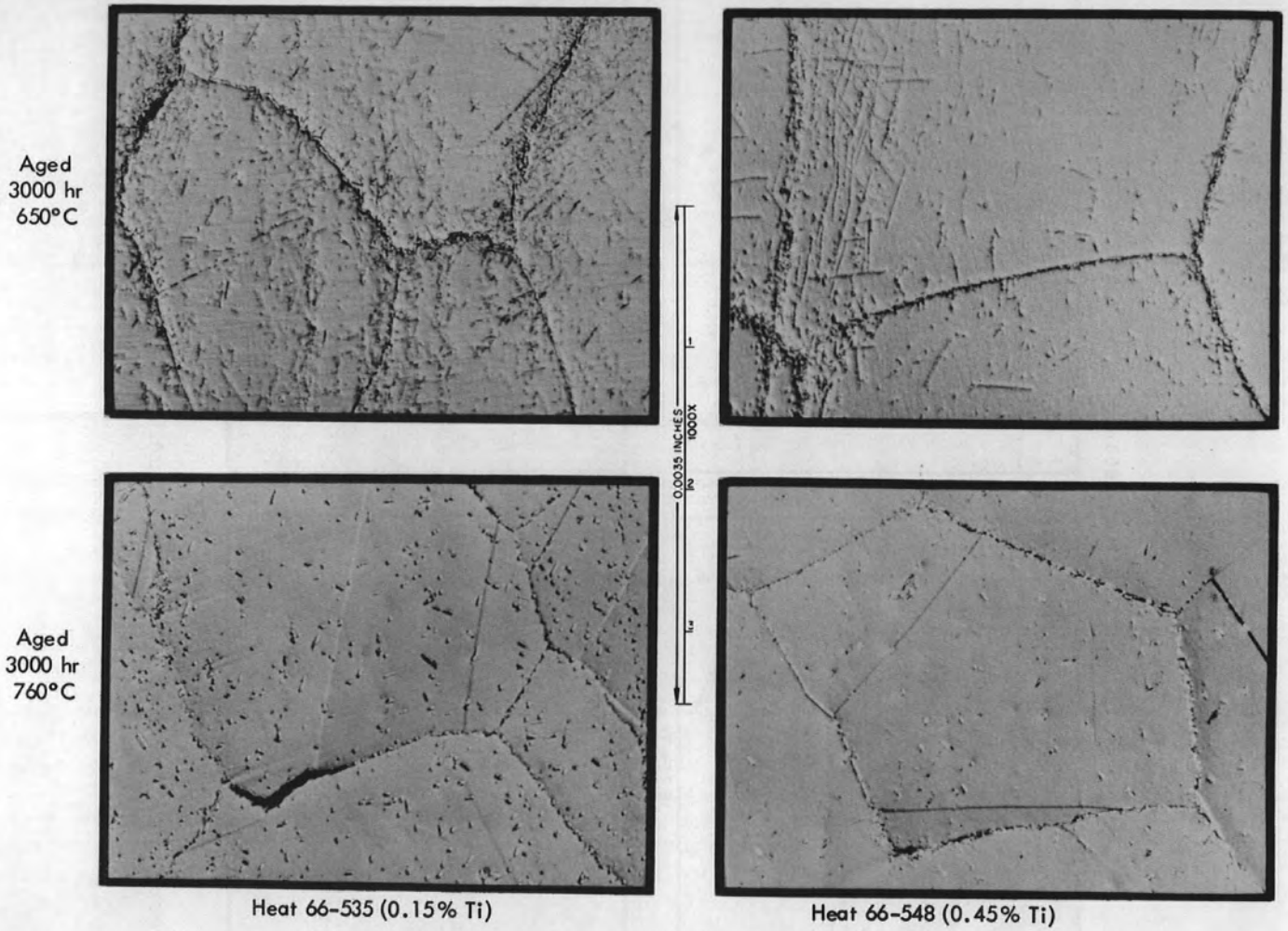

Figure 28. Comparison of structures of aged Ni-12% Mo-7% Cr-0.07% C alloys using interference contrast microscopy.

particles. Note that at this magnification (about 700×) a marked difference in the precipitate distribution is evident after aging at 650 and 760°C. For both levels of titanium shown, 0.15 and 0.45%, the 650°C structure is characterized by a continuous grain boundary precipitate and also by acicular carbide needles near the boundary. These needles are more apparent in this particular figure for the 0.45% Ti heat. The 760°C structure is characterized as having cleaner grain boundaries, but with coarse precipitate particles along the boundary and randomly distributed within the matrix.

C. Transmission Electron Microscopy

1. Laboratory heats. The amount of microscopy conducted on the alloys creep tested to determine the effect of carbon content was limited because of the large differencesin rupture lives and thus in time at temperature during testing. The structural differences were compared for the alloy with no titanium (heat 198) and with 0.5% Ti and 0.05% C (heat 196) after annealing 1500 hours at 760°C. The grain boundary carbide distributions are shown in Figure 29. The alloy without titanium, Figure 29(a), had only M_2C carbides and the predominate morphology is a smooth spherical precipitate, which forms a nearly continuous array of particles along grain boundaries as shown. Adding 0.5% Ti to this basic alloy promotes the formation of MC carbides as discussed previously, but some M_2C is also present. The morphology of the precipitates in the alloy with titanium, Figure 29(b), is significantly different than in the titanium-free alloy. The grain boundaries contain acicular

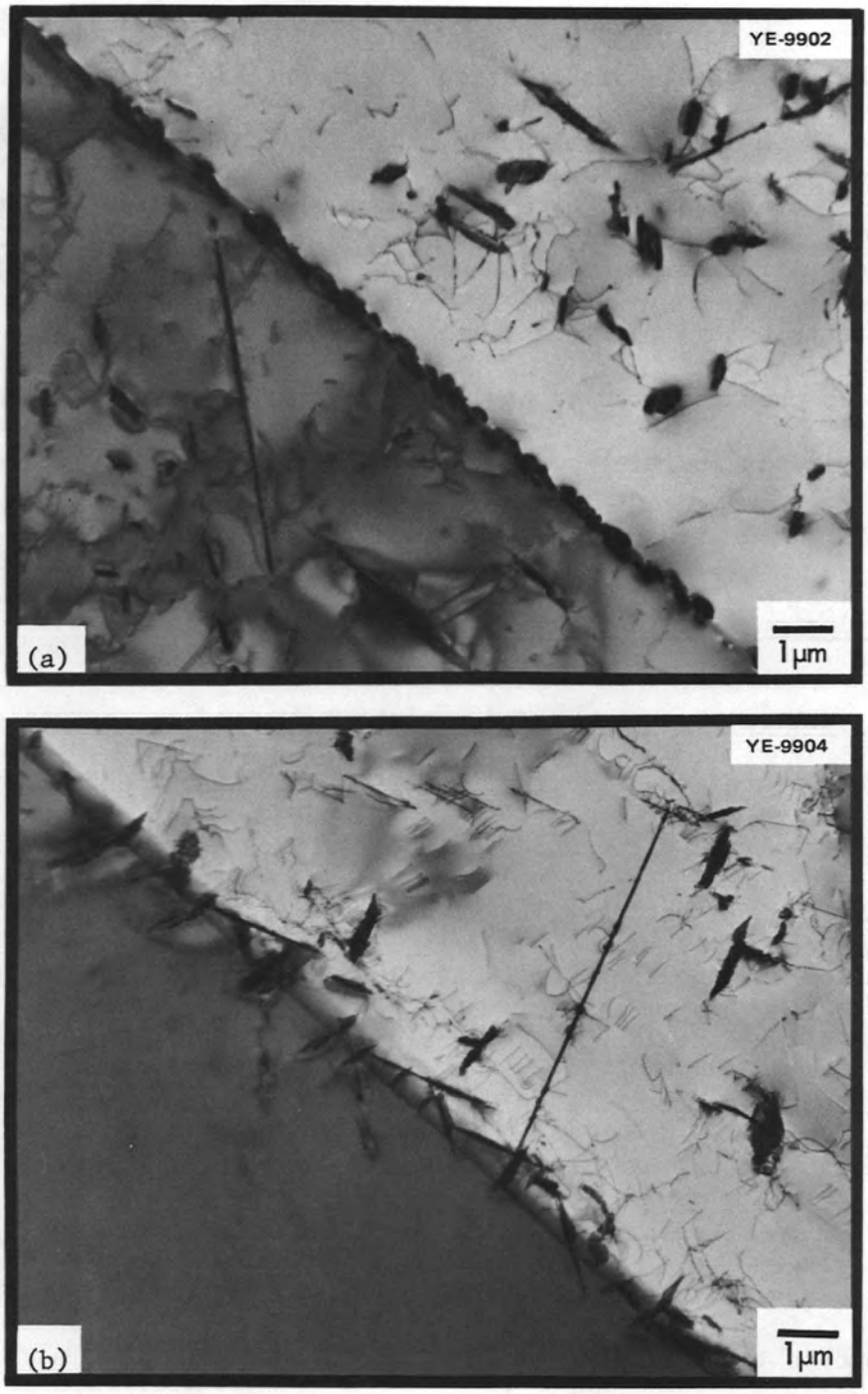

Figure 29. Grain boundary carbides in laboratory heats of Ni-12% Mo-7% Cr-0.05% C alloys after aging 1500 hours at 760°C. (a) Alloy 198, no titanium, (b) Alloy 196, 0.5% titanium.

precipitates (assumed to be MC-type) spaced at approximately 0.5 to 2 micron intervals and extending into the matrix.

2. Aged commercial heats. The structures produced as a function of titanium content, preage treatment, aging time, and aging temperature were assessed in order to correlate precipitate distribution and morphology with the corresponding creep and tensile behavior.

Precipitate distribution. Figures 30 and 31 compare the grain boundary precipitate distribution produced by an 1177°C solution anneal and 3000 hour age at either 650°C or 760°C. The figures, which are, unfortunately, at different magnifications, correspond to the samples exhibiting the tensile properties shown in Figure 13, page 60, and the creep properties in Figure 12, page 56. At 650°C (Figure 30) alloys with the intermediate and high titanium levels develop a pronounced grain boundary carbide distribution of MC, which was the only phase identified by x-ray diffraction. This carbide is characterized as follows: an apparently continuous array of precipitate within the boundary, a heavy concentration of rounded and elongated precipitates (0.1 to 2 microns long) adjacent to the boundary, and still others of the same form lying within the boundary but extending well into the grain interior. In the 0.15% Ti heat at 650°C, Figure 30, both MC and M_2C were identified by x-ray diffraction, and the precipitate morphologies include 1-micron rounded particles (M_2C type), spaced along grain boundaries at 1 to 2 micron intervals, and a second type of elongated precipitate within the matrix (presumed MC-type), which was 1 to 5 microns in length and 0.1 to 0.5 micron wide for this particular grain orientation.

Y-96031

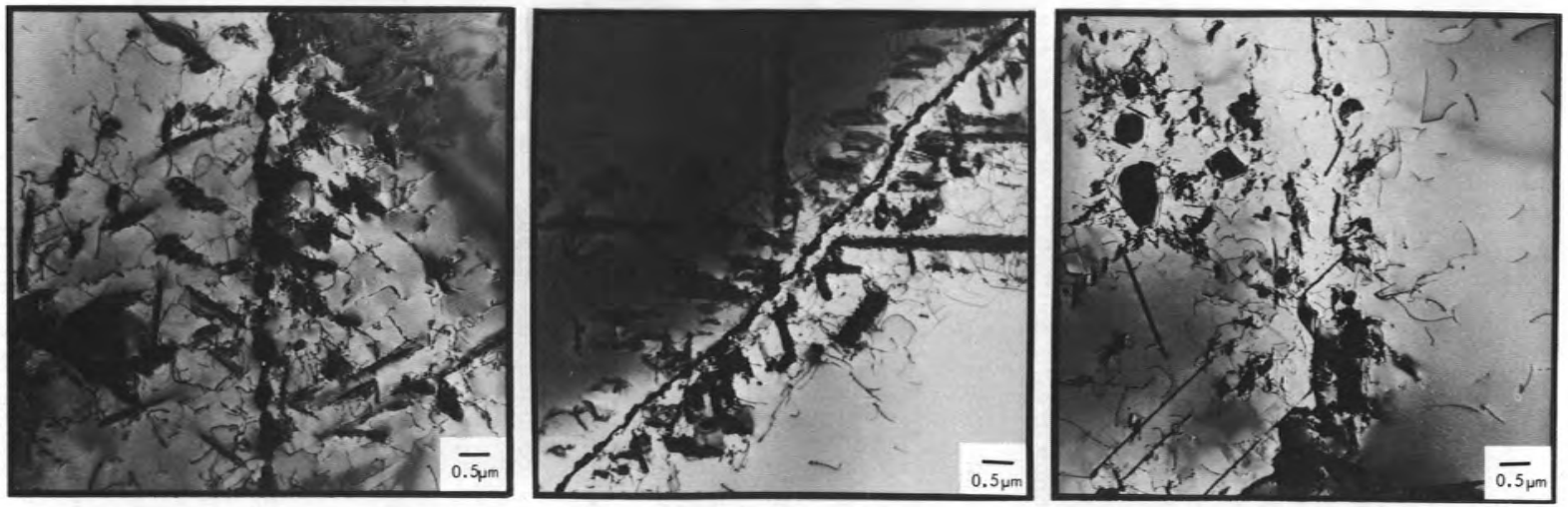

0.15% Ti M_2C + MC 0.45% Ti MC 1.2% Ti MC

Figure 30. Carbide distribution as a function of titanium content in Ni-12% Mo-7% Cr-0.07% C alloy after aging 3000 hours at 650°C (solution annealed one hour at 1177°C).

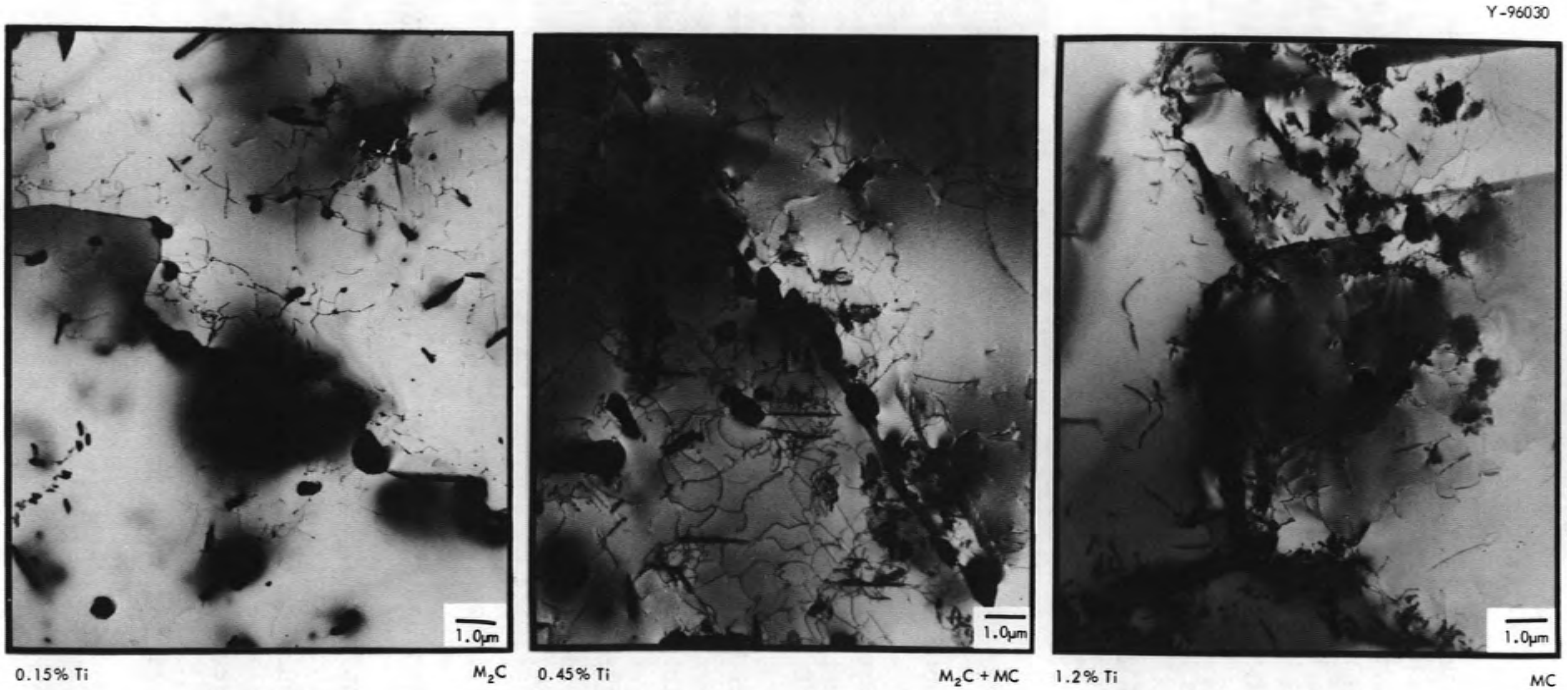

Figure 31. Carbide distribution as a function of titanium content in Ni-12% Mo-7% Cr-0.07% C alloy after aging 3000 hours at 760°C (solution annealed one hour at 1177°C).

After the 760°C aging treatment (Figure 31), the low titanium (0.15%) heat has a low concentration of rounded second phase particles along the grain boundaries and a large amount of precipitate within the matrix (both M_2C type). The intermediate and high titanium material exhibit less grain boundary precipitation than was found for these same heats at 650°C, but compared to the heats with lower titanium contents at 760°C the grain boundary precipitate density is appreciably higher. However, the 0.45% Ti alloy now contained some M_2C carbides in addition to the MC carbide (Table VII, page 77).

Although not shown, matrix precipitation within these alloys after aging 3000 hours was much more extensive at the lower titanium concentrations. Precipitates in the matrix of the 0.15% Ti alloy were heavy for the 650°C age, with primary MC carbides and elongated M_2C carbides being the predominate types observed. Aging this same alloy at 760°C produced a lower concentration of precipitate than found at 650°C, but the size was generally larger and the type was M_2C. In the 1.2% Ti heat the majority of the second phase was large primary MC carbides which were not put into solution during prior solution annealing. However, in some regions where a heavy concentration of primary carbides existed a different type of morphology, precipitates on stacking faults, was found. A discussion of this unusual precipitate morphology is given in the following section. Generally, the electron microscopy observations confirm the conclusions drawn from the optical microstructures shown in Figure 28, page 90, for these commercial alloys.

Precipitates on stacking faults. The main difference in precipitation on aging after an 1177° and a 1260°C solution anneal was that after the 1260°C treatment precipitates were found on stacking faults when observed in the electron microscope. The formation of this precipitate morphology was responsible for a large change in the mechanical properties of some of the alloys studied; thus, the conditions of its formation was investigated. The formation of this precipitate morphology apparently involves precipitation of a certain type of carbide on partial dislocations. The simultaneous growth of the precipitates and the separation of the two partial dislocations creates a stacking fault, the nature of which will be considered in the discussion of results. The appearance of this precipitate distribution is considered in this section.

Typical appearance of the stacking faults precipitate structure after solution annealing at 1260°C and aging 3000 hours at 650 and 760°C is shown in Figures 32-34 for the 1.2% Ti alloy. The most extensive formation of this type of precipitate occurred for the 1.2% Ti heat after annealing at 1260°C and aging at 760°C. This morphology was also found for the lowest titanium level, 0.15% Ti after the 1260°C anneal and 650 age, but was rarely observed in the 0.45% Ti alloy.

Precipitation on stacking faults was much more rapid at 760°C than at 650°C and the extent of growth of the stacking fault ribbons after 3000 hours of aging at these two temperatures is compared in Figure 32. In many instances, a primary MC carbide appears to be at the center of a stacking fault rosett, which implies that dislocations around the primary carbide may act to nucleate the stacking fault ribbons. The

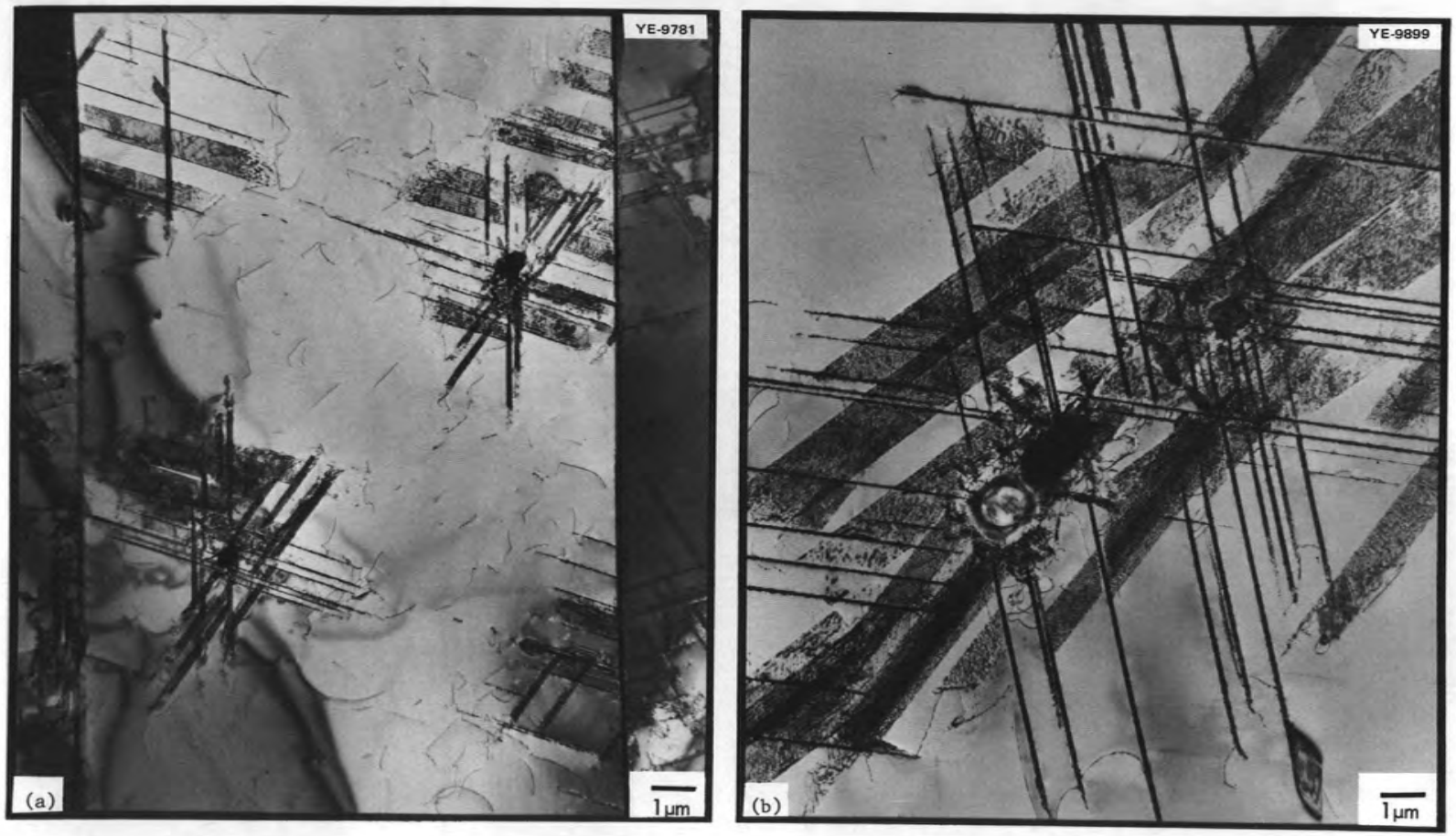

Figure 32. Precipitation of MC carbides on stacking faults in a Ni-12% Mo-7% Cr-1.2% Ti-0.08% C alloy (annealed at 1260°C and aged (a) 3000 hours at 650°C and (b) 3000 hours at 760°C).

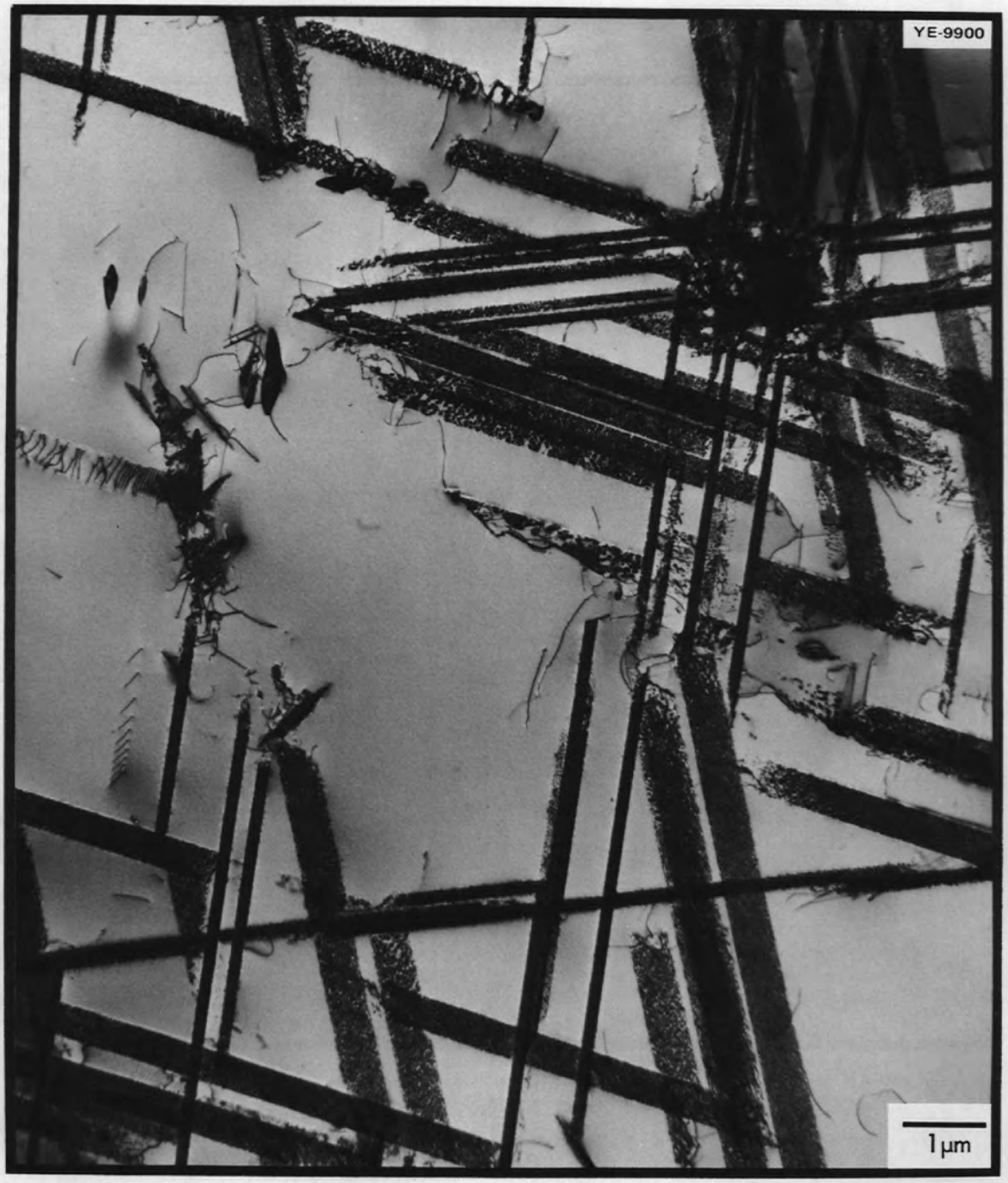

Figure 33. Precipitates on stacking faults in the 1.2% Ti heat of Hastelloy-N solution annealed one hour at 1260°C and aged 200 hours at 760°C.

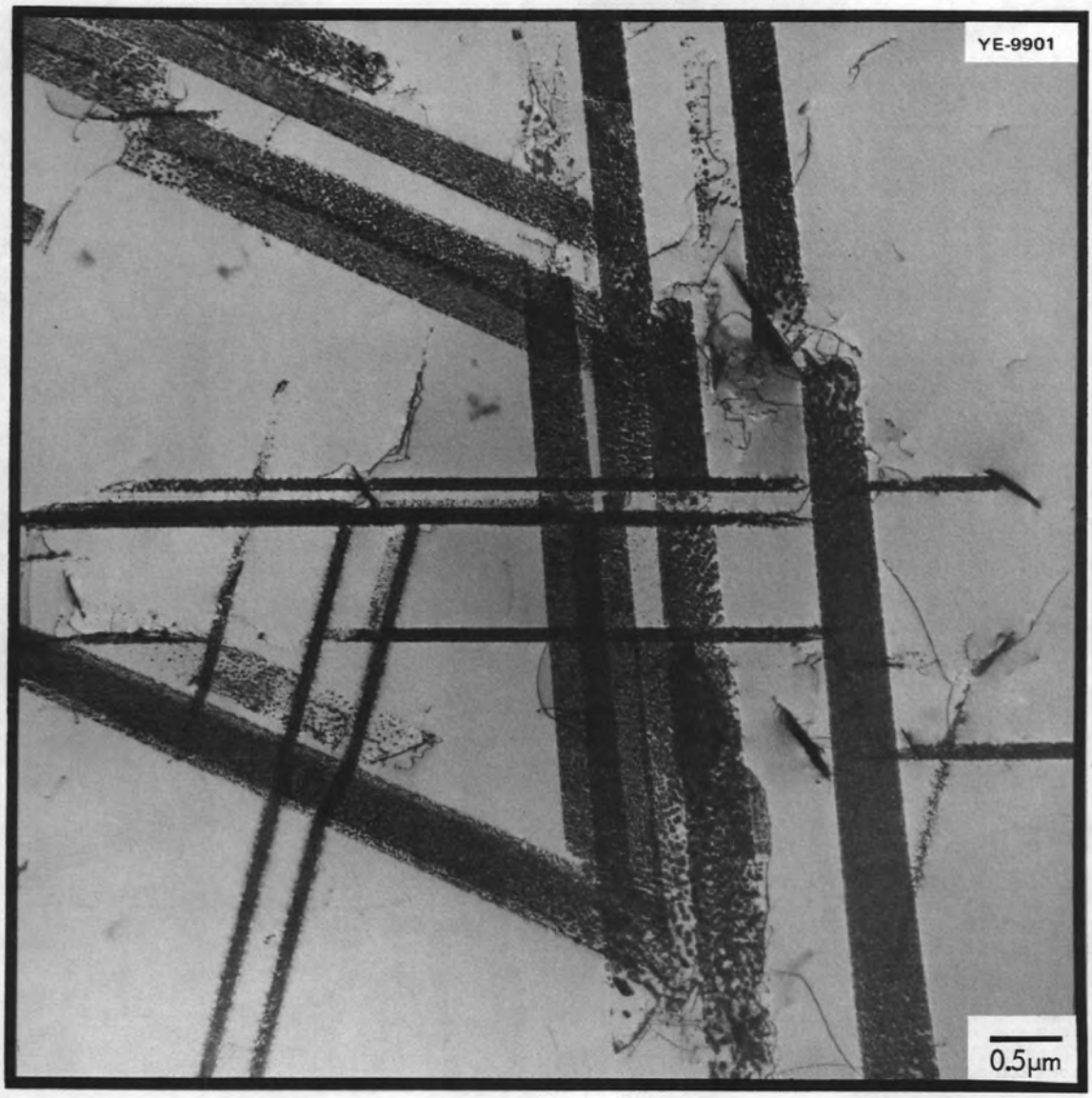

Figure 34. Precipitates on stacking faults in the 1.2% Ti heat of Hastelloy-N solution annealed one hour at 1260°C and aged 10,000 hours at 760°C.

relative size and distribution of the stacking fault precipitate formed at 650 and 760°C and shown in Figure 32 is representative. In Figure 32(a) a twin boundary visible in this microstructure appears to stop the growth of the stacking fault. No denuding of precipitate was evident at twin boundaries.

The development of the stacking fault precipitate as a function of aging time at 760°C is shown in Figures 33 and 34. The structures after 200 (Figure 33) and 10,000 hours (Figure 34) at 760°C show very little difference in the relative size and distribution of the stacking fault ribbons themselves, although the actual precipitate particles on the stacking faults are coarser in the 10,000-hour sample. For longer aging times the characteristic stacking fault contrast fringes were not evident. This indicates that the second phase precipitated and grew with the separation of the partial dislocations, but at some later time as the precipitates coarsened and coherency was lost the stacking fault contrast was eliminated probably by the partial dislocations recombining to form a total dislocation.

The distribution of stacking fault precipitates near grain boundaries is shown in Figure 35. In the grains in which the faults are in sharp contrast, there is a very small (0.1 micron) denuded region adjacent to the boundary. In the opposite grains there is a heavy concentration of faults at the boundary and extending into the matrix.

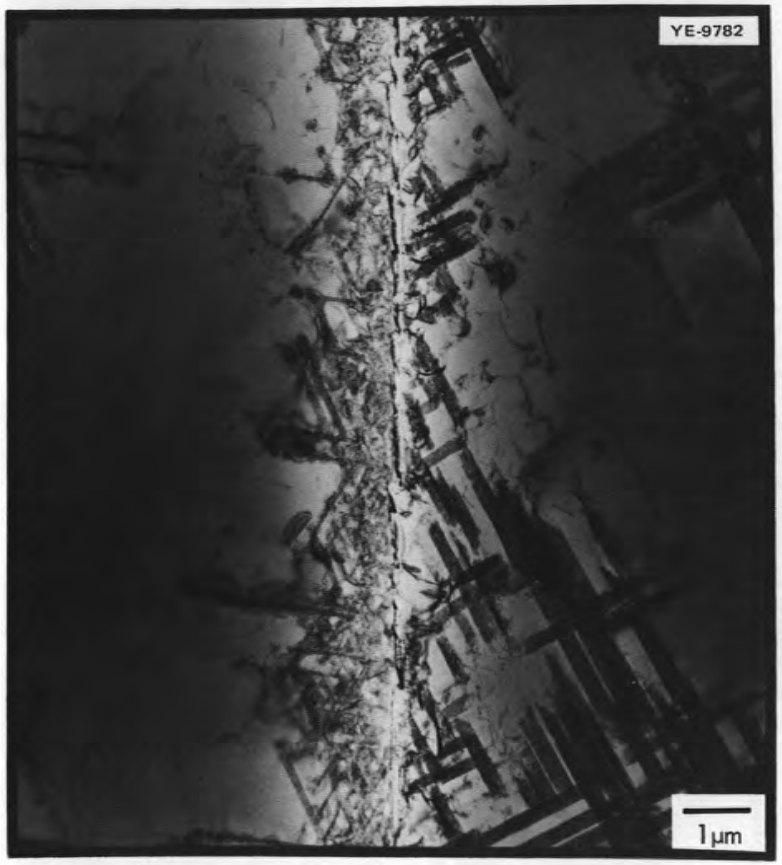

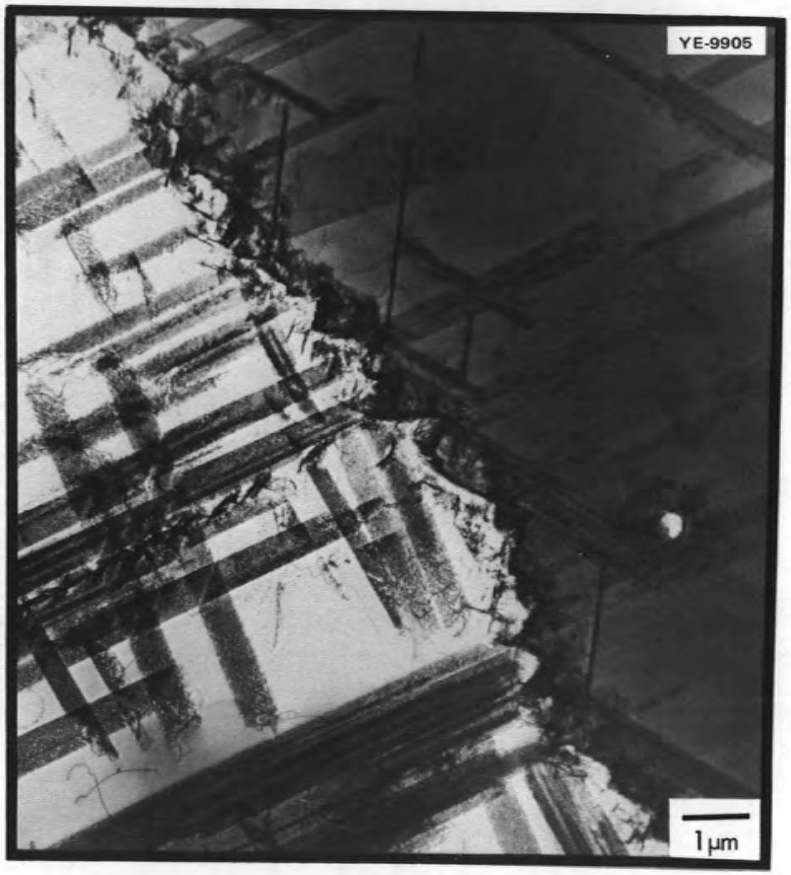

Figure 35. Grain boundary structures after a 1260°C solution anneal and 3000 hour age at 760°C in a sample of Hastelloy-N exhibiting stacking fault precipitates.

D. Precipitate Characterization from Extraction Replicas

As evident from Table VII, page 77, titanium in Hastelloy-N promotes the stability of MC rather than M_2C carbides. The relative amounts of these two phases depends on both the aging temperature and the titanium content of the alloy. At higher titanium contents only the MC phase was found.

Observing the precipitate morphology and distribution as a function of titanium content for alloys aged at 760°C defines the transition in structure that this composition change introduces. Figure 36 shows such a series of electron micrographs of extraction replicas obtained from the unstressed portion of tested tensile samples aged 3000 hours at 760°C after an 1177°C anneal. The phases present were determined by x-ray diffraction and are noted below each micrograph. Although a given phase can exist in a number of morphologies, the M_2C phase generally has the form of large (approximately 0.2 to 2.0 micron) elongated and irregularly shaped particles which are evident for the 0.15% Ti alloy in Figure 36. Matrix precipitation of MC occurred in two general morphologies: (1) large spherical primary carbide between 0.1 and 1.0 micron diameter, or (2) very fine particles (less than 0.1 micron) usually on stacking faults but within the matrix for some heat-treatments.

The primary MC carbides remain in large numbers after an 1177°C solution anneal (Figure 26, page 88), but the concentration was significantly reduced by annealing at 1260°C. However, in the 1.2% Ti heat after a 1260°C anneal and age treatment, the remaining primary MC precipitates were invariably associated with stacking fault precipitates

Y-94416

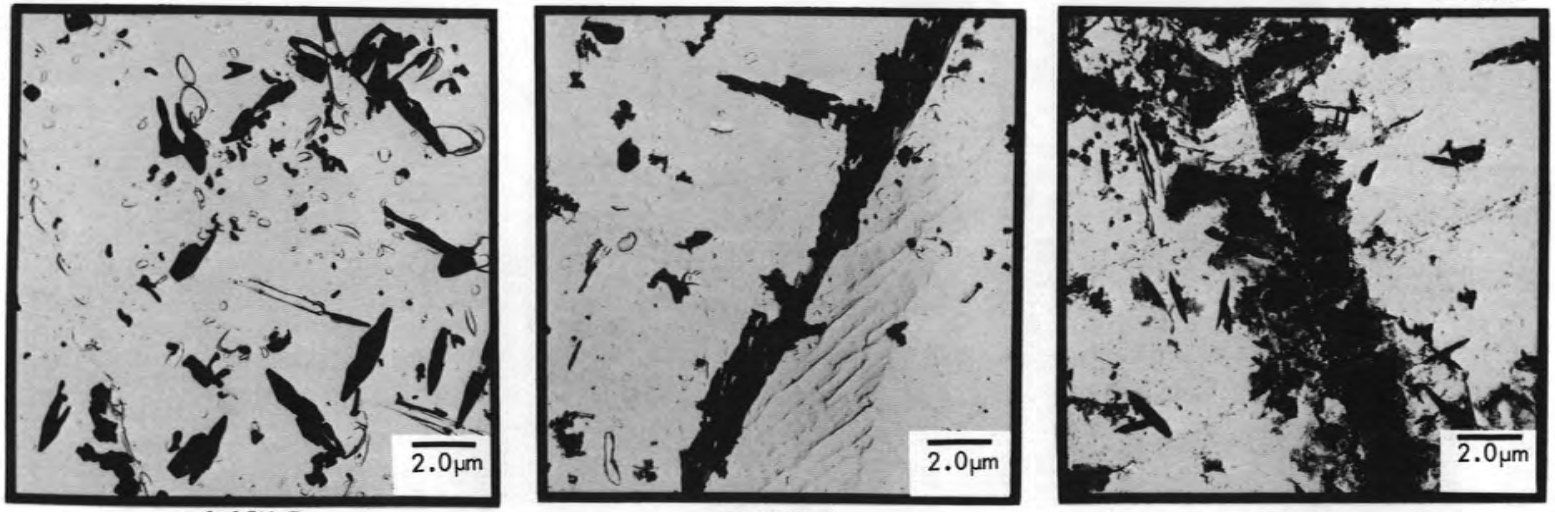

0.15% Ti
M_2C

0.45% Ti
$M_2C + MC$

1.2% Ti
MC

Figure 36. Precipitates on extraction replicas obtained from samples of Hastelloy-N solution annealed at 1177°C and aged 3000 hours at 760°C.

as shown in Figure 32, page 98. At the grain boundaries, the MC carbide takes the form of thin platelets (or discontinuous sheets) of precipitate that often appear quite massive, as shown for the 1.2% Ti heat in Figure 36.

E. Fracture Characterization

1. Optical examinations. The fracture behavior of these materials is a critical function of the precipitate phases and morphologies present after a given thermal treatment, as discussed previously. Although no specific experiments were aimed at studying the mechanistic aspects of the fracture process, several fractured samples were examined optically and by scanning electron microscopy. The fracture processes are considered to be controlled primarily by precipitation reactions in the nickel-molybdenum-chromium-carbon system. Binary nickel-titanium alloys were examined optically after both creep and tensile testing at 600°C.

Figure 37 compares the fracture of specimens creep tested at 650°C and 40,000 psi. These specimens represent the extremes of composition investigated in this study. In the top portion of the figure high and low carbon contents are shown for an alloy with Ni-12% Mo-7% Cr-0.5% Ti. In the bottom half of the figure two alloys with nominal carbon content (Ni-12% Mo-7% Cr-0.05% C) with and without 0.5% Ti are shown. The total creep elongation for the four samples in Figure 37 from top-left to bottom-right was 20, 15, 17, and 12%, respectively. Although the rate of creep deformation varied significantly for these four tests, the

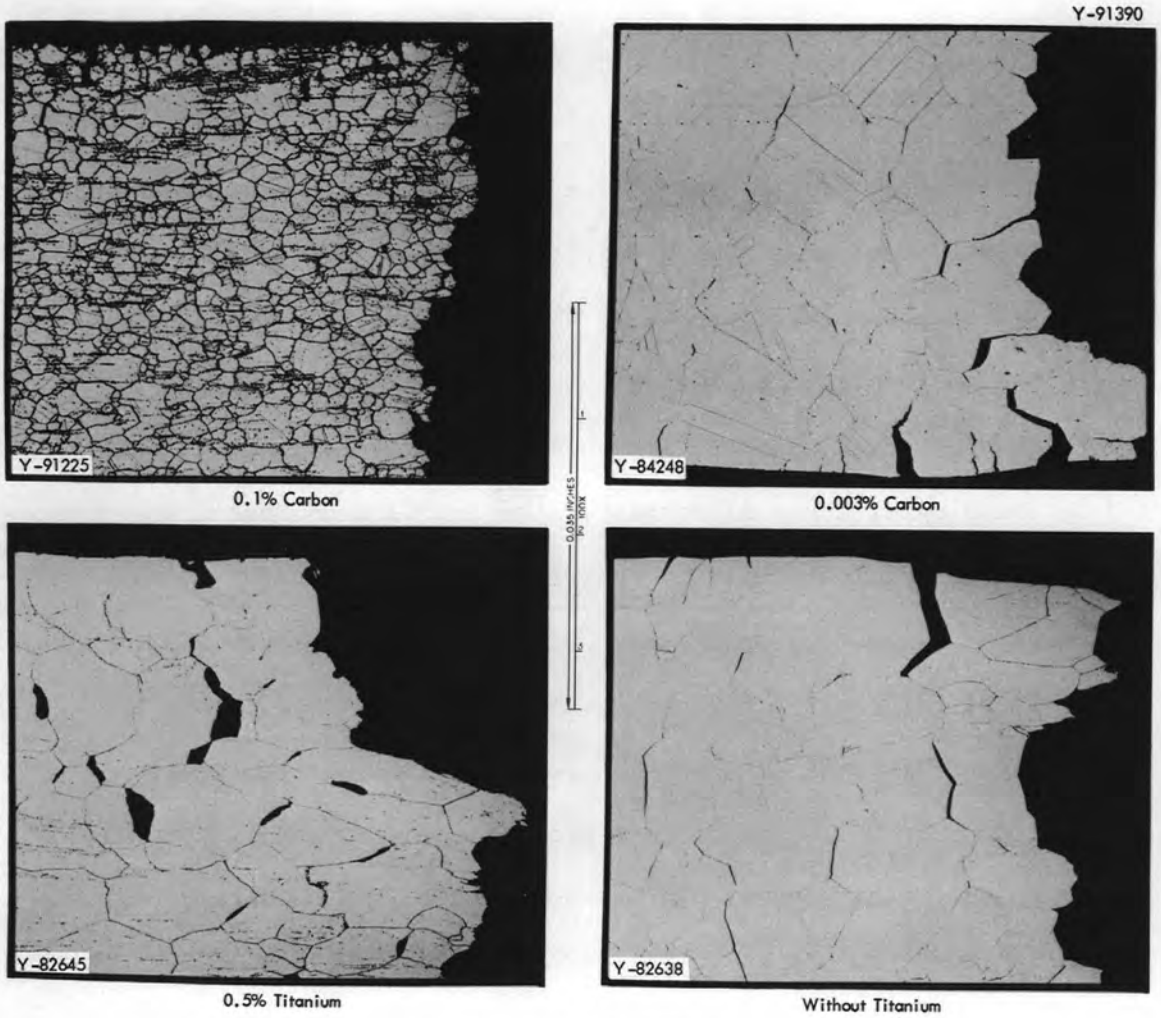

Figure 37. Effect of titanium and carbon on creep fractures at 40,000 psi and 650°C (solution annealed one hour at 1177°C and aged 100 hours at 870°C with the nominal composition Ni-12% Mo-7% Cr-0.5% Ti-0.05% C, except where noted).

ductility remained between 12 and 20%. The fracture of three of these four samples was completely intergranular, and only the 0.5% Ti (nominal 0.05% C) sample exhibited a mixture of trans- and intergranular fracture.

Figure 38 compares transgranular and intergranular tensile failures for the aged commercial heats. This material, with 0.45% Ti and 0.04% C, had 43% elongation when tested after aging at 650°C, and 21% after aging at 760°C. The amount of grain distortion in the two cases is noticeably different. Since the strength of these two alloys was virtually identical, the explanation for the loss of ductility must relate to the influence of the different carbide distributions (Figures 30 and 31, pages 94 and 95) on crack nucleation and/or propagation. An increased tendency for intergranular cracks to propagate would interrupt matrix-deformation and result in lower ductility at fracture. Thus, the electron microscopy studies of carbide morphologies and distributions should provide a better understanding of the factors controlling the ductility and the fracture mode. The specimens shown in Figure 38 exhibit typical high-temperature transgranular and intergranular fractures with a considerable difference in ductility. The intergranular fracture can be classified as "ductile-intergranular" failure since 21% elongation represents appreciable ductility for a nickel-base alloy at 650°C.

Figure 39 compares the macroscopic features of typical high-temperature fractures in the aged commercial alloys. The alloys, heat treatments, and measured ductilities for these 650°C tensile tests are given in the caption. The sample with lowest ductility, Figure 39(a), has a mixed trans- and intergranular failure. The next sample, Figure

Y-88786

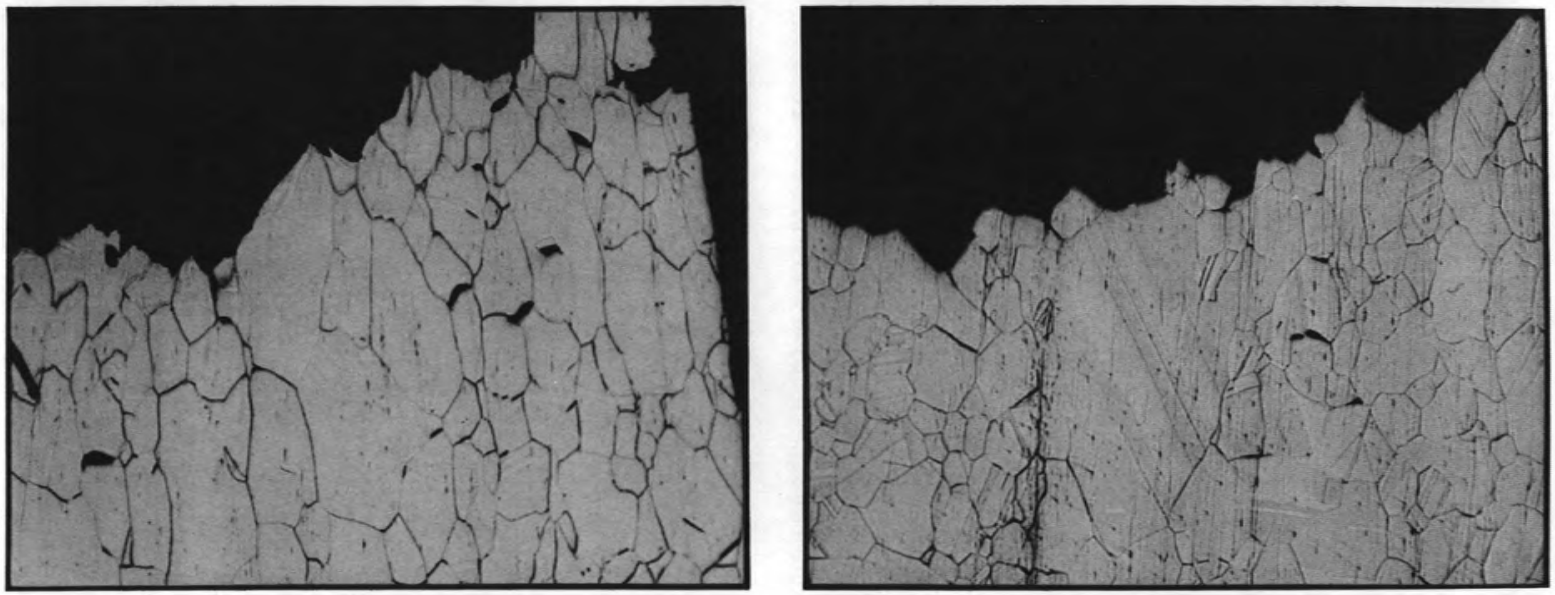

3000 HOURS AT 650° C

3000 HOURS AT 760° C

Figure 38. Tensile fractures in 0.45% Ti heat of Hastelloy-N tested at 650°C and 0.002 minute^{-1} strain rate after aging 3000 hours at either 650°C or 760°C.

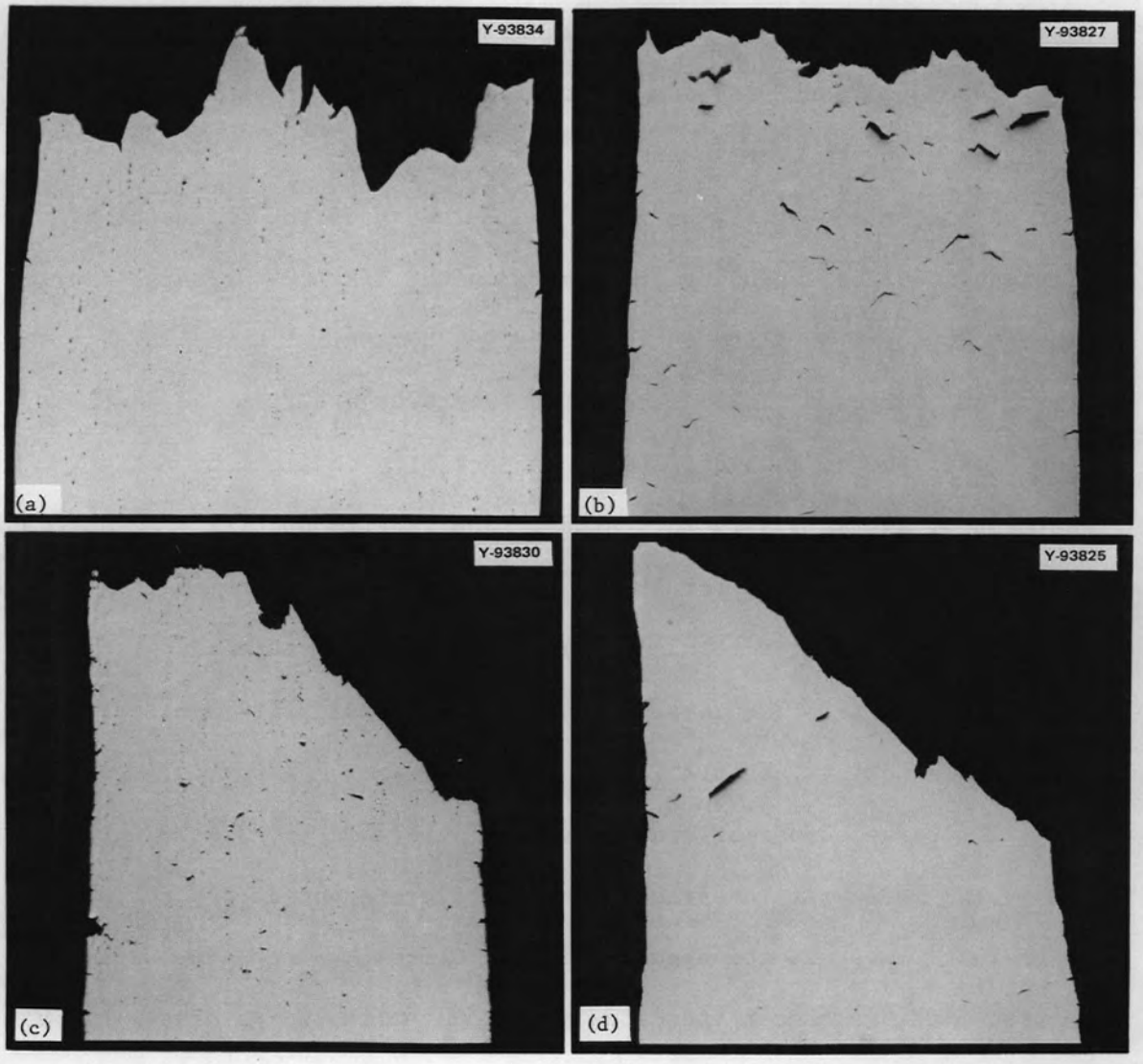

Figure 39. Comparison of tensile fractures of aged Hastelloy-N alloys (35X). (a) 1.2% Ti heat, annealed at 1260°C and aged 10,000 hours at 760°C, 12% elongation, 9.5% reduction of area (RA). (b) 0.15% Ti heat, annealed at 1177°C and aged 10,000 hours at 760°C, 17% elongation, 13% RA. (c) 1.2% Ti heat, annealed at 1177°C and aged 10,000 hours at 760°C, 44% elongation, 36% RA. (d) 0.45% Ti heat, annealed at 1177°C and aged 10,000 hours at 650°C, 43% elongation, 31% RA.

39(b), had 5% percentage points greater ductility than the previous sample (i.e., 17 vs. 12%), but this difference is due to the opening of intergranular voids along the gage length. The high ductility failures in Figures 39(c) and 39(d) show transgranular shear fractures which make 45° angles with the tensile axes.

A comparison of Figure 39(a) and 39(c) shows the influence of different solution annealing treatments on the fracture appearance after aging at 760°C. The alloy in this case was commercial Hastelloy-N with a titanium content of 1.2%. These two fractures are from the samples which showed the largest difference in ductility obtained by heat-treatment of any alloys in this study. The tensile ductility measured at 650°C was 12% and 44% for Figure 39(a) and 39(c) respectively: the difference in ductility relates primarily to the formation of precipitates on stacking faults. The sample with the lowest ductility had the precipitates on stacking faults.

The large number of cracks evident in Figure 39(c) were initiated at the carbide-matrix interface both at the grain boundaries and within the grains. However, the high ductility values (44%) obtained for this specimen with the cracks indicates that the nucleation of cracks has not adversely affected the ductility, but rather the inability of the cracks to propagate has allowed continued deformation, and thus promoted high ductility.

An unusual fracture from the 1.2% Ti heat aged 3000 hours at 650°C after a 1260°C solution anneal is illustrated in Figure 40. The sample elongated 20% and the fracture was predominately intergranular, but with

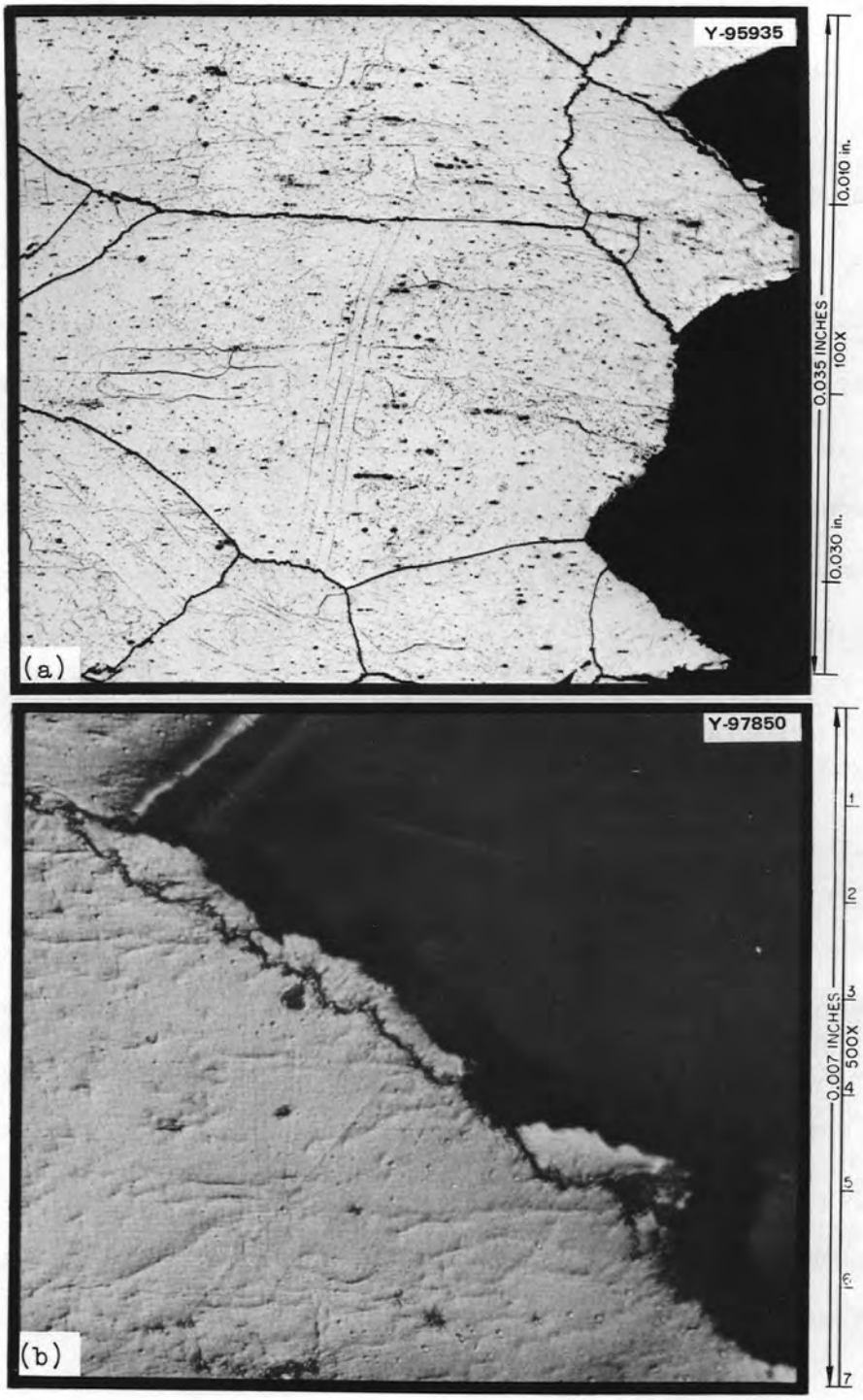

Figure 40. Mixed transgranular and intergranular tensile fracture of 1.2% Ti heat of Hastelloy-N heat-treated to produce stacking fault precipitates then tensile tested at 650°C. (a) 100X of fracture. (b) 500X of fracture.

some transgranular tearing as shown by the enlarged photograph, Figure 40(b). A large amount of precipitation has occurred as evidenced by the decorated subgrain and twin boundaries visible at the lower magnification.

The fracture appearance of pure nickel-270 and Ni-0.06% Ti after creep testing in argon at 12,000 psi and 600°C is compared in Figure 41. The low ductility (11% elongation) fracture in the nickel-270 sample is a mixed trans- and intergranular type, and there is wedge cracking along the gage length. Figure 41(c), taken in the vicinity of the fracture, shows second phase particles in addition to the cavities along serrated grain boundaries. Generally, the microstructure of the nickel-270 is more complex than that of the Ni-0.06% Ti alloy. The 25% ductility of the Ni-0.06% Ti alloy (Figure 18, page 71) reflects the fact that the fracture is transgranular, as shown in Figure 41(b). Near the point of fracture the large number of small grains and the mottled areas indicate that dynamic recrystallization has taken place during the creep test at 600°C. Stress relieving produced by recrystallization might account for the higher ductility of the Ni-0.06% Ti samples than of the nickel-270 which did not recrystallize. However, tensile fractures which were examined did not show recrystallization in the Ni-0.06% Ti alloys. Since the tensile ductility of this alloy was greater than for the pure nickel, the enhancement in tensile tests is not due to recrystallization. The structure of the Ni-0.06% Ti alloy (Figure 41(d)) is relatively simple with only a few scattered second phase particles present. The important point, however, is the difference in the amount of the cracking in two alloys. Much cracking is evident in the nickel-270 but none has occurred

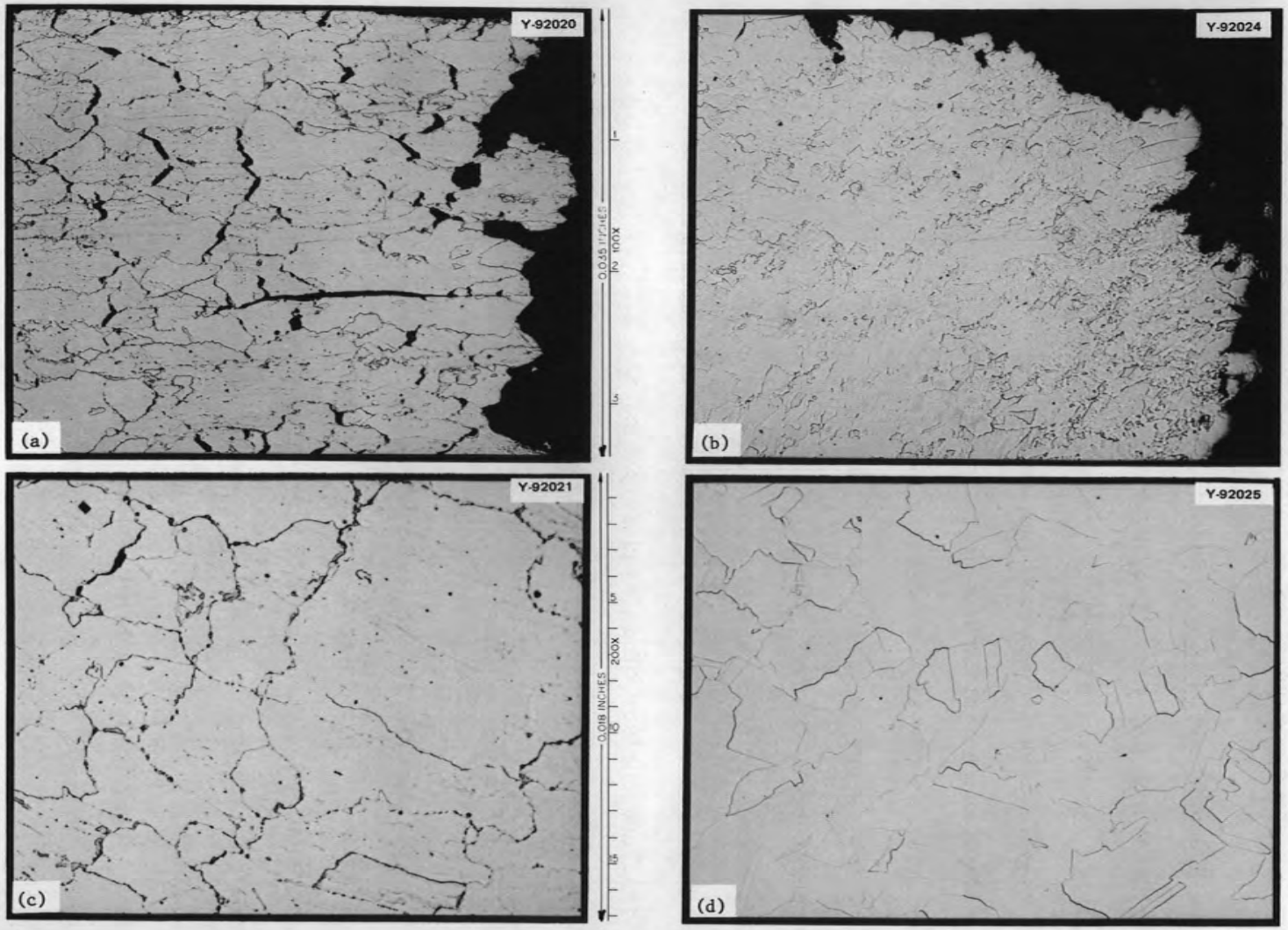

Figure 41. Creep fractures of commercially pure nickel and Ni-0.06% Ti alloy for tests in argon at 600°C and 12,000 psi. (a) Nickel-270. (b) Ni-0.06% Ti. (c) Nickel-270, near fracture. (d) Ni-0.06% Ti, near fracture.

in the Ni-0.06% Ti tested under identical conditions. No transmission microscopy or phase analysis was conducted on these nickel alloys.

2. Scanning microscopy. Scanning electron microscopy of tensile and creep fractures was conducted to help categorize the fracture modes of the alloys investigated in this program. Little is known about ductile and brittle high-temperature fracture. The observations made after elevated temperature testing may bear little relation to the fracture characteristics at the time of testing because of alteration of the fracture surfaces by the rapid surface diffusion and oxidation at elevated temperatures. However, the highlights of the observations made on samples tested at 650°C and at room temperature are given below.

Figure 42 shows a series of scanning micrographs made on the tensile fracture surface of an aged sample of the 1.2% Ti Hastelloy-N heat. This sample, after heat treating at 1260°C and aging 1500 hours at 760°C, was tested in tension at 650°C to failure with 11% total elongation, which was one of the lowest ductilities observed in this study. The micrographs show an intergranular fracture with the grain boundary surfaces covered with sheets of a dendritic material assumed to be carbides. At lower magnifications, Figure 42(b), the second phase has the appearance of a dendritic fern. At a higher magnification, Figure 42(d), the fern clearly consists of the high and low regions characteristic of a dendrite. The microstructure of this particular sample was previously shown to have a heavy concentration of stacking fault precipitates within the matrix.

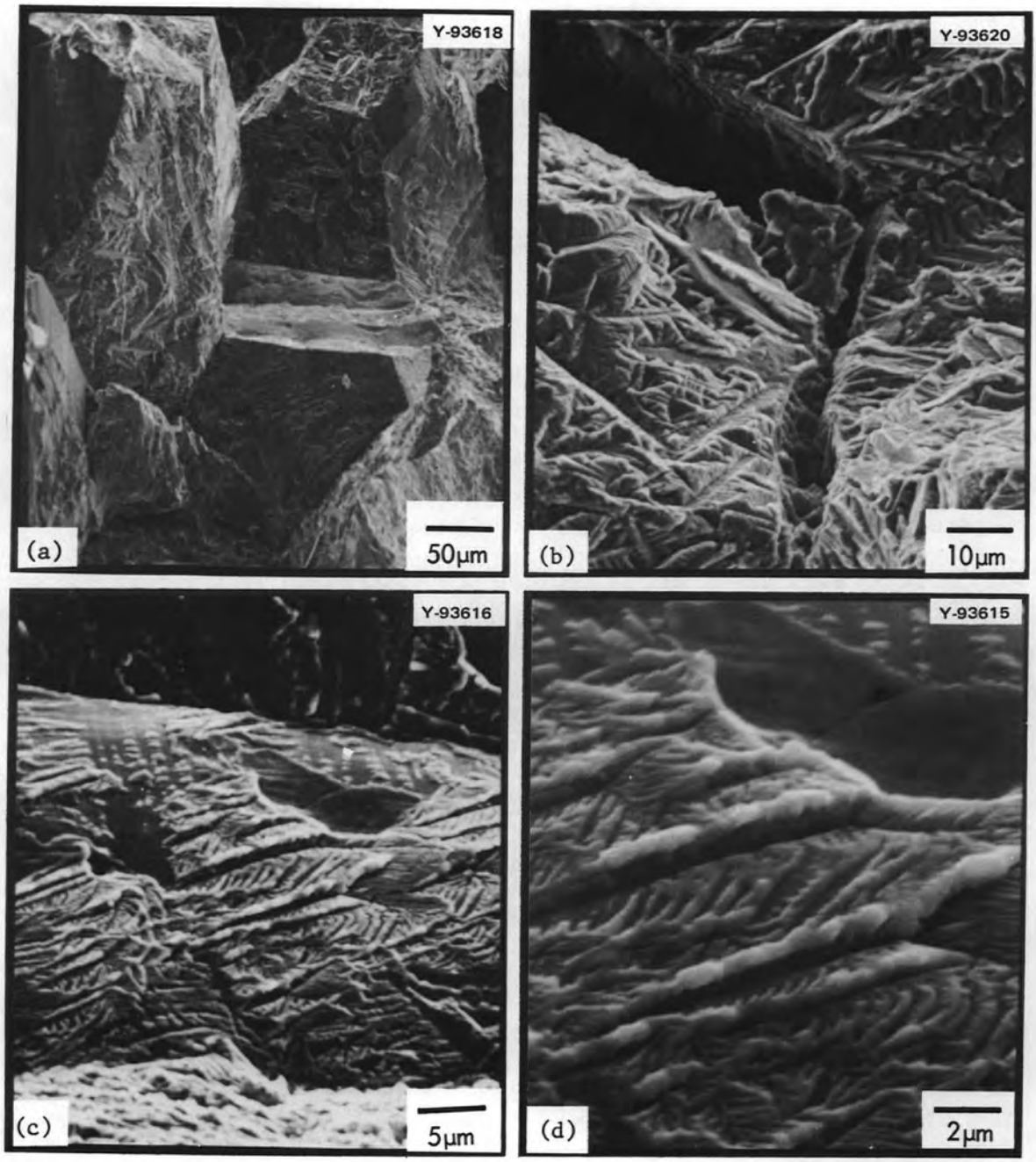

Figure 42. Electron scanning fractographs of intergranular fracture in 1.2% Ti heat of Hastelloy-N showing sheets of precipitate on grain boundaries (solution annealed at 1260°C and aged 1500 hours at 760°C, magnification increases progressive from (a) to (d)).

The fracture appearance (Figure 42) of this sample indicates failure along the carbide-matrix interface. Samples that did not have stacking fault precipitates showed high ductility, transgranular fractures in scanning microscopy which were quite different from those shown in Figure 42. However, heavy precipitate concentrations were also observed in transmission in the grain boundaries of the ductile alloys. Thus, apparently the distribution of the grain boundary precipitate is the important factor.

Although this study was concerned primarily with high temperature properties and fracture, some interesting observations were made at room temperature on samples which contained the stacking faults precipitate morphology. Figures 43 and 44 compare the appearance of two room temperature fractures for samples with thermal histories identical to those discussed in the previous paragraph and shown in Figure 42. The sample shown in Figure 43 was broken under "impact conditions" when attempting to cut the sample with a machine tool in a lathe. Figure 44 corresponds to a sample given the same thermal history and tested in slow tension (0.002 minute^{-1} strain rate) to 42% elongation at fracture. Thus, the difference between the room temperature fractures in Figures 43 and 44 is that one sample was fractured on "impact loading" and the other fracture occurred in slow tension. In Figure 43(a) and (b) the fracture appears to be a mixture of trans- and intergranular failure. The impact fracture, shown in Figure 43, displays mostly transgranular fracture characterized by large dimples, typical of ductile fracture of metals. There were several local areas, however, which showed the fracture to be

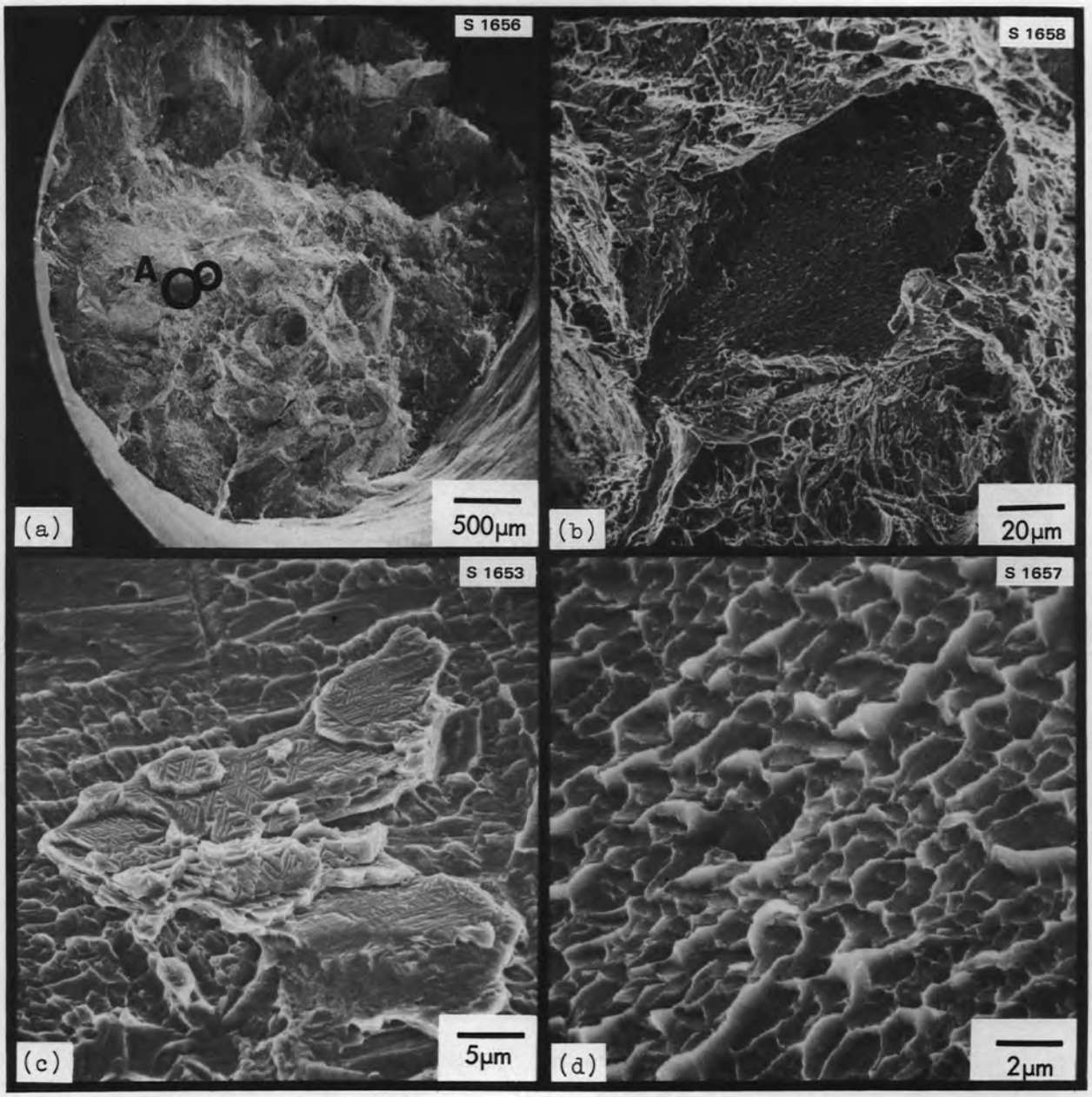

Figure 43. Room temperature fracture of sample with stacking fault precipitate morphology. (a) Fracture at 20X. (b) Region of intergranular fracture 500X. (c) Isolated region of transgranular failure on grain boundary 2000X. (d) Intergranular dimples 5000X.

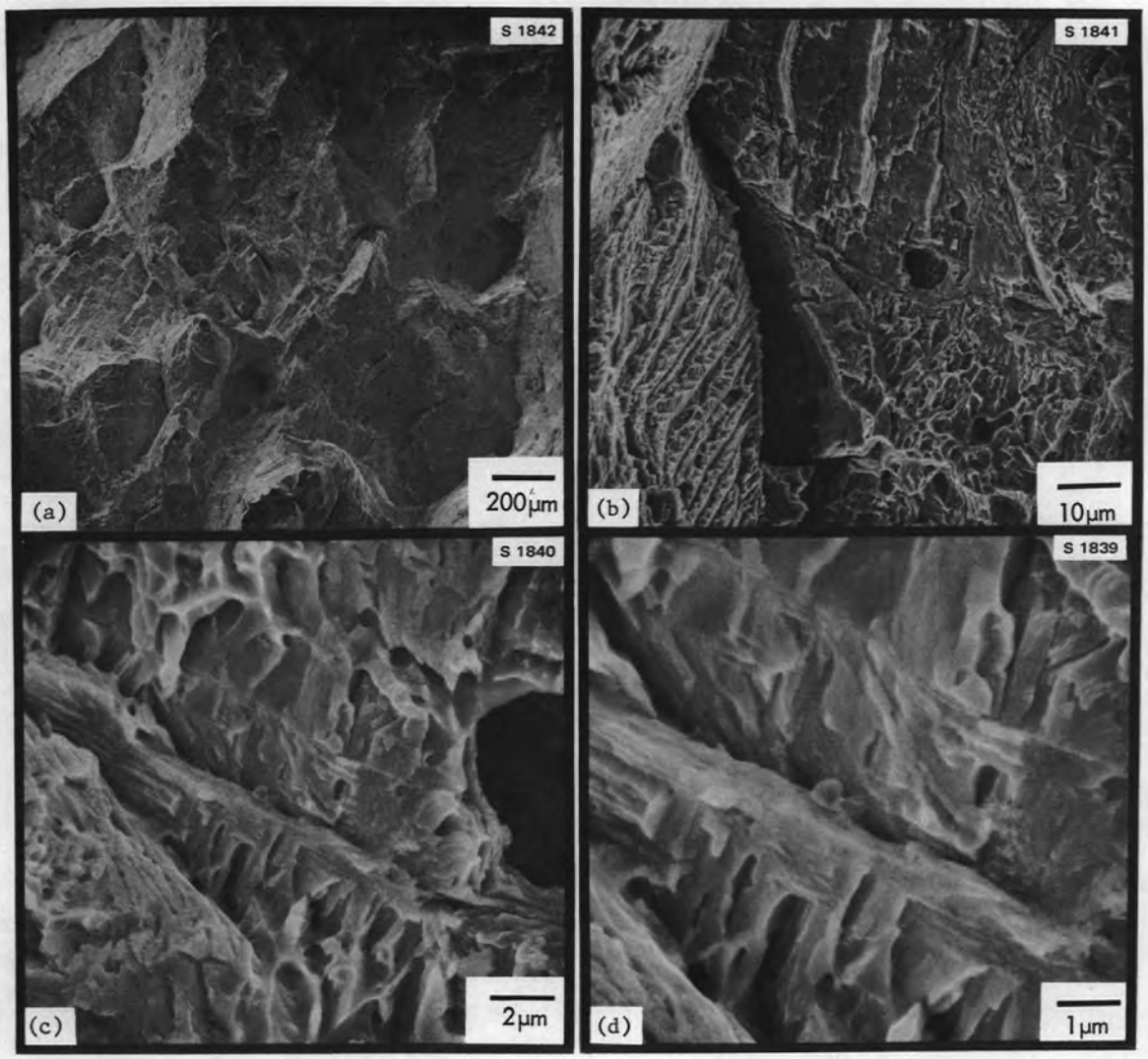

Figure 44. Scanning fractographs of 1.2% Ti heat of Hastelloy-N solution annealed at 1260°C and aged 1500 hours at 760°C to develop the stacking fault precipitate then tested in tension at room temperature. (Magnification increases progressively from (a) to (d)).

significantly influenced by grain boundaries or areas of highly concentrated precipitate particles. Two of these areas are encircled in Figure 43(a) and are shown at higher magnifications in Figure 43(b) through 43(d).

Figure 43(c) shows the area marked "A" at 2000X. This is apparently a region of "ductile" intergranular fracture as evidenced by the surrounding dimpled surface but with a distinctly different area in the center of the field. This rather striking area is seen to be terraced with a "checkered" pattern of surface markings. This regular matte pattern corresponds to the stacking fault ribbons that were shown in Figures 32-34, pages 98-100, and Figure 35, page 102. This object could be a portion of the opposite grain which has failed transgranularly and is now part of the fracture surface. The irregular matte pattern on the exposed surface of this feature corresponds to stacking fault ribbons on which precipitation has occurred as seen within the matrix in transmission microscopy. It is suggested that in this region (Figure 43(c)) the fracture propagated through the matrix, along planes of weakness within the sample, perhaps along a {111} plane weakened by the presence of precipitates on stacking faults. Other regions of this same sample show a "ductile-intergranular" fracture, which corresponds to the heavily dimpled grain boundary structure shown in Figure 43(d).

The dimpled structure in Figure 43(b) and (d) is similar to that found by Russ and Kabaya in fractured steels.[67] They found small discrete carbide precipitates located within individual dimples using scanning microscopy. The appearance of the dimples in Figure 43(d) also matches

the description of microvoid coalescence given by Beachem and Meyn.[68]

The fracture surface of the room temperature tensile sample, Figure 44, page 118, is different from the impact loaded specimen. At low magnification the fracture surface reflects considerable ductility. At higher magnification ductile shearing and microvoids formation can account for some of the features; however, the structures in Figures 44 (c) and (d) do not resemble any well known fracture mode. Since this particular sample had a high ductility at room temperature the grain boundary precipitates are not embrittling under this condition.

Based on this limited amount of fractography, unfortunately the question of whether or not carbides have influenced the tensile fracture process cannot be clearly resolved.

CHAPTER V

DISCUSSION OF RESULTS

The influence of dilute alloying additions on the high-temperature creep properties of metals is difficult to rationalize because of our limited understanding of three primary factors: (1) mechanisms of creep deformation, (2) mechanisms of fracture initiation and propagation, and (3) influence of impurities in metals. As a consequence, research in this area seldom terminates with a clear understanding of the phenomena observed but rather results in correlations of the observations and at least generation of some new insight into the underlying factors. This section is a discussion of the results presented in the previous chapter and attempts to define the role that titanium plays in enhancing the creep properties of nickel and the nickel-molybdenum-chromium alloys. The results for each phase of this study will first be discussed separately in the same order as the results in the previous chapter. The effect of titanium is considered in each section as follows: laboratory heats, Section I, commercial heats, Section II, binary nickel-titanium alloys, Section III, and phase stability and microstructure, Section IV. Finally, in Section V a model of precipitation on stacking faults during aging is considered and factors influencing crack nucleation and growth in creep are discussed. A model is proposed to account for the beneficial effect of some precipitate distributions on creep properties in the nickel-molybdenum-chromium-titanium alloy system.

I. EFFECT OF TITANIUM AND CARBON ON CREEP PROPERTIES

The initial experiments on the effect of the titanium-to-carbon ratio were intended to determine how the creep ductility in laboratory heats of a nickel-molybdenum-chromium alloy varied with composition, stress, and strain rate at a given test temperature. Whether titanium was acting as a solid solution strengthener or as a precipitation-hardening addition was another question which these first experiments we were designed to answer.

The effect of titanium on the strength of these alloys is significant. With 0.05% C, the presence of 0.5% Ti increases the 650°C creep-rupture life by a factor of from 5 to 20, depending on the heat-treatment and stress. The secondary creep rate was reduced by approximately a factor of 10 by 0.5% Ti. Carbon over the range investigated (0.003 to 0.3% C for an alloy containing 0.5% Ti) increased the rupture life and decreased the creep rate four orders of magnitude (a factor of 10,000). The influence of carbon in the absence of titanium was not investigated over a range of carbon concentration.

The influence of carbon on the creep ductility at 40,000 psi was shown in Figures 8 (page 49) and 9 and 10 (pages 51 and 52) to be significant over some ranges of test conditions. For carbon contents between 0.003 and 0.1% the total creep elongation for three different structures (produced by heat-treatment) varied only between approximately 10 and 20%. Little significance is placed on variations in creep ductility in this range. Carbon contents greater than 0.1% produced large amounts

of precipitate, a pronounced reduction in the average grain size, and a corresponding significant increase in the creep ductility. For these higher carbon concentrations (greater than 0.1%) the ductility was normally higher for the preaged (100 hours at 870°C) samples than for the same heats creep tested in the solution annealed condition.

The effect of titanium at the 0.05% C level on the creep ductility is small. The greatest increase in ductility due to titanium alone is found for preaged samples tested in creep (Figures 6 and 8, pages 45 and 49). Since titanium beneficially influences the creep ductility of preaged samples more than for the solution annealed conditions, one can conclude that the increased ductility is not caused by titanium in solid solution. This also suggests that changing the surface energy by titanium is not a factor in nucleation of cracks and implies that either the precipitate type or distribution is more important than titanium in solid solution in enhancing creep ductility. Thus, from this implication the research proceeded into an evaluation of the phases present and their distribution after aging as a function of titanium content in the Ni-12% Mo-7% Cr-0.07% C alloy, which is discussed in the next section.

Solution annealing at 1177° or 1260°C produced very little difference in the as-quenched microstructure, and at low carbon contents there are no differences in either the creep strength or creep ductility. For carbon contents greater than 0.05% an 1177°C solution anneal results in a higher creep rate and a higher ductility in creep than does a 1260°C anneal. Aging 100 hours at 870°C prior to creep testing does not have a large effect on properties for low carbon contents, but at higher

concentrations the influence of aging is greater, as one would expect. The rupture life is not significantly increased by aging, but the creep ductility at higher carbon levels is definitely enhanced by aging prior to testing. This was shown in Figures 4 and 8, pages 42 and 49.

Carbide precipitation during creep straining at 650°C greatly strengthens the alloy for both an 1177° and a 1260°C initial solution anneal. The 1260°C treatment resulted in lower creep rates and lower ductilities at the higher carbon contents, presumably because of the larger amount of precipitation during test which results from the larger amount of solute in solid solution. This conclusion discounts any influence of grain size on creep rate and ductility since the differences in grain size for these two heat treatments were normally less than a factor of two for the laboratory heats.

Since very little electron microscopy was conducted on the alloys with varying carbon content, it is impossible to specify the microstructural changes that accompanied the property changes. One can infer what the structures might be from the microstructural study of the aged commercial alloys. For example, one might expect that the precipitation on stacking faults observed for the commercial alloys could be a factor in the mechanical behavior of these laboratory heats, since it was found that differences in the tensile behavior for an 1177° and a 1260°C annealed material could be attributed to this unusual precipitate morphology.

Although one does not know the effect of stress on the rate of formation of stacking fault precipitate in this alloy system, this

factor has been investigated for NbC precipitation on stacking faults in stainless steels. Naybour[69] found that the density of stacking faults, caused by NbC precipitation and subsequent fault growth, in an Fe-18% Cr-12% Ni-0.8% Nb austenitic steel did increase with deformation at 650°C. Therefore, it is proposed that precipitation of MC carbides on stacking faults occurs during creep testing for the solution annealed Ni-12% Mo-7% Cr-0.5% Ti alloys. However, at low carbon contents and for lower solution annealing temperatures this type of precipitation would not be as extensive if the tendency for formation of precipitates on stacking faults in the laboratory heats follows the same trends as found for the commercial heats.

One additional point that should be made concerns the correlation of creep ductility with secondary creep rate (Figures 9 and 10, pages 51 and 52). For an 1177°C anneal and for an 1177°C plus 100 hour anneal at 870°C the relative influence of increasing the titanium or of increasing the carbon contents is identical; the effect is to increase the total elongation at fracture. Comparison of the creep curves for comparable rates of secondary creep indicates that titanium primarily influences the amount of tertiary strain, but does not appreciably change the fraction of the sample life spent in third stage creep. That is, whether titanium is present or not in a sample, approximately half of the time at temperature under stress can be classified as "third stage" creep. Thus, if third stage creep is controlled by the rate of crack growth or void formation, this suggests that the role of titanium, or more specifically the titanium induced carbide precipitation, has been to allow

additional straining to take place during this latter stage of creep. This could occur by inhibiting the propagation of grain boundary cracks.

II. DISCUSSIONS OF PHASE STABILITY ON AGING

The primary influence of titanium on the nickel-molybdenum-chromium system over the compositional range studied is to promote the formation of an MC-type carbide. For low titanium concentrations and high aging temperatures (i.e., 760°C) the MC carbide is not stable and is replaced by M_2C carbides. Although a number of different precipitate morphologies and distributions were observed for the MC and M_2C, the MC was often finer and usually the grain boundary concentration was much heavier than for the M_2C-type.

In general, the tensile and creep ductilities were greatest in alloys containing the MC carbides. Precipitation of MC at 650°C produced a structure that was both stronger and more ductile in tensile tests and had a greater rupture life and fracture strain in creep than structures containing M_2C. When M_2C was the predominate carbide (i.e., after 760°C aging) the tensile and creep ductilities were 50 to 70% lower than those found for the favorable MC precipitate distribution. These data suggest that the MC carbides produce better properties because of their morphology and/or distribution. This aspect of the correlation will be discussed later in relation to the microstructures and development of a fracture model in Section V. If one accepts the above conclusion that the MC-type carbide gives added strength and ductility, the enhancement of properties with increasing titanium content can be understood.

In this nickel-molybdenum-chromium alloy, titanium replaces chromium (or molybdenum) in the MC carbide structure. This appears to decrease the matrix solubility for the MC carbide and thereby increases the stability of the carbide that is more beneficial to the ductility at 650°C, the MC-type. No influence of titanium on the chemical analysis of the M_2C carbide was discernible from this study.

An interesting comparison can be made between the role of titanium in the nickel-molybdenum-chromium system and the molybdenum-titanium alloys investigated by Chang[55-59] and others. He found that maximum strengthening was obtained in Mo-0.5% Ti alloy for a titanium to carbon weight concentration ratio of four (atom ratio of one). This ratio suggests the formation of MC (i.e., TiC) rather than M_2C (i.e., Mo_2C), which was the equilibrium phase when either the titanium content was too low or the annealing temperature too high. Thus, the relative stability of MC and M_2C as a function of titanium content and aging temperature in the molybdenum system and the nickel-base system is similar for titanium concentrations up to approximately 1% Ti. However, the composition of MC and M_2C carbides differ significantly in the two systems. Chang[58] found TiC and Mo_2C in Mo-0.5% Ti, whereas, this study shows (Mo, Cr, Ti)C and $(Mo, Cr)_2C$ in the nickel-base alloy.

The observed carbide stability agrees with the standard free energy of formation.[70] The free energy data as a function of temperature for the TiC and Mo_2C carbides give a lower value for TiC formation at low temperatures and for Mo_2C formation at high temperature. The agreement between thermodynamic predictions and published observations on

related systems aids the obvious conclusion that although nickel constitutes approximately 75% of this alloy its primary role is in providing an inert solid state matrix in which the more reactive elements (molybdenum, chromium, and titanium) interact and compete for carbon to provide the beneficial strengthening precipitates of the MC-type or the M_2C-type. The M_2C distribution reduces the ductility by influencing the matrix and grain boundary behavior during hot deformation.

The relative contributions of matrix strengthening, grain boundary embrittlement, and strain aging[71] to the mechanical behavior in the nickel-molybdenum-chromium-titanium-carbon system are unknown. Detailed studies of these factors have been reported for the molybdenum-titanium-carbon system. Raffo[72] considered in detail the effects of small titanium additions on the mechanical behavior and microstructure in molybdenum base alloys and found that titanium caused dynamic strain aging. Raffo used the term dynamic strain aging to include the interaction of dislocations and precipitates as well as the classical inference of solute atom-dislocation reactions. He[72] reports that dynamic strain aging occurs over a limited range of temperature and strain rate and is characterized by a peak in the flow stress-temperature curve, serrated plastic flow, negative strain rate sensitivity,[73] and a rapid rate of work hardening. The replacement of titanium with hafnium or zirconium in molybdenum-carbon alloys resulted in these characteristic features for temperatures between 800° and 1375°C.[72] Raffo concludes that titanium strengthens the Mo-0.8% Ti-0.2% C alloy by causing precipitation of TiC during plastic deformation. This precipitation has two effects: it decreases the

mobile dislocation density by the pinning observed in electron microscopy and it possibly retards the rate of recovery by pinning of dislocation networks. Raffo concluded that titanium retarded recovery since the activation energy and stress dependence of creep did not change with alloying but the high-temperature strength was greater with titanium present.

In the present studies of the deformation of nickel-molybdenum-chromium-titanium alloys, several observations were made that can be related to strain aging. The following characteristics were observed from tensile tests: (1) serrated yielding could be eliminated by aging at 760°C, (2) higher rates of work hardening were produced by titanium additions, (3) precipitation occurred on dislocations, and (4) titanium additions and heat treatments produced large differences in the strain rate sensitivity of the plastic deformation. Thus, from a comparison of these factors with the reported[72] characteristic features of dynamic strain aging and from the effects of NbC in steels reported by Naybour[69] it is concluded that the strengthening benefit of titanium additions to the nickel-molybdenum-chromium system derives from both solute-dislocation interaction and precipitate-dislocation interactions during creep and tensile testing. However, a quantitative evaluation of the relative effects of solute and precipitate strengthening in this alloy system cannot be made from these currently available data.

For the highest titanium content investigated (1.2% Ti) some aging treatments increased the yield strength and total elongation and decreased the uniform elongation. Both the rate of work hardening and

strain rate sensitivity are undoubtedly affected (the value of n decreases and m increases in equations (7) and (8)) but the main effect of titanium is the enhanced ductility. Thus, precipitation in some cases is actually beneficial to both strength and ductility.

III. INFLUENCE OF TITANIUM IN PURE NICKEL

Small titanium additions to pure nickel significantly increase the fracture strain in creep and tensile tests at 600°C. For both tensile and creep tests a maximum ductility occurred for a titanium concentration of 0.26%, but at 0.06% Ti the ductilities were comparable. Thus, based on these results, a range of compositions (0.06 to 0.26% Ti) would be expected to produce enhanced ductility.

The temperature dependence of the tensile properties of alloys with and without the titanium additions showed a rapid drop in the uniform elongation with increasing temperature for each alloy. A similar drop for the total elongation was found for the pure nickel-270. The most striking feature of these data, however, is the large increase in total elongation with increasing test temperature for both titanium contents. The addition of titanium produced a positive temperature dependence of the tensile ductility whereas without titanium the temperature dependence of ductility was negative. Although it has previously been reported[74] that titanium additions to pure nickel could counteract the detrimental influence that some elements have on the intermediate temperature ductility it was not expected that as little as 0.06% Ti could actually change the temperature dependence of the ductility from negative to positive.

The tensile specimens of the alloy containing titanium exhibited appreciable necking and very little void formation prior to failure; thus, Hart's analysis[39] of tensile failure should apply to this case. Hart suggested that the large amount of plastic deformation found in some materials beyond the point of plastic instability (i.e., the non-uniform necking strain) was a manifestation of the large value of the strain rate sensitivity coefficient in equation (8). This suggests that the ductilizing effect produced by adding small amounts of titanium to pure nickel is related to the change in the strain rate sensitivity of the plastic deformation. This same conclusion was drawn from some of the effects of aging on the elongation of the nickel-molybdenum-chromium-titanium alloys (page 62). This is, however, a macroscopic explanation of the observed plastic deformation as related to the behavior of the tensile instability and does not in any way explain the microscopic influence of titanium on the deformation or fracture mechanisms in nickel. The question to be asked is, how can small amounts of titanium increase the strain rate sensitivity of nickel?

Aging at 650°C appeared to have no effect on the high temperature strength and ductility in these binary alloys. Since no transmission microscopy was conducted to carefully define the structural differences between the nickel and the Ni-0.06% Ti alloy, the only tangible evidence available concerning the ductilizing effect of titanium is the indication that recrystallization occurred during creep at 600°C in the Ni-0.06% Ti alloy and not in the nickel-270 material (see Figure 40, page 111). In addition, the Ni-0.06% Ti alloy crept at a slower rate than the pure nickel-270 for the two tests where a comparison can be made. This

indicates either a solid solution effect or a precipitation hardening effect of titanium. As the yield strength was equivalent with or without 0.06% Ti, titanium must operate through strengthening mechanisms that affect only the creep deformation. One way would be to affect the grain boundary shear and void nucleation characteristic, through chemical reaction with impurities located preferentially at grain boundaries.

A strong hint as to the effect of titanium is in its tendency to inhibit intergranular fracture, as shown in Figure 40, page 111. Using the fact that the ease of recrystallization is enhanced by adding a small amount of titanium, and assuming that aging is ineffective at temperatures below 650°C, it is proposed that the benefit of titanium is derived from the gettering of impurities from both the matrix and the grain boundaries. With titanium present the grain boundaries have greater mobility, since impurities no longer tend to pin the boundary, stress concentrations are relieved through boundary migration and grain boundary separation is inhibited. At high strains dynamic recrystallization occurs and fracture results from the reduction in cross-sectional area of the samples with little or no void formation or cracking. With no titanium present the nucleation and growth of grain boundary cavities in nickel increases the observed creep rate and leads to shorter rupture-lives and lower ductility as compared to nickel containing titanium.

These conclusions on the possible role of titanium on the deformation behavior of nickel are consistent with the findings of Robbins, Shepard, and Sherby.[75] These authors evaluated the effects of crystal structure, alloy purity, and test temperature on the ductility

of iron and concluded that the impurities present in the alloy controlled the grain boundary shearing characteristics and the ease of recrystallization of iron. However, in iron the diffusivity and the number of active slip systems changes drastically with the alpha to gamma phase transformation, so that factors other than purity are also important in the plastic deformation of iron.

IV. DISCUSSION OF MICROSCOPY

Optical, transmission, and scanning electron microscopy examinations were made to classify the precipitate distribution within the matrix and grain boundaries as a function of titanium content, carbon content, aging time, and temperature. The primary findings presented in Section IV of the previous chapter which will be discussed are as follows: (1) the correlation of observed structures and resulting mechanical properties after an 1177°C solution anneal, (2) the influence of the stacking fault precipitate morphology on the mechanical behavior at 25° and 650°C, largely following 1260°C anneals, and (3) the influence of several important variables on the tendency to form precipitates on stacking faults.

A. Relation of Structures to Properties

Palmer, Smith, and Warda[30] call attention to the fact that very little is known about the influence of size, shape, composition, and distribution of second phase particles on the ductile fracture characteristics of metals. For this reason a qualitative assessment of these factors was made in this nickel-molybdenum-chromium-titanium-carbon system.

The distribution of second phase precipitates along grain boundaries as a function of titanium and aging temperatures was shown in Figures 30 and 31, pages 94 and 95. The associated tensile and creep properties were given in Figures 12 and 13, pages 56 and 60, and correlated previously with MC and M_2C phases on page 126. These data show that the higher ductilities in both creep and tensile tests occur in those specimens with the heaviest grain boundary MC carbide distribution and that alloys with lower values of ductility have lower concentrations of M_2C carbide particles at grain boundaries. The latter carbides are more rounded and more widely spaced than in the more ductile alloys. This observation is contrary to Garofalo's conclusion[6] that a rounded precipitate that is widely distributed would improve creep ductility. However, Garofalo's conclusion was derived from creep ductilities measured at the same secondary creep rate while this study compares different alloys, at the same stress but with different creep rates. This observation is in agreement with that of Weaver,[11] Betteridge and Franklin,[12] and Heslop[13] who studied nickel-base Nimonic alloys. They found greater ductility in creep for heat-treatments which precipitated large amounts of chromium carbides and $Ni_3(Al,Ti)$ at grain boundaries.

The observations on nickel-molybdenum-chromium-titanium can be rationalized by considering that the heavy (virtually continuous) grain boundary platelets and particles extending into the matrix impede grain boundary shear during slow deformation. The nucleation of grain boundary voids or cavities, which requires grain boundary sliding, is inhibited and matrix straining is not interrupted by intergranular failure. In

the case of cleaner grain boundaries, under creep conditions the tendency to localize the strain at grain boundaries may be greater since they are weaker than the heavily precipitated boundaries and, thus, undergo greater grain boundary deformation. This provides one of the main factors thought to be prerequisite to intergranular failure, grain boundary shear. These ideas are basic to the model developed in a subsequent section.

The relation of titanium content of the alloy to this process, as discussed, is to promote the formation of MC carbides which increases the grain boundary precipitate concentration, decreases the grain boundary shear under stress and thus promotes transgranular failure. While the increased ductility associated with a transition from intergranular to transgranular tensile fracture is a macroscopic observation of the high-temperature mechanical behavior, the type and distribution of the carbides is the microscopic factor determining the fracture elongation.

B. Stacking Fault Precipitation

In addition to the property changes connected with the distribution of MC and M_2C carbides discussed above, a drastic difference in strength, ductility, and microstructure was found for the different MC carbide morphologies produced by aging after different solution anneals. The transition in properties and structures due to different MC morphologies was most pronounced in the 1.2% Ti heat, in which the stacking fault precipitate morphology completely dominated the microstructure after a 1260°C solution anneal and 760°C aging treatment. The same trends with

solution anneal temperature, but to a lesser extent, were found in the 0.15% Ti heat. The 0.45% Ti heat exhibited smaller differences in microstructure and properties, undoubtedly because of the lower carbon content of that material (0.04% C compared with 0.07% C). No stacking fault precipitates were found for the titanium-free heat aged 1500 hours at 760°C, since in the absence of titanium the MC carbide does not form and the M_2C which forms does not precipitate on stacking faults (i.e., partial dislocation) because of its unfavorable size.[76]

Several volumes have been written about the mechanisms of precipitation on stacking faults in steels,[69,76-82] but observations in nickel base alloys are rather recent.[83,84] No detailed analyses were made in this study of the kinetics or crystallography of the stacking fault precipitation. Rather, the following discussion will contrast the published observations concerning mechanisms of formation in iron base alloys with the present electron microscopy observations in the nickel-molybdenum-chromium-titanium system. It will also relate this morphology to measured room temperature and 650°C mechanical properties.

The observation that the mechanical properties of the 1.2% Ti commercial heat of Hastelloy-N exhibited a large difference in aging response after an 1177° and a 1260°C solution anneal led to a detailed examination of the factors that could explain these differences. The following factors were the result of using the higher solution annealing temperature prior to subsequent aging: (1) a larger grain size by a factor of two to three, (2) the solution of considerably more primary MC carbides, (3) the occurrence of massive MC precipitation on stacking

faults during aging, and (4) less grain boundary precipitation. Since the strength and ductility in the as-annealed condition did not differ significantly for the two annealing temperatures, factors (1) and (2) can be discounted as primarily responsible for the observed strengthening. The mechanical property differences after aging are thus a result of factors (3) and (4).

The reduction of 650°C tensile ductility from 42 to 17% on aging 200 hours at 760°C (Figure 15, page 63) is accompanied by a rapid hardening, with the yield strength increasing from 28,000 to over 56,000 psi. In only five hours of aging at 760°C the tensile ductility decreased to 30% and the yield strength increased to 46,000 psi. Examination of structures produced by aging five and 200 hours at 760°C showed that the stacking fault precipitate was well developed and, for some grain orientations discrete precipitate particles were resolvable within the faulted region, particularly for the 200-hour sample. No stacking fault precipitates were found for a sample aged 0.25 hour at 760°C; thus, the growth to an observable size occurs between 0.25 and 5 hours at 760°C. A good correlation exists between tensile property changes at 650°C and development of the stacking fault precipitate during aging at 760°C. A maximum in strength occurs after approximately 100 hours, whereas the ductility continues to drop for aging times up to 1500 hours, at which time it reaches an apparent minimum value of approximately 12%. Thus, the strengthening and ductility loss are produced by and proceed simultaneously with formation and growth of the precipitates on stacking faults. The time for maximum strengthening in this system agrees, coincidentally,

with reported times for maximum density of stacking fault precipitates in a steel at 700°C. Froes, Honeycombe, and Warrington[79] reported a maximum fault density (TaC precipitation on stacking faults) in a Fe-18% Cr-8% Ni-2% Ta-0.1% C steel after aging 100 hours at 700°C for a prior 1300°C anneal.

Comparison of the strengthening at room temperature and at 650°C caused by stacking fault precipitates can be made for material aged 1500 hours at 760°C. The room temperature yield strength (for the 1.2% Ti heat) increased from 36,000 to 60,000 psi (a 61% increase), and the ductility decreased from 68 to 42% (a 41% decrease) for aging at 760°C. The comparative changes in the 650°C properties were a yield strength increase from 29,000 to 47,000 psi (a 62% increase) and a ductility decrease from 42 to 11% (a 71% decrease). The formation of MC carbides on stacking faults has affected the high-temperature ductility to a much greater extent than the room-temperature ductility. Comparison of the effect of this precipitate morphology on the reduction in cross-sectional area can also be made from these tensile tests at room temperature and at 650°C. Comparing samples with and without the stacking fault precipitate one finds that the room-temperature reduction of area is decreased 27% and the 650°C reduction in area is decreased 65% due to the precipitation. This demonstrates once again that the precipitation on stacking faults is more detrimental to the high-temperature ductility than it is to the room-temperature ductility.

Because of the influence of precipitation during test on the creep behavior of these materials the effect of a precipitate

distribution is difficult to assess. However, ignoring the influence of grain size allows comparison of creep properties after aging 3000 hours at 760°C, for an 1177° and a 1260°C solution anneal. The structures for these two treatments are shown in Figures 31 and 32, pages 95 and 98. The rupture lives (1454 and 1335 hours at 40,000 psi) and creep rates (0.01 and 0.016% per hour) are equivalent for tests with these two aged structures, but the creep elongation was a factor of two lower for the sample with the stacking fault precipitate morphology (i.e., 20% versus 37% elongation). Thus, it is concluded that a previously established stacking fault precipitate distribution has no greater strengthening effect in creep (at 40,000 psi and 650°C) than does the precipitate distribution developed after an 1177°C anneal and 760°C age, but it does tend to reduce the ductility. On the other hand, precipitation on stacking faults during the creep test would be expected to strengthen the alloy. This speculation is consistent with the measured difference in the creep rates of the as-annealed material and also the work of Naybour[69] in a related system.

A final comparison of the influence of the stacking fault precipitate morphology on the deformation at 650°C can be made for identical structures evaluated in creep and tensile tests. Samples aged 3000 hours at 760°C after the 1260°C anneal exhibited 15.4% elongation in tension and 20.4% elongation in creep. This higher ductility in creep than in tensile tests is unusual when one considers the normal strain rate effects on fracture ductility (i.e., lower ductility with decreasing strain rate), but indicates either (1) that the effectiveness of the

stacking fault precipitate as barriers to dislocation motion is not sensitive to strain rate or (2) that time for recovery is the important factor in determining the ductility. Obviously, the stacking fault precipitate because of its size and extensive formation (at least for the 1.2% Ti heat) would be a difficult barrier for dislocation to climb around in either type of test. On this basis, the available time at temperature for recovery processes is more likely the important factor in rationalizing the ductility values of these two tests.

V. DISCUSSION OF MODELS

A. Nucleation of Precipitates on Stacking Faults

Precipitation on stacking faults in certain austenitic steels after particular heat-treatments was extensively investigated from 1960 to 1965. Small additions of certain strong carbide formers produce a susceptibility to this type of precipitation. Most of the studies concerned conditions and mechanisms of precipitation of NbC in such steels as Fe-18% Cr-12% Ni-1% Nb. However, other alloying additions which cause precipitation of a carbide with a simple, rock-salt type, crystal structure can promote precipitation on stacking faults. The following carbides have been observed[76] to precipitate in this morphology in steels: NbC, ZrC, TaC, TiC, VC and V_4C_3. Kotval[83,84] has reported precipitation of NbC in the nickel base alloy Inconel 625 (Ni-20% Cr-8% Mo-5% Fe-3.5% Nb-0.05% C). Other precipitation processes such as matrix and grain boundary precipitation often proceed simultaneously with

formation of precipitates on stacking faults in these systems. A detailed theory of this latter process has been presented.

The model for the nucleation and growth of stacking fault precipitate proposed by Silcock and Tunstall[76] involves the following steps: (1) segregation of solute atoms to dislocations, (2) the dissociation of a dislocation into partials by the reaction

$$\frac{a}{2}[110] \rightarrow \frac{a}{3}[111] + \frac{a}{6}[11\bar{2}] \ , \qquad (9)$$

(3) nucleation of MC carbides on the tension side of the $\frac{a}{3}[111]$ Frank partial dislocation, and (4) simultaneous growth of the stacking fault and MC precipitates with the vacancies, emitted in the dislocation climb process, accommodating the increased misfit strain imposed by precipitate growth.

Silcock and Tunstall considered the possibility of a more energetically favorable dislocation reaction that results in two Shockley partials, one of which could glide to cause growth of the fault. However, from electron diffraction contract analysis they identified a Frank partial at the boundary of the extrinsic fault, and thus proposed the above less energetically favorably reaction, equation 9, and associated model to describe the nucleation and growth of the precipitates on the stacking fault. Silcock and Tunstall[76] point out that a normal $\frac{a}{2}[110]$ dislocation cannot split as shown by equation (9) and argue that climb of dislocation loops associated with the initially decorated dislocation is a step that precedes growth of the stacking fault precipitate. They apparently mean

by this from considering the energy of the $\frac{a}{2}[110]$ dislocation reaction, which is proportional to the square of the Burgers' vector, that the energy is not decreased by dissociation. However, calculations by Teutonico[86] have shown that by considering the anisotropy of the face centered cubic structure certain orientations of $\frac{a}{2}[110]$ dislocations can dissociate with an energy decrease. Thus, dissociation can be energetically favorable for equation (9).

Six factors given by Silcock and Tunstall[76] as necessary for this type of precipitation on stacking faults follow:

1. A matrix with a low stacking fault energy.
2. A high solute size factors so that segregation to dislocations will occur.
3. Favorable strain energy considerations so that nucleation of precipitates occurs at dislocations.
4. An expansion on formation of the precipitate.
5. A small critical nucleus size, so one interface dislocation can accommodate its thickness.
6. A precipitate with a simple relationship to the matrix structure.

A comparison of these factors for the steel studied by Silcock and Tunstall and for the Ni-12% Mo-7% Cr-1.2% Ti alloy of this investigation is of interest. The requirement of a low matrix stacking fault energy for stacking fault precipitation must not be a necessary requirement. Although the stainless steels have low stacking fault energies (of the order of 13 ergs per square centimeter[77]) nickel is usually reported to have a high value (approximately 150 ergs/cm^2).[31,85] The stacking fault energy of this nickel-molybdenum-chromium-titanium alloy

is intermediate between the austenetic steels and pure nickel. Both molybdenum and chromium are reported[85] to lower the stacking faults energy of nickel; however, carbon is reported to have an opposite effect, which is probably related to its ability to remove solutes from solid solution. The influence of titanium on the stacking fault energy of the Ni-12% Mo-7% Cr-alloy is not known, but titanium is also reported to lower the stacking fault energy of pure nickel.[84,85] One could argue that titanium also decreases the stacking fault energy of the alloy since one observes growth of the faults when titanium is present but no stacking faults are found in alloys without titanium. Whether the titanium changes the stacking fault energy of the bulk alloy or changes the energy only in the vicinity of the dislocation is not known. Previous attempts to measure bulk changes in the stacking fault energy of a steel due to the addition of 1% Nb gave conflicting results.[77,82] The argument that solute segregation to dislocation changes the stacking fault energy in a local region near the dislocation cannot be disputed; however, when precipitation occurs on the partial dislocation the separation of partials is a function of factors other than the stacking fault energy of the matrix. Nevertheless this study shows stacking fault precipitates in an alloy with "intermediate" stacking fault energy in contrast to factor (1) above.

The relative size factor (2) is similar for the two systems. The misfit parameter (i.e., relative difference in atomic size) of niobium atoms in iron is 13% and for titanium in nickel is 16%. Although niobium atoms are larger than titanium atoms, the matrix lattice parameter of

the stainless steel and the Hastelloy are comparable and segregation to the tension side of the dislocation would be expected in each case to lower the energy of the system. Nucleation of precipitates on dislocations (3) is favorable when titanium is present and MC carbides form but not when M_2C carbides precipitate. The factor concerning expansion on formation of the precipitate (4) is favorable in the Ni-Mo-Cr-Ti alloy. The NbC has a 20% larger unit cell than does the austenitic matrix and the MC-type carbides in Hastelloy-N are approximately 17% larger than the matrix from which they precipitate. Apparently a small critical nucleus size (factor 5) is formed in the Hastelloy-N; however, no observations were made which could evaluate this criteria, except the faults themselves. The simple carbide structure (factor 6) of MC which is NaCl-type face center cubic (FCC) in a FCC nickel matrix is the same as for the NbC precipitate and the austenitic steel matrix.

In this study the MC carbides, with composition approximately $(Mo_{0.5}Ti_{0.4}Cr_{0.1})C$ and lattice parameter of 4.28 Å, are actually the first complex carbides found to precipitate on stacking faults.

Obviously the dislocation density, solute concentration, and vacancy concentration can influence the tendency toward formation of stacking fault precipitation if the above model governs the process. Low carbon and low titanium contents were found to inhibit this morphology. The higher annealing temperature enhances both the solute supersaturation and the vacancy concentration, but should decrease the dislocation density. A large dislocation density was associated with primary MC carbides, particularly in the commercial heats, and a

decrease in the number of primary carbides also decreases the dislocation density. Nucleation of this morphology in the nickel-molybdenum-chromium-titanium system was often associated with primary MC precipitates that were present after a 1260°C anneal. The distribution of dislocations around primary precipitate particles suggests that those may be prismatic dislocations punched out by the difference in coefficient of thermal expansion of the carbide and metal matrix. If so, they have Burger vectors of a type $\frac{a}{2}[110]$. An energetically favorable edge dislocation reaction would be their dissociation into a Frank and Shockley partial by the reaction[86]

$$\frac{a}{2}[\bar{1}01] \rightarrow \frac{a}{3}[\bar{1}11] + \frac{a}{6}[\bar{1}\bar{2}1] \quad . \tag{10}$$

If such a reaction occurs, one might argue that the local matrix composition favors the faulted structure. Hence, the absence of faults in deformed structures not having this heat treatment would be explained.

A precipitate free zone was observed around many primary carbides particles in agreement with Kotval.[83] Contrary to Kotval's observations in other nickel alloys, not all grain boundaries were denuded in this system. In most cases the stacking fault precipitation continued up to the boundary if nucleated in the matrix, but no primary nuclei were observed along the grain boundaries Kotval's[84] explanation of denuding of stacking fault precipitates near grain boundaries was that dislocations in this region could not achieve the proper orientation to dissociate because of the low vacancy concentration. The presence of faults

near boundaries in the Ni-12% Mo-7% Cr-1.2% Ti alloys must indicate that either (1) greater numbers of dislocations are favorably orientated for dissociation in this system or (2) that the role of vacancies on the stacking fault precipitate process is not that suggested by Kotval[84] and others.[76-82]

Since precipitation on stacking faults occurred primarily after the 1260°C solution anneal for the 1.2% Ti heat, but not following the 1177°C anneal, a series of solution anneal and age treatments were given to better establish the influence of solute supersaturation on this process. One sample was solution annealed one hour at 1260°C, then annealed one hour at 1177°C and finally aged 200 hours at 760°C. Following the heat treatment the sample was tensile tested at 650°C and a coupon heat treated with the specimens was evaluated in transmission microscopy. This treatment was expected to dissolve primary carbide, increase the grain size, and then to establish a solute supersaturation characteristic of 1177°C. The results of this experiment are listed in Table XVI of the Appendix. The strength and ductility after this treatment was virtually identical to that obtained by aging directly after a 1260°C anneal. Examination of the microstructure indicated extensive development of the stacking fault precipitate, but in addition rather coarse precipitates not associated with stacking faults were also present. This experiment shows that the increased solute supersaturation characteristic of the 1260°C anneal is not the only important factor in causing precipitation on stacking faults. This conclusion is in agreement with that of Pickering[81] for NbC precipitation on stacking faults in steels. This

experiment may, however, suggest that other processes take place or that other configurations are created at 1260°C which are not affected at 1177°C. These processes contribute to nucleation of precipitates on stacking faults in this alloy in addition to the supersaturation. Enhanced segregation of solute atoms (titanium, for example) to dislocations is one obvious process that could be enhanced at 1260°C and would significantly promote the subsequent precipitation of titanium-containing MC carbides on stacking faults.

In general, the mechanism proposed by Silcock and Tunstall[76] for precipitation of NbC carbides on stacking faults also applies to precipitation of MC carbides on stacking faults in the Ni-12% Mo-7% Cr-0.07% C alloys for titanium concentrations from 0.15 to 1.2%. Using the diffraction contrast techniques discussed by Silcock and Tunstall, the faults in this nickel base alloy were found to be extrinsic. The nature of the faults thus agrees with that reported by Kotval in Inconel[83] and by Silcock and Tunstall in stainless steels.[76] Additions of other alloying elements that promote formation of an MC carbide (i.e., niobium, zirconium, hafnium, tantalum and vanadium) would also be expected to result in the formation of stacking fault precipitates in this nickel base alloy. One would also expect from the implication of this study that small additions of these active elements should promote a marked strengthening due either to dynamic strain aging or strain induced precipitation.

B. Model of Creep Cracking

In order to discuss the influence of crack initiation and propagation on the ductility one must relate the precipitate

distributions to matrix and grain boundary deformation. Unfortunately, for each carbide distribution the creep behavior was restricted to one test at 40,000 psi and 650°C. It is also pointed out that for the most part the influence of titanium has been based upon single heats of material with different titanium contents. These factors have introduced some reservation into the validity of the correlations which are discussed below. However, it is presumed that the trends observed are not influenced by heat-to-heat property variation and, thus, reflect primarily the influence of titanium content. The model that is proposed to account for the observed influence of titanium on the creep ductility involves a modified Chen-Machlin[5] cavity nucleation mechanism and imposes the added influence of titanium induced precipitation on inhibiting grain boundary sliding. The model considers only the influence of a pre-existing precipitates distribution, established after an 1177°C anneal and aging treatment and does not take into account the influence of precipitation on stacking faults.

Steigler _et al._[9] concluded from studies of three dimensional creep cavities in tungsten that cavities undoubtedly grow by slip, grain boundary sliding, and stress induced vacancy diffusion. Further, the relative contribution of these depends on the conditions of temperature and stress. They also concluded that the characteristic r- and w-type creep cavities are limiting extremes of a common over-all process. Thus, the creep behavior and the characteristic appearance of the grain boundary cavities is a function of the applied stress and the test temperature.[9] They further observed that cavities were not preferentially

nucleated at triple grain junctions as proposed by Zener,[1] but rather were simply created by grain boundary sliding over discontinuities within the more common boundaries between two grains. Since Chen and Machlin[5] proposed that grain boundary shear over pre-existing jogs was the nucleation step for cavity formation, one could adopt their idea but consider the carbide precipitate rather than grain boundary jogs as the nucleation site. Grain boundary cracks were observed around carbide particles in these tests. The observation that a considerable amount of cracking occurred for alloys with high ductility (Figure 39, page 109) indicates that the rate of crack growth or link-up was probably more important than crack nucleation in determining the creep ductility. Taplin[87] showed from his work on aluminum-magnesium and 70/30 alpha brass that the major factor controlling creep ductility was not the rate of crack nucleation, but was the ease with which voids were able to interlink to form cracks of a critical length for propagation. Weaver also observed that good ductility was obtained when the extent of grain boundary crack growth was limited by the interparticle spacing.[11] Thus, apparently the ability of a material to inhibit crack growth often enhances ductility in complex alloys even though crack initiation at carbide particles is relatively easy.

Several possible explanations can be given to account for this inhibitation of crack propagation including the following factors:

1. A decrease in the rate of grain boundary sliding.
2. A decrease in the stress concentration at the crack tip by recovery processes or by blunting the tip.

3. An increase in the cohesion of the precipitate-matrix interface.

All of these factors could be operating to limit the rate of extension of previously initiated grain boundary cracks.

Consider the influence of these three factors on the intergranular crack propagation for the alloy with 0.45% Ti solution annealed at 1177°C and aged 3000 hours at 650°C (Figure 30, page 94) or 760°C (Figure 31, page 95). For this alloy the grain boundary structure is characterized by a heavy concentration of MC carbides after the 650°C age and widely spaced predominately M_2C-type carbide after the 760°C age. The creep ductility for these two structures was 41 and 17% for the MC and M_2C distributions respectively, but the creep rates were essentially equivalent (0.04 and 0.053%/hr.). One could argue that the heavy precipitate, which actually extends from the boundary out into the matrix, locks the boundary by increasing its effective width and, therefore, tends to distribute rather than concentrate the stress. Also, a decrease in grain boundary shear for heavy precipitate concentrations at the boundary would be expected on the basis of the rate of matrix deformation. Studies of the effect of grain boundary shear have shown that, when other factors are equal, the rate of boundary sliding for a given stress is proportional to the overall creep rate.[88] Therefore, the presence of 0.5% Ti in the Ni-12% Mo-7% Cr-0.05% C alloy should decrease the rate of grain boundary sliding because the measured secondary creep rate was approximately a factor of ten lower (at 40,000 psi) than when no titanium was present (Figure 7, page 47).

The effect of a solute depleted zone near a grain boundary on relieving stress concentrations and increasing ductility was discussed by Weaver for a Nimonic alloy.[11] He argued that the lower chromium concentration due to grain boundary precipitation of chromium-carbide allowed greater mobility of this adjacent region and, thus, this region could relieve the stress concentrations caused by continued grain boundary sliding in creep. Differences in the amount of solute depletion in the alloys of this study with and without 0.5% Ti could be expected based on the results of metallography and phase analysis. Differences in the amount of solute depletion is expected based on the amount of precipitate at the boundary and also the different stoichiometry of the carbides when titanium is present (i.e., MC versus M_2C). Given a larger depleted zone for the samples with dense MC grain boundary precipitates, then following Weaver's arguments, even if the amount of grain boundary sliding was the same for the two carbide distributions, greater stress relieving could be expected for the material with the highest solute depletion near the boundary. However, the before mentioned inhibition of grain boundary sliding is probably a more important factor in reducing the rate of crack growth.

A difference in the cohesion between the particle and the matrix could also affect the continued growth of a previously nucleated crack. That is, the rate of crack growth under a mechanical shearing process (for example) is a function of the energy expended in creating the new interface. Thus, if the cohesion of the carbide to the matrix is large, a lower rate of crack propagation would be expected for a given energy

input than if the carbide-matrix binding energy was small. Although the cohesion is a function of orientation and other factors, work in other systems supports the argument. Guard[47] reported in the case of molybdenum and titanium carbides in molybdenum alloys that Mo_2C actually has a lower interfacial tension than TiC when dispersed within a molybdenum matrix and that this interfacial tension is a factor in the less potent effect of Mo_2C on raising the recrystallization temperature and inhibiting recovery of molybdenum alloys. If the M_2C and MC phases in nickel also have the same relative interfacial tension as do Mo_2C and TiC in molybdenum, then one could argue that crack propagation and/or nucleation at an M_2C carbide should be easier than at an MC carbide if all other factors are equal. Thus, cohesion of the carbide-matrix interface could be an important factor in inhibiting crack growth.

CHAPTER VI

SUMMARY AND CONCLUSIONS

This investigation of the influence of small titanium additions on the deformation and fracture of nickel-base alloys involved (1) measurement of creep-rupture properties as a function of carbon and titanium content for laboratory nickel-molybdenum-chromium alloys, (2) definition of the effect of titanium on the phase stability, phase morphology, and mechanical properties of commercial nickel-molybdenum-chromium alloys, and (3) determination of the effects of titanium on the deformation behavior of pure nickel.

The benefits of titanium in the nickel-molybdenum-chromium alloy at 650°C are small and subtle, unless the alloy is aged prior to mechanical testing. The fracture mode (whether trans- or intergranular) is affected by titanium primarily for the aged condition. In pure nickel, however, titanium drastically increases the creep and tensile ductility for all heat treatments, and the fracture mode is changed from intergranular to transgranular by the addition of as little as 0.06% Ti.

The mechanisms of the beneficial influence of titanium in these two systems is related to the effects on carbide precipitation in the complex alloy and probably to the gettering of interstitial impurities in the pure nickel. More detailed conclusions for these two systems are listed below. Reference to effects on mechanical properties are based primarily on creep and tensile behavior at 650°C for the nickel-

molybdenum-chromium-titanium alloy and on properties at 600°C for the nickel-titanium alloy.

The major conclusions drawn from the investigation of the influence of titanium and carbon on the Ni-12% Mo-7% Cr alloy are as follows:

1. Carbon and titanium both raise the strength and ductility in creep. The ductility increase is most evident for carbon contents above 0.1% and for the addition of 0.5% Ti the ductility is enhanced only for creep tests at low stresses.
2. Higher titanium contents favor the formation of an MC-type carbide. Titanium substitutes for chromium or molybdenum in the compound, increases the lattice parameter, and tends to stabilize the MC carbide at higher solutioning or aging temperatures. At low titanium concentrations there is a marked tendency for M_2C or a mixture of MC plus M_2C to form as the aging temperature is increased.
3. The transition from MC to M_2C type of carbide, as the titanium content is lowered or the aging temperature raised, is associated with a loss in the hot ductility at 650°C as measured in both tensile and creep tests.
4. Titanium is effective in these alloys in promoting a carbide morphology which results in enhanced mechanical properties.

5. The enhanced tensile ductility of higher titanium alloys is not due to an increase in uniform elongation, but is rather the result of greater nonuniform straining.
6. The precipitation of MC carbides on stacking faults in the nickel-molybdenum-chromium-titanium alloy is enhanced by increases in the titanium contents, carbon contents, or the solution annealing temperatures.
7. Precipitation on stacking faults can appreciably raise the tensile strength and lower the ductility, particularly after short times at 760°C where the precipitation is rapid.

Some specific conclusions which were drawn from the limited investigation of the nickel-titanium binary alloys are the following:

1. A maximum in the 600°C creep and tensile ductility occurs in the vicinity of Ni-0.2% Ti.
2. A marked change in the 600°C tensile fracture mode from intergranular to transgranular is produced by the addition of 0.06% Ti to nickel and results in a large increase in fracture ductility.
3. It is tentatively concluded that under creep test conditions the main influence of titanium in pure nickel is to getter impurities.
4. By removing the impurities, or by changing their distribution along the grain boundary either (a) the grain boundary has greater mobility for stress relieving migration or

recrystallization or (b) the absence of the impurities decreases the number of possible intergranular void nucleation sites, so that fewer stress concentrations are present under mechanical test conditions.

BIBLIOGRAPHY

BIBLIOGRAPHY

1. Zener, C., Elasticity and Anelasticity of Metals. Chicago, Illinois: University of Chicago Press, 1948.

2. McLean, D., "A Note on the Metallography of Cracking During Creep," Journal of the Institute of Metals, 85:468-472, 1967.

3. Stroh, A. N., "The Formation of Cracks as a Result of Plastic Flow," Proceedings of the Royal Society (London), Series A, 223:404-414, 1954.

4. Smith, E., and J. T. Barnby, "Crack Nucleation in Crystalline Solids," Metal Science Journal, 1:56-64, March 1967.

5. Chen, C. W., and E. S. Machlin, "On a Mechanism of High Temperature Intercrystalline Cracking," Transactions of the Metallurgical Society of AIME, 209:829-835, July 1957.

6. Garofalo, F., Fundamentals of Creep and Creep-Rupture in Metals. New York: Macmillan, 1965.

7. Weaver, C. W., "Application of Stroh's Theory to Intercrystalline Creep Cracking," Acta Metallurgica, 8:343-344, 1960.

8. Balluffi, R. W., and L. L. Seigle, "Growth of Voids in Metals During Diffusion and Creep," Acta Metallurgica, 5:449-454, 1957.

9. Stiegler, J. O., K. Farrell, B.T.M. Loh, and H. E. McCoy, "Nature of Creep Cavities in Tungsten," Transactions of the American Society for Metals, 60:494-503, September 1967.

10. Chang, H. C., and N. J. Grant, "Mechanism of Intercrystalline Fracture," Transactions of the Metallurgical Society of AIME, 206: 544-553, May 1956.

11. Weaver, C. W., "Intergranular Cavitation, Structure, and Creep of a Nimonic 80A-Type Alloy," Journal of the Institute of Metals, 88:296-300, 1960.

12. Betteridge, W., and A. W. Franklin, "The Effects of Heat-Treatment and Structure on the Creep and Stress-Rupture Properties of Nimonic 80A," Journal of the Institute of Metals, 85:473-479, 1956-57.

13. Heslop, J., "Creep Fractures in Nickel-Chromium Base Creep-Resistant Alloys," Journal of the Institute of Metals, 91:28-33, 1962.

14. Gifkins, R. D., "A Mechanism for the Formation of Intergranular Cracks When Boundary Sliding Occurs," Acta Metallurgica, 4:98-99, 1956.

15. Harris, J. E., Central Electric Generating Board Report RD/B/N 325. September 1964.

16. Dieter, G. E., "Introduction to Ductility," Ductility. Metals Park, Ohio: American Society for Metals, 1967. Pp. 1-30.

17. Stiegler, J. O, and J. R. Weir, "Effect of Irradiation on Ductility," Ductility. Metals Park, Ohio: American Society for Metals, 1967. Pp. 311-342.

18. Edelson, B. I., and W. M. Baldwin, "The Effect of Second Phases on the Mechanical Properties of Alloys," Transactions of the American Society for Metals, 55:230-250, 1962.

19. Brindley, B. J., "The Mechanism of Ductile Fracture in an Fe-21% Cr-0.05% C Alloy," Acta Metallurgica, 16:587-595, April 1968.

20. Webster, D., "Grain Boundary and Recrystallization in Thoria Dispersed Nickel and Nichrome," Transactions of the Metallurgical Society of AIME, 242:640-648, April 1968.

21. Rhines, F. N., and P. J. Wray, "Investigation of the Intermediate Temperature Ductility Minimum in Metals," Transactions of the American Society for Metals, 54:117-128, 1961.

22. Reed-Hill, R. E., C. R. Smeal, and F. N. Rhines, "Development of the Microstructure of Nickel-200 During Hot Plastic Deformation," Metallurgica, 23(115):419-427, June 1967. (Translated from Portuguese for Oak Ridge National Laboratory, ORNL-tr-2011).

23. Shapiro, E., and G. E. Dieter, "Fracture of Metals During Deformation Processing Under Conditions of Hot Working," Final Report from Drexel Institute of Technology to the Naval Air Systems Command, Philadelphia: Drexel Institute of Technology, April 1968.

24. Smith, T. C., Investigation of the Elevated Temperature Ductility Minima of Pure Nickel, M.S. Thesis, The University of Tennessee, 1963.

25. Sessions, C. E., Effect of Sulfur on the Elevated Temperature Ductility of Nickel, M.S. Thesis, The University of Tennessee, 1964.

26. Bloom, E. E., Effect of Grain Size and Strain Rate on the Elevated Temperature Ductility of Nickel, M.S. Thesis, The University of Tennessee, 1964.

27. Werner, W. J., An Investigation of the Effect of Certain Minor Elements on the Elevated Temperature Ductility of Incoloy 800, M.S. Thesis, The University of Tennessee, 1968.

28. Orava, R. N., "The Effect of Dynamic Strain Rate on Room Temeprature Ductility," Proceedings of First International Conference on High Energy Forming. Denver, Colorado: University of Denver, 1967.

29. Rogers, H. C., "The Effect of Material Variables on Ductility," Ductility. Metals Park, Ohio: American Society for Metals, 1968. Pp. 31-61.

30. Palmer, I. G., G. C. Smith, and R. D. Warda, "Some Aspects of Ductile Fracture in Metals," Conference Proceedings - Physical Basis of Yield and Fracture, Conference Series No. 1, A. C. Stickland, editor. London: Institute of Physics and the Physical Society, 1966. Pp. 53-59.

31. Christian, J. W., and P. R. Swann, "Stacking Faults in Metals," Alloying Behavior and Effects in Concentrated Solid Solutions (Metallurgical Society of AIME Conference Proceedings, Cleveland, Ohio, Oct. 21, 1963). New York: Gordon & Breach, 1965. Pp. 105-269.

32. Garofalo, F., "Ductility in Creep," Ductility. Metals Park, Ohio: American Society for Metals, 1967. Pp. 87-132.

33. Grant, N. J., and A. G. Bucklin, "On the Extrapolation of Short-Time Stress Rupture Data," Transactions of the American Society for Metals, 42:720-751, 1950.

34. Garofalo, F., R. W. Whitmore, R. W. Domis, and F. von Gemmingen, "Creep and Creep-Rupture Relationships in an Austenitic Steel," Transactions of the Metallurgical Society of AIME, 221:310-319, 1961.

35. Monkman, F. C., and N. J. Grant, "An Empirical Relationship Between Rupture Life and Minimum Creep Rate in Creep Rupture Tests," Transactions of the American Society for Metals, 56:593-620, 1956.

36. Bowing, P., P. W. Davies, and B. Wilshire, "The Strain-Dependence of Density Changes During Creep," Metal Science Journal, 2:168-171, 1968.

37. Hoff, N. J., "The Necking and Rupture of Rods Subjected to Constant Tensile Loads," Transactions of the American Society of Mechanical Engineers, 75:105-108, 1953.

38. Kennedy, A. J., Processes of Creep and Fatigue in Metals. Edinburgh, Scotland: Oliver & Boyd, 1962.

39. Hart, E. W., "Theory of the Tensile Test," Acta Metallurgica, 15: 351-355, 1967.

40. Glen, J., "An Experimental Study of the Strength and Ductility of Steels at Elevated Temperatures," Symposium on Strength and Ductility of Metals at Elevated Temperatures, ASTM Special Technical Publication 128. Philadelphia: American Society for Testing and Materials, 1953. Pp. 184-221.

41. Comstock, G. F., and S. F. Urban, "Titanium in Steels," Metals Handbook, Taylor Lyman, editor. Novelty, Ohio: American Society for Metals, 1948. Pp. 478-482.

42. Bardgett, W. E., "High Temperature Steels," Behavior of Metals at Elevated Temperatures. London: Iliffe and Sons, 1957. Pp. 93-122.

43. White, J. E., and J. W. Freeman, "Metallurgical Principles Governing the Creep-Rupture Strength of Type 321 (18-8 + Ti) Austenitic Steel Superheating Tubing with Limited Extension to Type 304 (18 Cr-8 Ni) and Type 316 (18 Cr-8 Ni + Mo) Austenitic Steels," Journal of Engineering for Power, 85:119-146, 1963.

44. Nakagawa, Ryuichi, Yoshikuni Kawabe, and Yasuo Otoguro, "Effect of Ti and Nb Additions on Structures and Properties of Cr-Ni Stainless Steels," Transactions of National Research Institute for Metals (Tokyo), 8:8-14, 1966.

45. Leslie, W. C., and R. J. Sober, "Yielding and Plastic Flow in a Polycrystalline Interstitial-Free Fe-0.15% Ti Alloy," Transactions of the American Society for Metals, 60:99-111, 1967.

46. Bloom, E. E., and J. R. Weir, Jr., "Development of Austenitic Stainless Steels with Improved Resistance to Elevated-Temperature Irradiation Embrittlement," Effects of Radiation on Structural Metals, ASTM Special Technical Publication 457. Philadelphia: American Society for Testing and Materials (to be published).

47. Guard, Ray W., "Alloying for Creep Resistance," Mechanical Behavior of Materials at Elevated Temperatures, J. E. Dorn, editor. New York: McGraw-Hill, 1961. Pp. 270-287.

48. Hazlett, T. H., and E. R. Parker, "Effects of Some Solid Solution Alloying Elements on the Creep Properties of Nickel," Transactions of the American Society for Metals, 46:701-715, 1954.

49. Ancker, Betty, and E. R. Parker, "Quantitative Substructure and Tensile-Property Investigation of Nickel Alloys," Journal of Metals, 6:1115-1162, October 1954.

50. Lund, C. H., Physical Metallurgy of Nickel-Base Superalloys, Battelle Memorial Institute, DMIC Report 153, May 1961.

51. Sims, C. T., "A Contemporary View of Nickel-Base Superalloys," Journal of Metals, 18:1119-1130, October 1966.

52. Beattie, H. J., Jr., and F. L. VerSnyder, "The Influence of Molybdenum on Phase Relationships of a High Temperature Alloy," Transactions of the American Society for Metals, 49:883-904, 1957.

53. Decker, R. F., and J. W. Freeman, "The Mechanism of Beneficial Effects of Boron and Zirconium on Creep Resistance of a Complex Heat-Resistant Alloy," Transactions of the Metallurgical Society of AIME, 218:277-285, 1960.

54. McCoy, H. E., and J. R. Weir, Jr., "Development of a Titanium-Modified Hastelloy N with Improved Resistance to Radiation Damage," Effects of Radiation on Structural Metals, ASTM Special Technical Publication 457. Philadelphia: American Society for Testing and Materials (to be published).

55. Chang, W. H., "Effects of Carbide Dispersion in Molybdenum Alloys," Transactions of the Metallurgical Society of AIME, 218:254-255, 1960.

56. Chang, W. H., "The Effect of Heat Treatment on Strength Properties of Molybdenum-Base Alloys," Transactions of the American Society for Metals, 56(1):107-124, March 1963.

57. Chang, W. H., "Effects of Titanium and Zirconium on Microstructures and Tensile Properties of Carbon Strengthened Molybdenum Alloys," Transactions of the American Society for Metals, 57(2):527-553, June 1964.

58. Chang, W. H., and I. Perlmutter, "Solutioning and Aging Reactions in Molybdenum-Base Alloys," High Temperature Materials Part II, Metallurgical Society of the AIME Conference, Vol. 18. New York: Interscience Publishers, 1963. Pp. 347-370.

59. Chang, W. H., "Strain Induced vs. Pre-Existing Precipitation in the Mo-TZC Alloy," Transactions of the American Society for Metals, 57:565-567, 1964.

60. Keith, G. H., Interactions of Titanium and Molybdenum Additions with Interstitial Impurities in Vanadium, United States Department of the Interior-Bureau of Mines, RI-7262, May 1969.

61. King, R. T., E. M. Thomas, and H. E. McCoy, "The Computer - An Aid for Analyzing and Processing Creep Rupture Data," Journal of Metals, 21(11):62-68, November 1969.

62. DuBose, C. K. H., and J. O. Stiegler, Semiautomatic Preparation of Specimens for Transmission Electron Microscopy, Oak Ridge National Laboratory, ORNL-4066, February 1967.

63. Kimoto, S., and J. C. Russ, "The Characteristics and Applications of the Scanning Electron Microscope," American Scientist, 57(1): 112-133, 1969.

64. Scanning Electron Microscopy - 1969 (Proceedings of Second Annual Scanning Electron Microscopy Symposium). Chicago, Illinois: Illinois Institute of Technology Research Institute, 1969.

65. Kuz'ma, Yu. B., and T. F. Fedorov, "Phase Equilibria in the System Molybdenum-Chromium-Carbon," Soviet Powder Metallurgy and Metal Ceramics, 1(25):920-922, 1965. [Translated from Poroshkovaya Metallurgiya, No. 11(35):62-65, November 1965.]

66. Pearson, W. B., A Handbook of Lattice Spacings and Structures of Metals and Alloys, Vol. 2. New York: Pergamon Press, 1967.

67. Russ, John C., and Akira Kabaya, "Use of a Non-Dispersive X-Ray Spectrometer on the Scanning Microscope," Scanning Electron Microscopy - 1969 (Proceedings of Second Annual Scanning Electron Microscopy Symposium). Chicago, Illinois: Illinois Institute of Technology Research Institute, 1969.

68. Beachem, C. D., and D. A. Meyn, "Fracture by Microscopic Plastic Deformation Processes," Electron Fractography, ASTM Special Technical Publication 436. Philadelphia: American Society for Testing and Materials, 1967. Pp. 59-88.

69. Naybour, R. D., "Hardening During Deformation of an 18 Cr/12 Ni/Nb Austenitic Steel at 650°C," Acta Metallurgica, 13:1197-1207, 1965.

70. Elliott, J. F., and M. Gleiser, Thermochemistry for Steelmaking. Reading, Massachusetts: Addison-Wesley, 1960.

71. Klein, M. J., and C. N. Reid, Metal Deformation Processing Volume 1, Battelle Memorial Institute, DMIC Report 208, August 1964.

72. Raffo, Peter J., Dynamic Strain Aging During Creep and Tensile of a Molybdenum-Titanium-Carbon Alloy, National Aeronautics and Space Administration, Lewis Research Center, NASA TN-D5169, January 1969.

73. Wilcox, B. A., and A. R. Rosenfield, "On Serrated Yielding and Negative Strain-Rate Sensitivity," Materials Science and Engineering, 1(4):201-205, November 1966.

74. Bieber, C. G., and R. F. Decker, "The Melting of Malleable Nickel and Nickel Alloys," Transactions of the Metallurgical Society of AIME, 221:629-636, 1961.

75. Robbins, Jack L., O. C. Shepard, and Oleg D. Sherby, "Role of Crystal Structure on the Ductility of Pure Iron at Elevated Temperatures," Journal of the Iron and Steel Institution (London), 199: 175-180, October 1961.

76. Silcock, Jeanne M., and W. J. Tunstall, "Partial Dislocations Associated with NbC Precipitation in Austenitic Stainless Steels," The Philosophical Magazine, 10:360-389, 1964.

77. Silcock, Jeanne M., "Precipitation of NbC in Niobium Stabilized Austenitic Steels Observed by Thin Film Electron Microscopy," Journal of the Iron and Steel Institute (London), 204:409-421, 1963.

78. Van Aswegan, J. S. T., R. W. K. Honeycombe, and D. H. Warrington, "Precipitation on Stacking Faults in Cr-Ni Austenitic Steels," Acta Metallurgica, 12:1-13, January 1964.

79. Froes, F. H., R. W. K. Honeycombe, and D. H. Warrington, "Conditions Controlling Matrix and Stacking Fault Precipitation," Acta Metallurgica, 15:157-159, 1967.

80. Honeycombe, R. W. K., J. S. T. Van Aswegen, and D. H. Warrington, "The Role of Stacking Faults in Precipitation Processes," The Relation Between the Structure and Mechanical Properties of Metals, National Physical Laboratory Conference, Vol. 1. London: Her Majesty's Stationery Office, 1963. Pp. 379-396.

81. Pickering, F. B., "The Precipitation of Niobium Carbide in Austenitic Creep Resisting Steels," The Relation Between the Structure and Mechanical Properties of Metals, National Physical Laboratory Conference, Vol. 1. London: Her Majesty's Stationery Office, 1963. Pp. 397-407.

82. Van Aswegen, J. S. T., and R. W. K. Honeycombe, "Segregation and Precipitation in Stacking Faults," Acta Metallurgica, 10:262-264, 1962.

83. Kotvol, P. S., "Carbide Precipitation on Imperfections in Superalloy Matrices," Transactions of the Metallurgical Society of AIME, 242:1651-1656, August 1968.

84. Kotvol, P. S., "The Microstructure of Superalloys," Metallography, 1(3/4):251-285, January 1969.

85. Kotvol, P. S., and O. N. Nestor, "The Effect of Solute Additions on the Stacking Fault Energy of a Nickel-Base Superalloy," Transactions of the Metallurgical Society of AIME, 245:1275-1278, June 1969.

86. Teutonico, L. J., "The Dissociation of Dislocations in the Face-Centered Cubic Structure," Acta Metallurgica, 11:1283-1289, December 1963.

87. Taplin, D. M. R., "A Note on the Relationship Between Cavitation and Ductility," Journal of the Australian Institute of Metals, 10:336-339, 1963.

88. Conrad, Hans, "The Role of Grain Boundaries in Creep and Stress-Rupture," Mechanical Behavior of Materials at Elevated Temperature, John E. Dorn, editor. New York: McGraw-Hill, 1961. Pp. 218-269.

APPENDIX

TABLE VIII

HEAT TREATMENT DESIGNATIONS

Designation	Solution Anneal		Age Treatment	
	Time (hr)	Temperature (°C)	Time (hr)	Temperature (°C)
22	1	1177	100	870
112	1	650	0	--
121	1	1177	0	--
123	1	1260	0	--
130	1	1177	1500	650
131	1	1177	1500	760
132	1	1177	3000	650
133	1	1177	3000	760
134	1	1177	10000	650
135	1	1177	10000	760
136	1	1260	1500	650
137	1	1260	1500	760
138	1	1260	3000	650
139	1	1260	3000	760
140	1	1260	10000	650
141	1	1260	10000	760
190	5	1177	0	--
191	1	1260	5	760
192	1	1260	50	760
193	1	1260	100	760
194	1	1260	200	760
195	1	1260	100	650
196	1	1177	200	760
197	1	1177 and 1260	0	--
198	1	1177 and 1260	100	760
199	1	1177 and 1260	200	760
200	5	1177	0	--

TABLE IX

CREEP-RUPTURE DATA AT 650°C FOR LABORATORY HEATS OF HASTELLOY-N VARYING TITANIUM AND CARBON CONCENTRATION

Heat	Heat Treatment	Test Number	Stress (psi)	Rupture Life (hr)	Secondary Creep Rate (%/hr)	Total Elongation (%)	Reduction in Area (%)
193	22	6552	47000	0.0	0.0000	21.67	27.30
193	22	6551	32350	6.1	0.2850	11.18	16.45
193	22	6546	40000	0.1	32.6000	15.12	26.59
193	121	6545	32350	13.0	0.0975	10.91	20.25
193	121	6544	40000	0.1	3.4500	22.57	26.89
193	121	7243	20000	3049.4	0.0012	7.20	3.68
193	121	7244	25000	110.8	0.0264	7.70	6.65
193	121	6735	32500	1.8	1.9500	7.31	14.24
193	123	6548	40000	0.0	0.0000	14.27	25.44
193	123	6556	47000	0.0	0.0000	21.76	29.06
193	123	6555	32350	7.2	0.2650	10.48	16.91
193	123	7245	25000	147.2	0.0151	8.40	13.88
194	22	6474	40000	0.7	1.9000	14.90	23.60
194	22	6476	55000	0.0	0.0000	26.36	30.71
194	22	6475	47000	0.0	0.0000	20.10	23.67
194	121	6485	40000	0.5	1.0400	13.47	24.84
194	121	6483	32350	19.7	0.0700	10.15	18.43
194	121	6484	47000	0.0	0.0000	19.45	33.99
194	121	7246	20000	3049.6	0.0015	6.60	3.67
194	121	7247	25000	252.6	0.0096	8.00	12.77
194	121	6749	32350	3.6	0.1950	15.32	15.09
194	123	6465	40000	0.4	1.8600	14.10	19.87
194	123	6467	55000	0.0	0.0000	26.58	30.06
194	123	6466	47000	0.0	0.0000	18.19	20.17
194	123	6734	32350	28.5	0.0375	9.43	19.30

TABLE IX (continued)

Heat	Heat Treatment	Test Number	Stress (psi)	Rupture Life (hr)	Secondary Creep Rate (%/hr)	Total Elongation (%)	Reduction in Area (%)
195	22	6461	55000	4.8	0.8750	27.10	25.82
195	22	6460	47000	19.7	0.3000	23.50	21.67
195	22	6459	40000	169.4	0.0440	20.20	19.68
195	22	6753	32350	1332.2	0.0118	27.20	22.36
195	121	6470	32350	1121.1	0.0050	19.04	20.51
195	121	6446	47000	51.0	0.0390	20.70	22.12
195	121	6439	40000	176.7	0.0210	17.40	17.86
195	121	7248	55000	15.3	0.1800	25.50	27.97
195	123	6488	55000	0.1	25.0000	28.10	36.08
195	123	6487	47000	8.4	0.2860	17.50	26.21
195	123	6486	40000	87.0	0.0364	12.40	22.40
195	123	6756	32350	575.8	0.0063	20.46	21.15
196	22	6550	32350	1257.1	0.0117	23.10	22.71
196	22	6529	40000	133.8	0.0611	16.95	18.97
196	22	6549	47000	33.5	0.2213	17.06	17.07
196	22	7250	55000	5.6	0.6750	16.40	21.43
196	121	6542	47000	138.7	0.0138	17.70	16.83
196	121	6541	40000	533.4	0.0067	16.42	15.69
196	121	6543	32350	2555.9	0.0015	16.41	8.43
196	121	7249	55000	15.7	0.0850	21.80	27.16
196	123	6547	40000	363.5	0.0050	19.07	28.86
196	123	6553	47000	21.5	0.0850	12.95	22.01
196	123	6554	32350	1353.4	0.0040	15.99	15.96
196	123	6750	32350	1181.9	0.0048	16.61	12.74

TABLE IX (continued)

Heat	Heat Treatment	Test Number	Stress (psi)	Rupture Life (hr)	Secondary Creep Rate (%/hr)	Total Elongation (%)	Reduction in Area (%)
197	22	6473	55000	30.1	0.6000	34.25	33.12
197	22	6471	40000	415.6	0.0557	41.40	39.69
197	22	6472	32350	1557.2	0.0134	44.10	49.05
197	22	6754	47000	704.5	0.0263	42.83	46.46
197	121	6482	40000	838.8	0.0125	41.70	40.58
197	121	6481	47000	401.1	0.0250	42.30	44.50
197	121	6480	32350	2478.6	0.0039	37.62	43.35
197	121	7252	70000	13.2	0.4100	16.10	16.95
197	121	7251	55000	36.5	0.2220	18.60	16.16
197	123	6464	55000	32.9	0.2670	16.90	15.47
197	123	6463	47000	118.5	0.1140	29.95	27.72
197	123	6462	40000	442.5	0.0270	32.17	32.53
197	123	6732	32350	2949.9	0.0009	3.45	10.94
197	123	6732R*	35000	172.2	0.0013	0.47	--
197	123	6732RR*	40000	800.0	0.0101	10.28	--
198	22	6456	40000	18.1	0.1680	12.00	12.51
198	22	6458	55000	1.4	2.5000	21.60	21.75
198	22	6457	47000	4.7	0.6700	15.80	18.34
198	22	6755	32350	66.2	0.0331	5.95	8.93
198	22	7255	25000	35.7	0.0121	4.90	9.73
198	121	6438	55000	0.3	25.8000	28.90	27.95
198	121	6437	47000	1.6	0.7000	19.80	26.49
198	121	6432	40000	8.5	0.1300	14.00	17.52
198	121	7253	25000	885.1	0.0020	7.20	4.30
198	121	7254	20000	1471.1	0.0014	5.70	2.85
198	121	6733	32350	132.5	0.0144	9.90	8.31
198	123	6489	40000	2.0	0.5000	13.60	17.29

TABLE IX (continued)

Heat	Heat Treatment	Test Number	Stress (psi)	Rupture Life (hr)	Secondary Creep Rate (%/hr)	Total Elongation (%)	Reduction in Area (%)
198	123	6491	32350	59.1	0.0280	7.47	12.66
198	123	6490	47000	1.4	0.8330	19.40	23.44
198	123	6736	47000	0.1	6.4300	22.37	22.73
238	22	6908	40000	231.4	0.0444	20.30	19.85
238	22	6907	47000	56.5	0.1920	18.80	16.34
238	22	6906	55000	11.7	0.5100	16.60	18.90
238	121	6923	40000	842.3	0.0053	16.90	13.29
238	121	6922	47000	222.4	0.0114	10.50	14.39
238	121	6921	55000	51.3	0.0613	15.10	17.76
238	121	7256	70000	11.0	0.1800	18.90	18.15
238	123	6938	40000	493.6	0.0031	13.70	17.37
238	123	6937	47000	176.9	0.0053	18.10	16.29
238	123	6936	55000	42.0	0.0250	22.90	20.32
239	22	7110	40000	302.2	0.0525	25.4	20.5
239	22	7109	47000	46.4	0.257	19.8	17.2
239	22	7108	55000	9.5	1.145	17.4	16.2
239	121	7106	40000	647.6	0.0097	20.4	18.0
239	121	7105	47000	321.2	0.0152	18.8	18.5
239	121	7095	55000	88.7	0.0432	16.3	17.1
239	121	7107	70000	10.8	0.385	18.1	16.7
239	123	7114	40000	1118.3	0.0043	13.6	23.6
239	123	7113	47000	347.1	0.008	13.7	12.2
239	123	7112	55000	60.5	0.0483	15.5	13.2

TABLE IX (continued)

Heat	Heat Treatment	Test Number	Stress (psi)	Rupture Life (hr)	Secondary Creep Rate (%/hr)	Total Elongation (%)	Reduction in Area (%)
242	22	6920	40000	255.6	0.0800	41.20	34.52
242	22	6919	47000	87.8	0.2417	40.10	36.66
242	22	6918	55000	14.2	1.4670	31.40	28.01
242	121	6933	55000	58.6	0.1256	25.20	26.85
242	121	6935	40000	896.3	0.0110	28.90	29.64
242	121	6934	47000	408.9	0.0187	29.10	27.55
242	121	6950	40000	1003.7	0.0087	30.40	26.71
242	121	7260	70000	13.0	0.5550	16.20	16.56
242	123	6949	47000	277.9	0.0200	11.90	22.85
242	123	6948	55000	45.7	0.1672	18.00	23.94

*Stress was increased to 35000 psi after 2950 hr (3.45% ϵ) and later increased to 40000 psi.

TABLE X

CREEP-RUPTURE DATA FOR NICKEL AND NICKEL-TITANIUM ALLOYS
TESTED IN ARGON AT 600°C

Heat	Heat Treatment	Test Number	Stress (psi)	Rupture Life (hr)	Secondary Creep Rate (%/hr)	Total Elongation (%)	Reduction in Area (%)
222	112	7328	9000	586.0	0.0244	37.40	72.25
222	112	7063	12000	87.3	0.0883	25.30	87.53
222	112	7622	9000	863.4	0.0034	6.00	4.15
222	112	7497	14000	34.3	0.6338	43.50	93.83
226	112	7105	12000	326.2	0.0142	16.70	87.37
226	112	7312	14000	68.2	0.1960	25.90	89.33
253	112	7058	12000	7.1	0.6938	11.30	21.93
253	112	7313	4000	2176.2	0.0014	7.90	9.08
253	112	7167	9000	20.0	0.1930	10.20	13.72
253	112	7194	7500	216.2	0.0118	9.12	9.11
253	112	7205	7500	71.4	0.0500	8.70	13.61

TABLE XI

CREEP-RUPTURE PROPERTIES AT 40000 PSI AND 650°C FOR COMMERCIAL HEATS OF HASTELLOY-N USED TO EVALUATE THE THERMAL STABILITY

Heat	Heat Treatment	Test Number	Rupture Life (hr)	Secondary Creep Rate (%/hr)	Total Elongation (%)	Reduction in Area (%)
466535	121	7130	166.5	0.0133	9.50	10.60
466535	123	7132	50.9	0.0119	13.60	24.39
466535	131	7277	136.5	0.0489	11.30	17.36
466535	132	7368	137.8	0.0630	13.60	14.27
466535	133	7369	63.6	0.0683	9.50	13.19
466535	138	7336	217.5	0.0346	13.70	15.22
466535	139	7340	26.2	0.0868	8.30	9.51
466541	121	7133	341.6	0.0060	15.20	17.75
466541	123	7135	189.0	0.0080	21.50	26.61
466541	131	7276	217.0	0.0538	18.90	19.48
466541	132	7370	507.6	0.0315	27.60	26.93
466541	133	7371	67.8	0.0692	10.50	18.42
466541	138	7337	50.0	0.0716	9.70	12.96
466541	139	7341	41.2	0.0844	9.90	17.62
466548	121	7136	358.0	0.0117	16.70	22.31
466548	123	7138	125.1	0.0110	19.30	28.19
466548	130	7024	569.6	0.0203	27.20	30.09
466548	131	7275	594.0	0.0251	42.10	34.19
466548	132	7372	574.6	0.0391	41.30	41.30
466548	133	7373	135.5	0.0535	16.70	21.94
466548	138	7338	345.5	0.0968	29.10	37.27
466548	139	7342	175.2	0.0660	24.10	37.54

TABLE XI (continued)

Heat	Heat Treatment	Test Number	Rupture Life (hr)	Secondary Creep Rate (%/hr)	Total Elongation (%)	Reduction in Area (%)
467548	121	7434	1207.6	0.0144	36.60	33.44
467548	123	7141	2472.9	0.0038	21.60	17.62
467548	131	7303	1006.2	0.0195	32.40	47.74
467548	132	7374	1582.7	0.0159	54.40	47.74
467548	133	7375	1335.2	0.0162	36.80	35.17
467548	138	7339	2095.5	0.0072	24.50	26.93
467548	139	7343	1454.2	0.0099	20.40	28.64

TABLE XII

TENSILE DATA AT 650°C FOR COMMERCIAL HEAT 466535 FOR VARIOUS HEAT TREATMENTS

Specimen Number	Heat Treatment	Test Temperature (°C)	Strength (psi)		Elongation (%)		Reduction in Area
			Yield	Ultimate Tensile	Uniform	Total	
			$\times 10^3$	$\times 10^3$			
5989	121	650	29.3	71.4	24.0	24.6	27.28
5991	121	650	28.6	76.1	30.4	30.9	21.18
6019	123	650	26.1	66.7	29.0	30.0	22.61
6017	123	650	24.5	64.5	31.8	33.0	32.09
5993	130	650	38.7	77.5	24.9	27.7	26.61
6040	130	650	40.7	81.9	27.0	32.5	23.40
5994	131	650	35.2	73.9	15.9	16.4	17.59
6041	131	650	35.2	76.2	16.6	17.4	13.54
5999	132	650	39.3	73.9	18.5	18.8	22.93
6000	133	650	32.7	66.2	13.4	13.8	16.71
6001	134	650	36.2	62.6	14.8	15.1	11.49
6002	135	650	32.3	73.4	16.6	16.9	13.29
6021	136	650	33.1	66.1	21.0	21.6	24.20
6022	137	650	33.0	66.7	13.8	16.5	17.43
6027	138	650	35.2	57.5	12.1	12.6	17.73
6028	139	650	30.5	63.3	14.3	16.0	17.86
6029	140	650	38.4	62.2	10.2	10.7	10.54
6030	141	650	31.9	65.3	13.7	14.4	17.36
5997	130	25	61.5	135.9	40.5	40.8	29.54
5998	131	25	53.3	139.1	43.5	46.0	47.81

TABLE XIII

TENSILE DATA AT 650°C FOR COMMERCIAL HEAT 466541 FOR VARIOUS HEAT TREATMENTS

Specimen Number	Heat Treatment	Test Temperature (°C)	Strength (psi)		Elongation (%)		Reduction in Area (°C)
			Yield	Ultimate Tensile	Uniform	Total	
			$\times 10^3$	$\times 10^3$			
6090	121	650	26.5	68.8	29.2	30.6	28.41
6092	121	650	27.5	76.2	33.7	34.6	28.30
6121	123	650	21.5	54.4	31.8	33.4	31.22
6119	123	650	21.4	53.9	29.7	30.5	41.14
6128	123	650	21.8	53.6	29.8	31.3	27.48
6094	130	650	35.1	77.3	35.1	43.7	38.68
6095	131	650	33.3	68.8	17.8	18.3	23.17
6101	132	650	34.6	74.3	32.9	39.6	35.31
6102	133	650	31.4	63.4	15.4	16.0	20.73
6103	134	650	33.8	69.8	28.6	34.6	27.36
6104	135	650	28.3	61.0	19.0	19.5	16.01
6123	136	650	26.6	46.8	16.4	17.4	26.43
6124	137	650	31.3	59.2	15.5	16.7	15.92
6129	138	650	29.9	46.1	10.4	11.4	25.41
6120	139	650	29.7	57.6	13.6	14.9	16.03
6131	140	650	36.0	48.5	7.4	8.9	10.39
6132	141	650	31.0	58.1	13.1	14.7	13.57
6099	130	25	54.3	125.6	52.5	53.7	41.88
6100	131	25	42.4	110.5	50.1	52.3	40.64

TABLE XIV

TENSILE DATA AT 650°C FOR COMMERCIAL HEAT 466548 FOR VARIOUS HEAT TREATMENTS

Specimen Number	Heat Treatment	Test Temperature (°C)	Strength (psi)		Elongation (%)		Reduction in Area (%)
			Yield	Ultimate Tensile	Uniform	Total	
			$\times 10^3$	$\times 10^3$			
6268	121	650	25.2	66.6	28.2	29.2	35.43
6270	121	650	24.2	66.9	30.4	31.9	26.33
6299	123	650	20.3	54.2	29.8	32.2	27.74
6297	123	650	20.6	55.3	30.2	32.9	34.73
7400	130	650	29.7	76.6	40.4	43.3	40.10
7402	131	650	30.1	79.2	35.3	37.7	28.94
6279	132	650	29.9	74.3	39.6	42.9	41.38
6280	133	650	30.1	67.3	20.1	20.8	27.04
6281	134	650	29.4	71.9	35.4	43.3	31.45
6282	135	650	28.9	70.3	23.6	24.3	20.41
6301	136	650	24.3	71.6	47.2	49.8	46.04
6302	137	650	27.2	86.5	32.3	33.5	27.64
6307	138	650	26.1	68.6	44.4	46.2	52.56
6308	139	650	25.8	61.8	24.9	26.2	23.42
6309	140	650	29.6	72.4	39.3	41.7	40.83
6310	141	650	27.0	63.9	24.9	26.2	26.33
6277	130	25	47.6	124.1	57.4	59.0	41.79
6278	131	25	48.1	129.6	53.6	55.4	50.95

TABLE XV

TENSILE DATA AT 650°C FOR COMMERCIAL HEAT 467548 FOR VARIOUS HEAT TREATMENTS

Specimen Number	Heat Treatment	Test Temperature (°C)	Strength (psi)		Elongation (%)		Reduction in Area (%)
			Yield	Ultimate Tensile	Uniform	Total	
			$\times 10^3$	$\times 10^3$			
6313	121	650	39.4	96.3	29.8	35.3	31.58
6315	121	650	33.8	96.7	39.3	42.9	31.22
6341	123	650	29.7	74.6	39.4	40.8	39.95
6343	123	650	28.6	82.4	43.2	43.9	28.53
6317	130	650	46.5	92.1	28.3	50.2	45.00
6355	130	650	42.9	93.6	25.7	45.4	38.51
6357	131	650	41.1	94.5	26.5	44.7	37.44
6318	131	650	41.8	92.8	25.9	45.0	39.99
6323	132	650	43.1	87.9	26.1	43.3	42.18
6324	133	650	40.8	87.1	24.5	42.1	41.05
6325	134	650	38.2	84.3	26.7	44.1	35.74
6326	135	650	36.6	83.1	25.5	44.1	36.05
6345	136	650	42.7	83.3	24.4	25.7	24.07
6346	137	650	46.3	71.5	9.6	11.0	10.60
6351	138	650	44.8	79.0	17.3	20.1	27.41
6352	139	650	44.6	91.7	13.3	15.4	18.51
6353	140	650	49.6	81.4	14.0	15.2	18.29
6354	141	650	49.8	76.4	10.8	11.7	9.52
6321	130	25	61.3	145.6	50.5	52.0	41.21
6322	131	25	50.1	121.3	47.8	49.0	43.57

TABLE XVI

TENSILE DATA FROM AUXILIARY EXPERIMENTS ON HEAT 467548 TO DEFINE CONDITIONS OF FORMATION OF THE STACKING FAULT PRECIPITATE MORPHOLOGY

Specimen Number	Heat Treatment	Test Temperature (°C)	Strength (psi)		Elongation (%)		Reduction in Area (%)
			Yield	Ultimate Tensile	Uniform	Total	
			$\times 10^3$	$\times 10^3$			
6315	121	650	33.8	96.7	39.3	42.9	31.2
6343	123	650	28.6	82.4	43.2	43.9	28.5
6344	123	25	35.7	104.9	67.0	68.2	18.1
8779	197	650	34.6	92.2	34.2	34.7	33.9
8992	198[a]	650	37.5	75.7	29.1	39.3	26.2
6350	199	650	40.9	72.6	17.1	18.5	17.6
8993	199[a]	650	38.7	78.1	32.0	32.8	25.5
8899	191	650	46.1	89.4	29.4	30.2	20.0
8900	192	650	48.0	82.2	19.9	20.7	21.3
8780	193	650	54.9	94.9	16.2	17.4	17.1
8781	195	650	38.2	102.2	36.0	36.9	28.2
8901	194	650	46.3	75.7	15.2	17.2	11.4
6345	136	650	42.7	83.3	24.4	25.7	24.1
6346	137	650	46.8	71.5	9.6	11.0	10.6
6989	137	25	59.6	122.6	41.6	41.7	36.7
6351	138	650	44.8	79.0	17.3	20.1	27.4
6352	139	650	44.6	91.7	13.3	15.4	18.5
6353	140	650	49.6	81.4	14.0	15.2	18.3
6354	141	650	49.8	76.4	10.8	11.7	9.5
8782	190	650	35.9	105.4	38.5	42.4	29.5

[a]Samples furnace cooled from 1260°C to 1177°C in approximately 10 minutes.

TABLE XVIII

TENSILE DATA FOR NICKEL AND NICKEL-TITANIUM ALLOYS TESTED IN ARGON AT 600°C AND 0.002 MINUTE^{-1} STRAIN RATE

Heat	Specimen Number	Heat Treatment	Test Temperature	Yield Strength (psi)	Ultimate Tensile Strength (psi)	Uniform Elongation (%)	Total Elongation (%)	Reduction in Area (%)
222	7011	112	400	4880	29300	43.0	52.7	84.7
222	7012	112	500	6590	24700	47.5	59.1	96.1
222	7010	112	600	5340	20860	36.7	66.0	100.0
222	7013	112	600	5530	18300	39.2	57.3	81.9
222	7016	112	600	6760	18500	33.8	51.2	63.9
222	7022	112	700	6160	12100	16.8	81.8	96.9
222	7023	112	800	4420	7260	12.6	64.0	67.0
222	10004	112	600	9450	19100	20.0	--	12.3
223	7040	112	600	8210	23700	33.8	60.8	87.5
223	10016	112	25	9700	54600	47.4	56.2	85.6
224	7049	112	600	23050	32600	17.2	36.2	78.9
226	7086	112	25	13100	68100	41.9	47.9	72.7
226	7085	112	400	14900	64000	33.2	42.2	76.5
226	7078	112	500	14100	49600	42.2	49.7	74.1
226	7079	112	600	10900	37800	35.5	62.4	51.1
226	7075	112	700	10850	21300	28.0	58.3	65.3
226	10062	112	800	7560	10500	19.4	79.7	83.0
253	7178	112	25	6800	45760	49.0	54.1	70.6
253	7202	112	25	7070	48200	49.0	56.0	69.4
253	7183	112	400	6240	27900	34.2	35.8	--
253	7181	112	500	7590	22700	37.8	40.2	33.6
253	7200	112	600	6620	17900	13.3	14.1	16.9
253	7177	112	600	6010	16800	22.9	29.6	25.9
253	7188	112	600	4200	16600	26.6	34.2	30.4
253	7189	112	700	1490	8420	11.0	14.6	9.4
253	7186	112	800	3700	4710	5.7	8.9	7.9

TABLE XVIII

TENSILE DATA FOR NICKEL AND NICKEL-TITANIUM ALLOYS TESTED IN ARGON AT 600°C AND 0.002 MINUTE^{-1} STRAIN RATE

Heat	Specimen Number	Heat Treatment	Test Temperature (°C)	Strength (psi)		Elongation (%)		Reduction in Area (%)
				Yield	Ultimate Tensile	Uniform	Total	
222	7011	112	400	4880	29300	43.0	52.7	84.7
222	7012	112	500	6590	24700	47.5	59.1	96.1
222	7010	112	600	5340	20860	36.7	66.0	100.0
222	7013	112	600	5530	18300	39.2	57.3	81.9
222	7016	112	600	6760	18500	33.8	51.2	63.9
222	7022	112	700	6160	12100	16.8	81.8	96.9
222	7023	112	800	4420	7260	12.6	64.0	67.0
222	10004	112	600	9450	19100	20.0	--	12.3
223	7040	112	600	8210	23700	33.8	60.8	87.5
223	10016	112	25	9700	54600	47.4	56.2	85.6
224	7049	112	600	23050	32600	17.2	36.2	78.9
226	7086	112	25	13100	68100	41.9	47.9	72.7
226	7085	112	400	14900	64000	33.2	42.2	76.5
226	7078	112	500	14100	49600	42.2	49.7	74.1
226	7079	112	600	10900	37800	35.5	62.4	51.1
226	7075	112	700	10850	21300	28.0	58.3	65.3
226	10062	112	800	7560	10500	19.4	79.7	83.0
253	7178	112	25	6800	45760	49.0	54.1	70.6
253	7202	112	25	7070	48200	49.0	56.0	69.4
253	7183	112	400	6240	27900	34.2	35.8	--
253	7181	112	500	7590	22700	37.8	40.2	33.6
253	7200	112	600	6620	17900	13.3	14.1	16.9
253	7177	112	600	6010	16800	22.9	29.6	25.9
253	7188	112	600	4200	16600	26.6	34.2	30.4
253	7189	112	700	1490	8420	11.0	14.6	9.4
253	7186	112	800	3700	4710	5.7	8.9	7.9

ORNL-4561
UC-25 — Metals, Ceramics, and Materials

INTERNAL DISTRIBUTION

1–3. Central Research Library
4–5. ORNL — Y-12 Technical Library
Document Reference Section
6–25. Laboratory Records
26. Laboratory Records, ORNL RC
27. ORNL Patent Office
28. R. K. Adams
29. G. M. Adamson, Jr.
30. R. G. Affel
31. J. L. Anderson
32. R. F. Apple
33. W. E. Atkinson
34. C. F. Baes
35. J. M. Baker
36. S. J. Ball
37. C. E. Bamberger
38. C. J. Barton
39. H. F. Bauman
40. M. S. Bautista
41. S. E. Beall
42. R. L. Beatty
43. M. J. Bell
44. M. Bender
45. R. G. Berggren
46. C. E. Bettis
47. E. S. Bettis
48. D. S. Billington
49. R. E. Blanco
50. F. F. Blankenship
51. J. O. Blomeke
52. E. E. Bloom
53. R. Blumberg
54. E. G. Bohlmann
55. B. S. Borie
56. C. J. Borkowski
57. H. I. Bowers
58. C. M. Boyd
59. G. E. Boyd
60. M. A. Bredig
61. R. B. Briggs
62. H. R. Bronstein
63. G. D. Brunton
64. O. W. Burke
65. D. A. Canonico
66. S. Cantor
67. D. W. Cardwell
68. R. W. Carpenter
69. J. H. Carswell, Jr.
70. W. L. Carter
71. G. I. Cathers
72. J. E. Caton
73. O. B. Cavin
74. J. M. Chandler
75. C. J. Claffey
76. F. H. Clark
77. R. E. Clausing
78. W. R. Cobb
79. H. D. Cochran
80. W. A. Coghlan
81. Nancy Cole
82. C. W. Collins
83. E. L. Compere
84. K. V. Cook
85. S. W. Cook
86. W. H. Cook
87. J. W. Cooke
88. G. L. Copeland
89. L. T. Corbin
90. B. Cox
91. C. M. Cox
92. R. S. Crouse
93. J. L. Crowley
94. F. L. Culler
95. D. R. Cuneo
96. J. E. Cunningham
97. J. M. Dale
98. D. G. Davis
99. R. J. DeBakker
100. J. H. DeVan
101. J. R. DiStefano
102. S. J. Ditto
103. R. G. Donnelly
104. F. A. Doss
105. A. S. Dworkin
106. I. T. Dudley
107. D. A. Dyslin
108. W. P. Eatherly
109. J. R. Engel
110. E. P. Epler
111. J. E. Epperson

112. K. Farrell
113. J. I. Federer
114. J. Feltner
115. D. E. Ferguson
116. L. M. Ferris
117. A. P. Fraas
118. J. K. Franzreb
119. H. A. Friedman
120. D. N. Fry
121. J. H Frye, Jr.
122. W. Fulkerson
123. L. C. Fuller
124. W. K. Furlong
125. C. H. Gabbard
126. R. B. Gallaher
127. R. E. Gehlbach
128. J. H. Gibbons
129. L. O. Gilpatrick
130. G. Goldberg
131. G. M. Goodwin
132. R. J. Gray
133. W. R. Grimes
134. A. G. Grindell
135. R. H. Guymon
136. J. P. Hammond
137. R. L. Hamner
138. B. A. Hannaford
139. T. H. Handley
140. P. H. Harley
141. D. G. Harman
142. W. O. Harms
143. C. S. Harrill
144. P. N. Haubenreich
145. F. K. Heacker
146. R. E. Helms
147. P. G. Herndon
148. D. N. Hess
149. R. F. Hibbs
150. J. R. Hightower
151–153. M. R. Hill
154. E. C. Hise
155. B. F. Hitch
156. H. W. Hoffman
157. D. K. Holmes
158. P. P. Holz
159. R. W. Horton
160. A. Houtzeel
161. T. L. Hudson
162. W. R. Huntley
163. H. Inouye
164. W. H. Jordan
165. P. R. Kasten
166. R. J. Kedl
167. C. W. Kee
168. M. T. Kelley
169. M. J. Kelly
170. C. R. Kennedy
171. T. W. Kerlin
172. H. T. Kerr
173. J. J. Keyes
174. R. T. King
175. D. V. Kiplinger
176. S. S. Kirslis
177. H. W. Kline
178. R. L. Klueh
179. L. R. Koffman
180. J. W. Koger
181. R. B. Korsmeyer
182. A. I. Krakoviak
183. T. S. Kress
184. J. W. Krewson
185. C. E. Lamb
186. J. A. Lane
187. J. J. Lawrence
188. J. M. Leitnaker
189. M. S. Lin
190. R. B. Lindauer
191. C. T. Liu
192. G. H. Llewellyn
193. E. L. Long, Jr.
194. A. L. Lotts
195. M. I. Lundin
196. R. N. Lyon
197. R. L. Macklin
198. R. E. MacPherson
199. J. C. Mailen
200. D. L. Manning
201. C. D. Martin
202. W. R. Martin
203. H. V. Mateer
204. T. H. Mauney
205. H. McClain
206. R. W. McClung
207. H. E. McCoy
208. D. L. McElroy
209. C. K. McGlothlan
210. C. J. McHargue
211. B. McNabb
212. L. E. McNeese
213. J. R. McWherter
214. H. J. Metz
215. A. S. Meyer

216. R. L. Moore
217. C. A. Mossman
218. D. M. Moulton
219. T. W. Mueller
220. M. L. Myers
221. H. A. Nelms
222. H. H. Nichol
223. J. P. Nichols
224. E. L. Nicholson
225. T. S. Noggle
226. E. D. Nogueira
227. L. C. Oakes
228. S. M. Ohr
229. N. H. Packan
230. P. Patriarca
231. A. M. Perry
232. T. W. Pickel
233. H. B. Piper
234. C. B. Pollock
235. B. E. Prince
236. G. L. Ragan
237. J. L. Redford
238. J. D. Redman
239. D. M. Richardson
240. M. Richardson
241. P. L. Rittenhouse
242. G. D. Robbins
243. J M Robbins
244. R. C. Robertson
245. K. A. Romberger
246. M. W. Rosenthal
247. J. Roth
248. J. P. Sanders
249. H. C. Savage
250. W. T. Schaffer
251. A. C. Schaffhauser
252. C. E. Schilling
253. Dunlap Scott
254. J. L. Scott
255. H. E. Seagren
256. J. D. Sease
257–271. C. E. Sessions
272. J. H. Shaffer
273. W. H. Sides
274. G. M. Slaughter
275. A. N. Smith
276. F. J. Smith
277. G. P. Smith
278. O. L. Smith
279. P. G. Smith
280. I. Spiewak
281. R. C. Steffy
282. R. L. Stephenson
283. J. O. Stiegler
284. W. C. Stoddart
285. H. H. Stone
286. R. A. Strehlow
287. R. D. Stulting
288. D. A. Sundberg
289. R. W. Swindeman
290. J. R. Tallackson
291. E. H. Taylor
292. W. Terry
293. R. E. Thoma
294. P. F. Thomason
295. L. M. Toth
296. A. L. Travaglini
297. D. B. Trauger
298. Chia-Pao Tung
299. W. E. Unger
300. R. A. Vandemeer
301. R. A. Waddell, Jr.
302. T. N. Washburn
303. G. M. Watson
304. J. S. Watson
305. H. L. Watts
306. C. F. Weaver
307. B. H. Webster
308. A. M. Weinberg
309. J. R. Weir, Jr.
310. W. J. Werner
311. K. W. West
312. H. L. Whaley
313. M. E. Whatley
314. J. C. White
315. R. P. Wichner
316. F. W. Wiffen
317. R. O. Williams
318. L. V. Wilson
319. M. H. Yoo
320. Gale Young
321. H. C. Young
322. J. P. Young
323. E. L. Youngblood
324. F. C. Zapp
325. C. M. Adams (consultant)
326. Leo Brewer (consultant)
327. L. S. Darken (consultant)
328. Walter Kohn (consultant)

EXTERNAL DISTRIBUTION

329. G. G. Allaria, Atomics International, P. O. Box 309, Canoga Park, California
330. J. G. Asquith, Atomics International, P. O. Box 309, Canoga Park, California
331. C. R. Brooks, the University of Tennessee
332. D. F. Cope, RDT, SSR, AEC, Oak Ridge National Laboratory
333. G. W. Cunningham, AEC, Washington
334. A. R. DeGrazia, AEC, Washington
335. G. K. Dicker, Division of Reactor Development and Technology, AEC, Washington
336. H. M. Dieckamp, Atomics International, P. O. Box 309, Canoga Park, California
337. David Elias, AEC, Washington
338. J. E. Fox, AEC, Washington
339. A. Giambusso, AEC, Washington
340. D. H. Gurinsky, Battelle-Northwest Laboratory, P. O. Box 999, Richland, Washington 99352
341. F. D. Haines, AEC, Washington
342. C. E. Johnson, AEC, Washington
343. W. L. Kitterman, AEC, Washington
344. Kermit Laughon, RDT, AEC, OSR, Oak Ridge National Laboratory
345. C. L. Matthews, RDT, OSR, AEC, Oak Ridge National Laboratory
346. C. F. Leitten, Jr., Union Carbide Corporation Materials System Division Technology, P. O. Box 24184, 1500 Polco Street, Indianapolis, Indiana 46224
347. J. J. Lombardo, NASA, Lewis Research Center
348. A. B. Martin, Atomics International, P. O. Box 309, Canoga Park, California
349. D. G. Mason, Atomics International, P. O. Box 309, Canoga Park, California
350–351. T. W. McIntosh, AEC, Washington
352. G. W. Meyers, Atomics International, P. O. Box 309, Canoga Park, California
353. D. E. Reardon, AEC, Canoga Park Area Office, Canoga Park, Calif.
354. D. R. Riley, AEC, Washington
355. H. M. Roth, AEC, Oak Ridge Operations
356. T. G. Schleiter, AEC, Washington
357. M. Shaw, AEC, Washington
358. P. G. Shewmon, Argonne National Laboratory, 9700 South Cass Avenue, Argonne, Illinois 60439
359. J. M. Simmons, Division of Reactor Development and Technology, AEC, Washington
360. W. L. Smalley, AEC, Washington
361. J. E. Spruiell, the University of Tennessee
362. S. R. Stamp, AEC, Canoga Park Area Office, Canoga Park, Calif.
363–372. E. E. Stansbury, the University of Tennessee
373. D. K. Stevens, AEC, Washington
374. J. A. Swartout, Union Carbide Corporation, New York
375. R. F. Sweek, AEC, Washington

376. A. Taboada, Division of Reactor Development and Technology, AEC, Washington
377. A. Van Echo, Division of Reactor Development and Technology, AEC, Washington
378. James Watson, Gulf General Atomic, Inc., San Diego, California
379. C. E. Weber, AEC, Washington
380. M. J. Whitman, AEC, Washington
381. R. F. Wilson, Atomics International, P. O. Box 309, Canoga Park, California
382. Laboratory and University Division, AEC, Oak Ridge Operations
383–587. Given distribution as shown in TID-4500 under Metals, Ceramics, and Materials category (25 copies – CFSTI)